ADVANCED ENERGY MATERIALS
www.advenergymat.de

Fast-Charging Lithium–Sulfur Batteries

Jakob Offermann, Sheikh Najeeb Ul Haq, Kai-Xing Wang, Rainer Adelung, Shu-Hao Chang, Binson Babu,* and Mozaffar Abdollahifar**

The growing demand for sustainable energy solutions has intensified research into lithium-sulfur batteries (LSBs) due to their potential for high energy density, though their commercialization is primarily hindered by challenges in achieving satisfactory cycle stability and energy density, with fast-charging capabilities also requiring significant improvement. This review explores strategies to enhance the fast-charging capabilities of LSBs, addressing critical issues such as lithium polysulfide (LiPSs) shuttling, sluggish reaction kinetics, and lithium dendrite formation. The review discusses the mechanisms of fast-charging, followed by a comprehensive analysis of key techniques and the crucial role of various battery components that can revolutionize fast-charging capabilities. It covers challenges related to electrical and ionic conductivity, optimizing Li-ion mobility, immobilizing LiPS, designing suitable electrolytes, integrating catalysts to accelerate LiPSs conversion, and engineering cathodes and separator modifications. Additionally, the review discusses scaling challenges for fast-charging LSBs, including electrolyte design, sulfur loading, polysulfide shuttle mitigation, and electrode stability. The review concludes by providing future perspectives on developing next-generation LSBs that could transform the energy storage landscape, with a sustainable, high-capacity, and rapid-charging alternative to current battery technologies, with significant implications for electric vehicles and portable electronics.

1. Introduction

The ever-increasing global demand for electrical and environmentally friendly energy generated from renewable energy resources pushes the existing energy storage solutions to their limits. The electrification of individual mobility demands portable electrochemical energy storage devices, particularly Li-ion batteries (LIBs), and the pursuit of improved LIBs has continued since their commercial inception. In addition, the demand for the LIB market is expected to reach a volume of ~6000 GWh by 2030.[1–3] However, the current LIB technology is limited by the energy density because it relies on insertion-type anode and cathode materials.[4–7] The utilization of conversion-type electrode materials that can accommodate more ions and electrons is a viable solution to achieve higher energy densities.[8–12]

Lithium–sulfur batteries (LSBs) are one of the most promising high-energy battery systems, utilizing Li-stripping/plating at the Li–metal anode and conversion reaction at the sulfur-cathode, significantly outperforming LIBs in terms of both gravimetric and volumetric capacity. Sulfur is a cheap, environmentally friendly, and one of the most abundant elements available on the Earth's crust, exhibits a high theoretical capacity of 1672 mAh g^{-1}, and has spurred a boom in LSB research in recent years (**Figure 1a**).[6,13–19] Although LSBs exhibit high energy density, their wide application and commercialization lag behind LIBs due to several challenges. These challenges include significant electrode volume expansion during charging and discharging, electrode degradation, and the shuttling of soluble LiPS between

J. Offermann, R. Adelung, M. Abdollahifar
Chair for Functional Nanomaterials
Department of Materials Science
Faculty of Engineering
Kiel University
Kaiserstr. 2, 24143 Kiel, Germany
E-mail: moza@tf.uni-kiel.de

The ORCID identification number(s) for the author(s) of this article can be found under https://doi.org/10.1002/aenm.202404383

DOI: 10.1002/aenm.202404383

S. N. Ul Haq, B. Babu
Department of Physics, School of Natural Sciences
Shiv Nadar Institution of Eminence
Delhi, Uttar Pradesh 201314, India
E-mail: binson.babu@snu.edu.in

K.-X. Wang, S.-H. Chang
Department of Chemical Engineering
Chung Yuan Christian University
320314 Taoyuan City, Taiwan
E-mail: changsh@cycu.edu.tw

R. Adelung, M. Abdollahifar
Kiel Nano, Surface and Interface Science (KiNSIS)
Kiel University
Kaiserstr. 2, 24143 Kiel, Germany

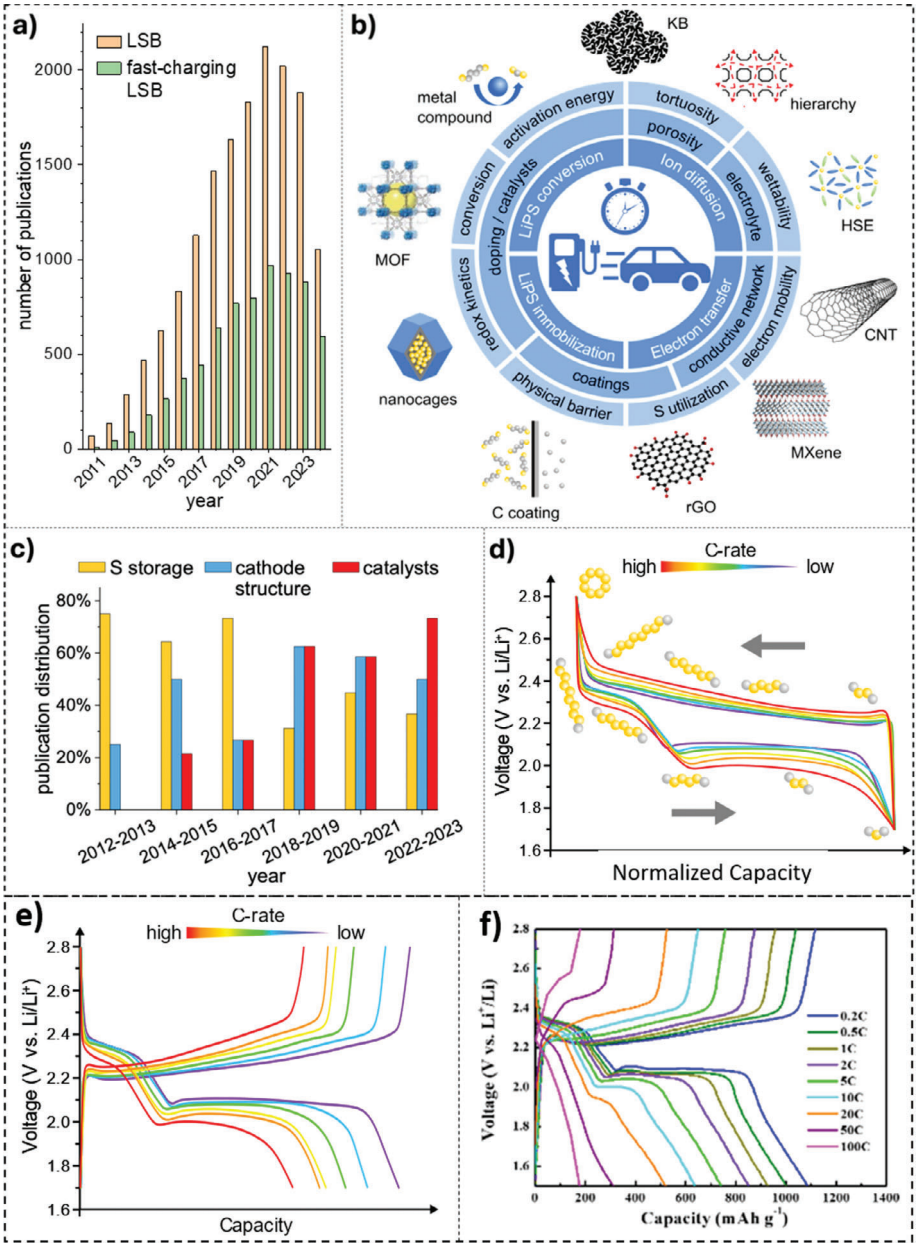

Figure 1. Research trends, key influencing factors, and characteristic electrochemical behavior of LSBs, particularly concerning fast-charging capabilities. a) Annual number of publications related to LSBs and fast-charging LSBs from 2011 to middle 2024 (from www.webofscience.com, with keywords: "fast-charging lithium-sulfur battery" as well as "high-rate lithium-sulfur battery" (green) and " lithium-sulfur battery" (orange)). b) Schematic overview highlighting key parameters, challenges, and strategies influencing LSB fast-charging. c) Histogram showing the changing research activities over the last 12 years on various cathode materials of LSBs to improve their high-power nature. d) Typical galvanostatic charge–discharge profiles (Voltage vs Li/Li^+) vs normalized capacity at various C-rates (color-coded), including schematic molecular discharge pathway (S_8 to Li_2S_x to Li_2S_2/Li_2S). e) Corresponding voltage profiles vs capacity, illustrating reduced capacity and increased voltage hysteresis at higher C-rates. Profiles in (d) and (e) represent data averaged across five studies.[28,35–38] f) Voltage profiles demonstrating performance under ultra-high C-rate conditions (0.2C to 100C). Reproduced with permission.[35] Copyright 2020, Elsevier.

electrodes, all of which limit the coulombic efficiency (CE) and cycling stability. Although the dissolution of LiPSs is inherent to the battery's operation, it is the subsequent shuttling of these dissolved species that poses a significant problem.[20–22]

Though substantial research activities have been conducted to address these challenges by developing novel electrode material composites, incorporating catalysts, designing innovative electrolyte compositions, and creating new cell configurations,[20,23–25] only a small portion of the research has focused on the issues related to the high-power applications of LSBs, which is a critical factor for electric vehicles. During fast-charging, the abovementioned challenges are exacerbated,

affecting the electrical integration of the sulfur, active mass loss, polysulfide shuttle effect, etc. However, the understanding of "fast-charging" has changed continuously in the last decade, and high rates progressed from 1C or 2C to 5C and more for LSBs.[26–30] In this review, we will primarily focus on strategies enabling performance at rates of "2C or higher" as indicative of significant progress towards fast-charging capabilities for LSBs.

Fast-charging and discharging of LSBs require excellent electrical and ionic conduction at the electrodes, high Li-ion mobility, effective immobilization, rapid conversion of LiPSs, prevention of dendrite formation on the Li-metal, and careful electrode engineering (porosity, pore sizes, and distribution, tortuosity, adhesion, and thickness), which can be designed from making slurry to electrode calendering (Figure 1b).[31] Significant progress has been made to enhance the high-rate performance of LSBs by improving electrical connectivity through the incorporation of highly porous and conductive materials with sulfur cathodes, introducing catalysts, a focus of significant attention in recent years, at the cathode and separator to accelerate LiPS conversion, and doping with electrolyte additives (Figure 1c).

The electrochemical consequences of operating LSBs at high rates are starkly illustrated in Figure 1d–f. Figure 1d,e compares typical galvanostatic charge-discharge profiles at low versus high C-rates. Key challenges immediately apparent at higher rates (e.g., red curves vs blue/purple curves) include substantially reduced capacity (Figure 1e), increased voltage hysteresis (the gap between charge and discharge curves in Figure 1d,e) reflecting higher polarization and energy inefficiency, and shifts in the characteristic voltage plateaus associated with LiPS conversions.[32–34] Furthermore, Figure 1f[35] showcases the extreme voltage penalties and capacity degradation observed under ultra-high C-rate conditions (up to 100C), emphasizing the severe kinetic limitations inherent in the system. (The fundamental electrochemical processes, reaction steps, and potentials underlying these voltage profile characteristics are discussed in detail in Section 2: Fundamentals of Lithium–Sulfur Batteries). Effectively mitigating these rate-dependent performance degradations, visually summarized in Figures 1d–f, is essential for realizing practical fast-charging LSBs.

Evaluating the effectiveness of strategies aimed at enhancing fast-charging capabilities requires monitoring several key performance indicators. Rate capability, expressed as the specific capacity retained at high current densities (C-rates $\geq$ 2C), is a primary metric. Equally important are the capacity retention ratio (comparing high C-rate capacity to low C-rate capacity) and the high-rate cycling stability, which measures capacity fade over extended cycles under fast-charging conditions. Analysis of voltage profiles reveals crucial information about polarization (voltage gaps between (dis)charge) and reaction kinetics, while high CE during high-rate cycling indicates minimal parasitic losses. These indicators, alongside impedance measurements where applicable, collectively assess both the speed and sustainability of fast-charging in LSBs, and will be used throughout this review to compare different approaches. This review addresses challenges in fast-charging LSBs, explores strategies to improve high-power performance, and provides guidelines for future advancements. We will commence with the fundamental principles of LSBs and fast-charging mechanisms and subsequently explore key techniques to revolutionize fast charging: cathode design optimization, electrolyte enhancement, separator refinement, and catalyst integration.

2. Fundamentals of Lithium–Sulfur Batteries

A typical LSB comprises a sulfur cathode, a metallic lithium anode, an organic electrolyte, and a separator.[17,39,40] Among the different forms of sulfur, the ring-structured octa sulfur S_8 is typically the most stable at room temperature.[41–43] Once the LSB is assembled, the cell initiates operation from the discharged state. Specifically, as the lithiation process commences, the lithium metal anode undergoes oxidation to generate Li^+ ions. These ions then migrate from the negative to the positive electrode through the electrolyte. On the positive electrode side, Li^+ ions react with sulfur to produce LiPSs (Li_2S_x, $1 \leq x \leq 8$) with the assistance of electrons transmitted from the external electrical circuit. In a typical LSB employing sulfur as a starting material, there is a continuous transition of sulfur species between S_8 and Li_2S during the discharge process. Conversely, during the sulfur cathode delithiation (charge process), Li_2S is oxidized to generate S_8 through multiple intermediate LiPSs. The overall electrochemical reaction corresponding to the Li/S redox reaction can be articulated as follows:

$$16\ Li + S_8 \leftrightarrow 8\ Li_2S \quad (1)$$

The characteristic multi-step electrochemical behavior of LSBs during charge and discharge is clearly visualized in typical galvanostatic profiles, such as those shown at various C-rates in Figure 1d,e.[28,35–38,44–47] Figure 1d (normalized capacity) highlights the profile shape and associated molecular transformations, while Figure 1e (specific capacity) illustrates the impact on delivered energy and the effect of C-rate. The molecular diagrams in Figure 1e depict the widely accepted discharge sequence: cyclic S_8 → linear long-chain LiPSs (Li_2S_x, x = 8, 6, 4) → short-chain LiPSs and lithium sulfide (Li_2S_2/Li_2S).[34,48–53] The complex sequence involves multiple phase transitions and intermediate lithium polysulfide (LiPS) species. **Table 1** provides a detailed summary correlating the key reaction steps,[54] their specific reported potentials, the corresponding phase transitions, the observed electrochemical features (plateaus) seen in Figure 1d,e, and explicitly contrasts the approximate voltages of these features observed at low versus high C-rates.

As summarized in Table 1 and illustrated in Figure 1d,e, the upper plateau and the sloping region in the voltage profile during the discharging of LSB indicate the dissolution of sulfur to higher-order polysulfides, whereas the lower plateau region, associated with the formation of less soluble Li_2S_2 and Li_2S, which contributes the maximum reversible capacity, is responsible for the high reversible capacity where the impact of polysulfide shuttling is significantly reduced.[54,55] The LSB discharge typically proceeds through an upper voltage plateau (e.g., ≈2.3 V at low C-rate) associated with the conversion of solid S_8 to soluble high-order LiPSs (Steps 1–2), followed by a lower voltage plateau (e.g., ≈2.1 V at low C-rate) corresponding to the conversion of intermediate LiPSs to solid Li_2S_2 and Li_2S precipitates (Steps 3–4). The charge process involves the reverse transformations at generally higher potentials.

Table 1. Summary of LSB discharge/charge steps, potentials, and C-rate effects.

Step	Description/phase transition	Corresponding electrochemical feature	Low C-rate (V vs Li/Li^+)[a]	High C-rate (V vs Li/Li^+)[a]
Discharge				
1	Solid (S_8) → Liquid (Li_2S_8)	Upper Discharge Plateau (Start)	≈2.3 V	≈2.15 V
2	Liquid (Li_2S_8) → Liquid (Li_2S_6) → Liquid (Li_2S_4)	Upper Plateau/Sloping Region	≈2.3 V	≈2.15 V
3	Liquid (Li_2S_4) → Solid (Li_2S_2)	Lower Discharge Plateau	≈2.15 V	≈1.95 V
4	Solid (Li_2S_2) → Solid (Li_2S)	Lower Discharge Plateau	≈2.1 V	≈1.95 V
Charge				
–	Solid (Li_2S, Li_2S_2) → Liquid (Li_2S_4) (Reverse Steps 4 and 3)	Lower Charge Plateau	≈2.2 V	≈2.3 V
–	Liquid (Li_2S_4, Li_2S_6, Li_2S_8) → Solid (S_8) (Reverse Steps 2 and 1)	Upper Charge Plateau	≈2.4 V	≈2.5 V

[a] Approximate observed plateau centers based on typical averaged experimental data (Figure 1d,e).

Crucially, the separate columns for low and high C-rates in Table 1, along with Figure 1e, clearly highlight the significant impact of kinetics and operating current. At higher C-rates, discharge plateau voltages drop significantly (e.g., lower plateau from ≈2.1 V to ≈1.95 V), charge plateau voltages rise (e.g., upper plateau from ≈2.4 V to ≈2.5 V), and the overall specific capacity decreases substantially.[32–34] This increased voltage hysteresis signifies greater energy inefficiency. These effects stem from several challenges inherent in the Li–S system, detailed further in Table 2: the insulating nature of S_8, Li_2S_2, and Li_2S imposes significant polarization; the multi-step reaction pathway involves sluggish kinetics, particularly the solid-state conversions (Step 4) and overcoming nucleation barriers (Step 3); and the dissolution of intermediate LiPSs (Step 2) leads to the detrimental shuttle effect, causing capacity fade and low coulombic efficiency, especially during extended cycling.[54,56,57]

Boosting the high-power performance of LSBs thus requires careful management of these complex sulfur species transitions and mitigation of the associated challenges summarized in Table 2. Curbing LiPS dissolution and shuttling while overcoming the kinetic barriers related to insulating species (S_8, Li_2S_2, Li_2S) and phase transitions (especially solid-state conversions) are paramount, particularly under fast-charging conditions. Therefore, developing advanced strategies such as optimizing porous cathode structures, modifying separators, utilizing electrocatalysts to lower activation barriers and speed up conversion reactions, and engineering electrolytes are essential approaches for achieving high-power LSBs, which will be further elucidated in subsequent sections.

3. Design Principles and Strategies for Fast-Charging LSBs

The development of fast-charging LSBs requires overcoming numerous challenges in materials science, electrochemistry, and engineering (**Figure 2**). Fast-charging in LSBs demands a careful balance between high energy density and rapid (dis)charge capabilities while addressing core issues like sulfur redox reactions (SRRs) and polysulfide shuttling, which can compromise battery performance at high current densities. Effective solutions require integrated advancements across cathode, separator, anode design, electrolyte composition, and system-wide optimizations.

3.1. Enhancing Conversion Kinetics through Material Design

The ability of LSBs to achieve rapid charging is fundamentally governed by the kinetics of the SRRs, particularly the conversion between different polysulfide species and the final formation of solid Li_2S. Material design plays a pivotal role in accelerating these sluggish kinetics, especially under the high current densities demanded by fast charging. For instance, engineering cathode architectures with interconnected conductive networks, such as those based on carbon nanotubes and graphene,[58,59] ensures efficient electron transport throughout the sulfur-active material, minimizing polarization and enabling faster reaction rates. The incorporation of highly porous structures facilitates rapid Li-ion diffusion, allowing for quicker access to reaction sites within the cathode.[60] Furthermore, the integration of catalytic materials, including metal oxides and single-atom catalysts (SACs),[61,62] significantly lowers the activation energy barriers for both the sulfur reduction and evolution reactions. These catalysts can promote the rapid conversion of soluble long-chain polysulfides to less soluble short-chain species and ultimately to Li_2S during discharge, as well as the reverse process during charge. By strategically designing materials with optimized electrical and ionic conductivity, high surface area, and catalytic activity, the kinetic limitations of LSBs can be effectively overcome, paving the way for high-performance fast-charging capabilities.

3.2. Establishing Electrical and Ionic Conductivity: the Foundation of Fast-Charging

The first step toward achieving fast-charging LSBs is to ensure high electrical and ionic conductivity at both cathode and anode electrodes and separator, which can be discussed as follows:

Cathode Engineering: The cathode must facilitate rapid electron transfer and efficient sulfur-Li_2S conversion during cycling. This requires incorporating conductive additives like nanocarbons, carbon nanotubes (CNTs), and graphene,[58,59] which create robust electron pathways to enhance charge transfer. The structural architecture of the cathode must be designed to balance porosity, active material loading, and mechanical stability, ensuring effective ionic and electronic transport without sacrificing energy density or long-term cycle life. For example, the use of highly porous 3D carbon frameworks combining CNTs and graphene has shown promise in providing both high

Table 2. Summary of key challenge areas limiting fast-charging in LSBs, their impact, and the corresponding enabling strategies discussed in Section 3.

Challenge area and primary mechanism (source section(s))	Fast-charging enablement and impact	Key strategy examples
Slow Kinetics (Sluggish SRR/SER) (3.1, 3.5)	• Accelerates chemical transformations for quicker charge acceptance/release.	• Catalyst integration (e.g., metal oxides, SACs) • Material design (porosity, surface area) • Interface engineering
Poor Transport (e^-/Li^+ Conductivity) (3.2, 3.6)	• Allows higher current density with less resistance/polarization.	• Conductive cathode architectures (e.g., 3D carbon) • High σ electrolytes • Optimized separator ion transport • Conductive interfaces
LiPS Shuttle (Active Material Loss) (3.3, 3.4, 3.5)	• Improves current efficiency by preventing parasitic reactions.	• Cathode confinement structures • Separator blocking/functional layers • Low-solubility/High-conc. electrolytes • Catalytic trapping and conversion
Anode Instability (Dendrite Growth) (3.2, 3.4)	• Ensures safety and longevity when applying high charging currents.	• Anode surface engineering • Electrolyte additives for SEI stabilization • Solid electrolytes as barriers • Separator protection/ion flux control
Interface Degradation (High Resistance) (3.7)	• Maintains efficient charge transfer under high-current stress.	• Protective coatings • Artificial SEI layers • Multi-functional/conductive interlayers
System Limitations (Heat, Control, Scale) (3.8)	• Enables sustained high rates safely and facilitates practical viability.	• Thermal management • Advanced BMS • Scalable manufacturing
Need for Integration (Overall Synergy) (3.9)	• Maximizes performance gains by combining complementary solutions.	• Integrated designs (e.g., catalyst + cathode structure) • Multi-functional components (e.g., separator + catalyst) • Optimized system-wide approach (e.g., electrolyte + additives)

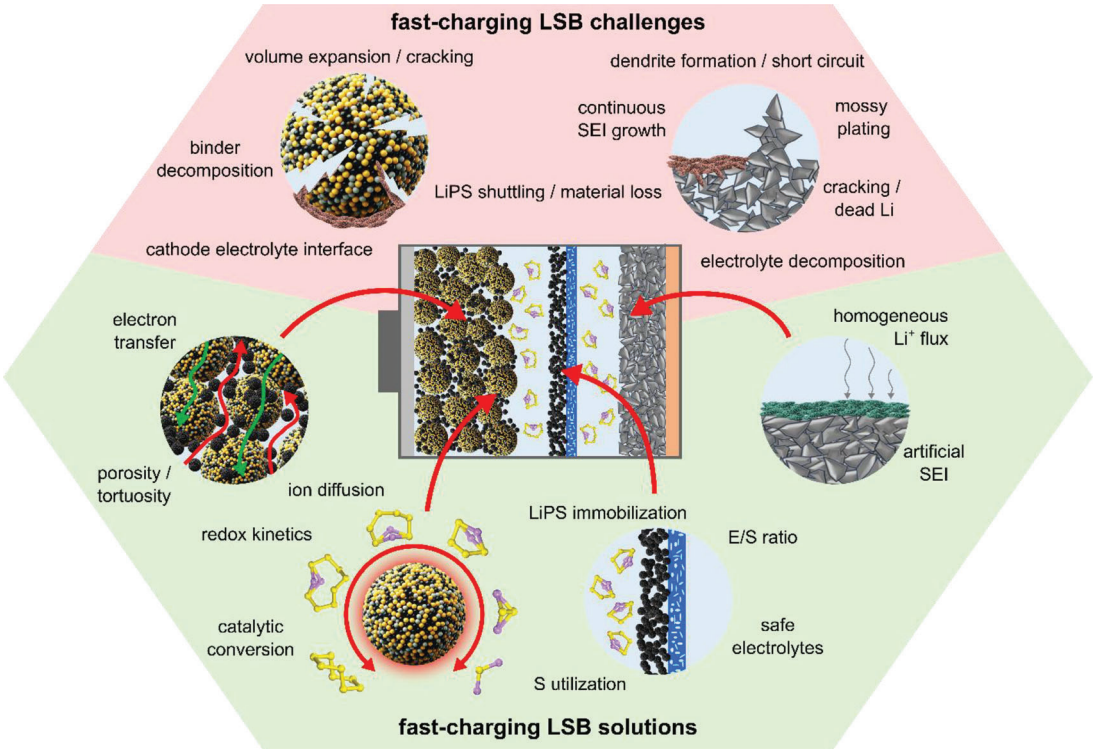

Figure 2. The diagram showcases the key challenges (red background) and potential solutions (green background) for fast-charging LSBs. Issues like cathode degradation, dendrite formation, polysulfide shuttling, and electrolyte decomposition are highlighted, along with the importance of efficient electron/ion transfer and sulfur utilization. Solutions such as artificial SEI layers, safe electrolytes, catalytic conversion, and electrode engineering offer promise for improved LSB performance and stability.

conductivity and sulfur storage.[63,64] Additionally, cathode designs must accommodate volume changes associated with sulfur expansion during cycling to maintain structural integrity, which is critical for high-rate performance. Encapsulating sulfur within nanostructured carbon materials can help manage this expansion.[65]

Anode Requirements: On the anode side, smooth and uniform lithium plating is essential to prevent dendrite formation, a common challenge at high current densities that can lead to short circuits and battery failure. Surface engineering strategies, including lithiophilic coatings and structured interfaces, promote uniform lithium deposition and mitigate dendrite growth. For instance, the use of electrolyte additives like $LiNO_3$ has been shown to stabilize the lithium metal surface and improve cycling stability.[66,67] The anode must also tolerate significant volume fluctuations during cycling and maintain a stable SEI layer, which ensures long-term stability and fast-charging performance.

Separator Refinement: The separator is vital in controlling ionic conductivity and managing polysulfide migration. Modifications, such as coating with carbon-based materials,[68] metal composites,[69] or metal–organic frameworks (MOFs),[70] can effectively reduce polysulfide crossover while enhancing the mechanical properties of the separators. These modifications contribute to maintaining the efficiency of the cell and stability, especially under high-rate conditions. For example, coating the separator with conductive carbon can improve electron transport and utilize adsorbed polysulfides,[68] while MOF-based coatings can act as ionic sieves, allowing Li-ion transport while blocking polysulfides.[70]

3.3. Optimizing Li-Ion Mobility and LiPSs Immobilization

Rapid charge transport in LSBs relies on high Li-ion mobility and effective LiPS immobilization. The electrolyte, crucial for ion transport between the cathode and anode, significantly impacts the overall performance of the battery. Advanced electrolyte formulations, such as high-concentration ether and solid-state electrolytes (SSEs), boost Li-ion mobility while minimizing polysulfide dissolution, a key factor in achieving stable, high-rate cycling.[71,72] For instance, the use of dual-salt high-concentration ether electrolytes has shown enhanced ionic conductivity and high-power performance.[73] SSEs, while facing challenges, offer the potential to eliminate polysulfide shuttling altogether, further contributing to stability.[74] The discovery of solid-to-solid reactions in carbonate-based electrolytes using γ-monoclinic sulfur offers a promising pathway to fast-charging while bypassing traditional challenges associated with the polysulfide shuttle effect.[71,75] This approach often involves specific cathode designs to facilitate the direct conversion of sulfur to Li_2S.[76] The uncontrolled LiPS migration degrades performance of LSBs, leading to capacity fading and reduced cycle life. Effective immobilization strategies involve integrating catalysts within the cathode[77] or separator[78] that accelerate the conversion of LiPSs, ensuring they are quickly reduced to less soluble species. Catalysts with high adsorption capacity, abundant active sites, superior electronic and ionic conductivity are essential for capturing soluble polysulfides and facilitating their rapid conversion into solid Li_2S during discharge, thereby mitigating the shuttle effect. For example, metal oxides like Fe_3O_4 have shown strong interactions with LiPSs and catalytic ability,[77] while separator modifications with materials like lepidolite have demonstrated accelerated conversion of polysulfides.[78]

3.4. Electrolyte Design for Fast-Charging LSBs

The electrolyte plays a decisive role in enabling fast-charging in LSBs.[71,72] The primary challenge is managing LiPSs dissolution while ensuring sufficient ionic conductivity for high-rate cycling. Ether-based electrolytes are commonly employed due to their favorable redox kinetics,[73] but pose risks related to polysulfide shuttling and lithium metal reactivity. Solid electrolytes[74] and high-concentration electrolyte formulations[79] are being explored to overcome these issues while maintaining rapid ion transport. For high energy densities, a low electrolyte/sulfur (E/S) ratio is essential, however, lean electrolytes often lead to poor polysulfide solubility and drying issues. Addressing these challenges requires careful electrolyte management and the development of formulations that sustain performance under practical, high-power conditions. Fast-charging at high current densities increases the risk of dendrite formation on the lithium-metal anode, which can be mitigated through electrolyte additives that stabilize the SEI layer [66,67] or with SSEs that act as physical barriers against dendrite penetration.[80] Both approaches contribute significant enhancement in safety and longevity of LSBs under fast-charging conditions.

3.5. Accelerating LiPSs Conversion via Catalyst Integration

Ideal catalysts have high activity for sulfur reduction reaction (SRR) and sulfur evolution reaction (SER), maintain structural integrity, and offer electrochemical stability, ensuring stable and efficient battery performance under high-rate conditions, enabling rapid conversion of LiPSs and preventing the detrimental shuttle effect and dendrite formation.[54] For example, metal oxides like MnO_2 and RuO_2 heterostructures have shown promise in regulating the energy barrier for LiPS transformation.[81] They reduce the activation energy needed for SRR and SER, enhancing reaction rates without altering thermodynamics.[54] Effective catalysts possess several key attributes, including strong LiPS adsorption,[82] abundant active sites,[62] and excellent electronic and ionic conductivities,[83] which can also be embedded in conductive materials to further enhance electron/ion transfer.[84] For instance, metal chalcogenides like CoS_2 exhibit strong polysulfide adsorption properties,[82] and SACs maximize the surface area of active sites.[62] Combining catalysts with conductive materials like CNTs can further improve electron transfer.[83] The active sites of these catalysts fulfill two critical functions: (i) capturing soluble polysulfides to mitigate the shuttling effect[85] and (ii) offering nucleation sites for Li_2S_2/Li_2S deposition, facilitating rapid liquid-solid transformation.[84] Selective catalysts, for example, can decelerate sulfur dissolution and simultaneously accelerate LiPSs conversion.[85] Ideal catalysts exhibit high activity for SRR and SER, maintain structural integrity, and offer electrochemical stability, ensuring stable and efficient battery performance under high-rate conditions.[86]

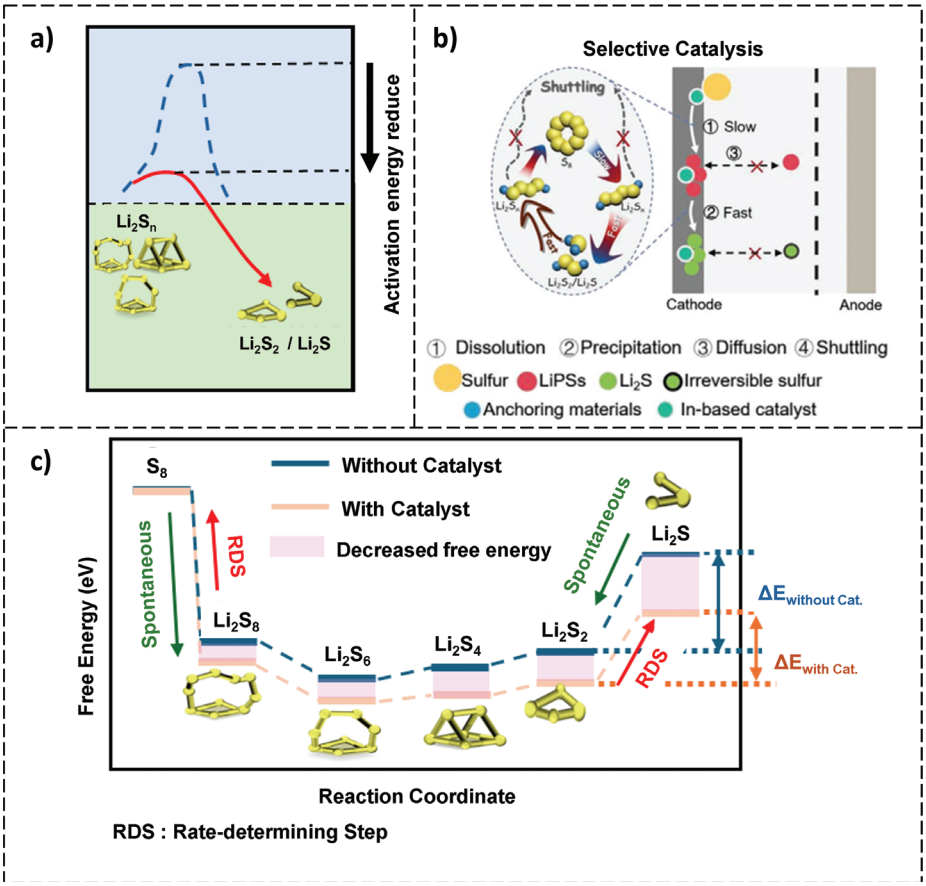

Figure 3. a) Illustration showing the reduction of activation energy for the transition from Li_2S_n to Li_2S_n/Li_2S with and without catalysts. b) Illustration of the selective catalysis mechanism explaining the inhibition of the shuttling effect. Reproduced with permission.[85] Copyright 2021, John Wiley and Sons. c) The Gibbs free energy profiles of lithium polysulfide (LiPS) conversions with and without catalysts.

Mechanisms: Catalysts reduce activation energy for both SRR and SER processes, enabling faster redox kinetics and enhancing charging speed.[87,88] For example, the use of organometallic-based homogeneous catalysts has shown reduced activation energy for LiPS conversion.[89] Selective catalysis allows for the controlled conversion of sulfur into LiPSs, while promoting their rapid transformation into Li_2S minimizes polysulfide buildup, and mitigates the shuttle effect.[87] In general, by providing alternative reaction pathways with lower energy barriers for the SRR and SER during discharging and charging, respectively, catalysts improve the efficiency of converting LiPSs into Li_2S, and vice versa (**Figure 3a**).[90] Thus, the accelerated redox reactions ensure the high performance of LSBs during fast-charging and discharging cycles. For instance, Zeng et al.[61] employed in situ Raman spectroscopy to investigate catalytic transformation in LSBs, comparing S/MIL-101(Cr) and S/MOF-TOC cathodes, demonstrating the superior catalytic effect of S/MOF-TOC in converting sulfur to lower-order polysulfides.

Active Sites and Conductivity: Effective catalysts provide high electrocatalytic activity,[91] ample active sites,[62] and superior electronic conductivity,[83] all essential for capturing soluble polysulfides and driving their conversion into stable discharge products.[92] For example, dual metallic single-atom pairs have shown high catalytic activity,[91] and SACs maximize active site utilization.[62] These properties ensure reliable performance even at high current densities. The presence of polar sites on cathode surfaces facilitates strong adsorption of LiPS, significantly lowering interfacial resistance and enabling efficient nucleation and lateral growth of Li_2S. The Li_2S formation follows a "nucleation–proliferation–growth" pathway, where nucleation is limited by interfacial charge transfer, and growth is mainly driven by LiPS diffusion, rather than electron conduction, which is restricted to nanometer-scale distances.[93] Notably, Sun et al.[94] developed a multifunctional GC-uNiCoP@NPC catalyst, featuring ultrafine NiCoP nanoparticles embedded in N, P co-doped carbon, which accelerates sluggish heterogeneous SRR steps and stabilizes Li_2S formation. Operando analyses confirmed enhanced redox kinetics, enabling high performance even at high sulfur loading and low E/S.

Selective Catalysis: Selective catalysis plays a pivotal role in enabling fast-charging in LSBs. Beyond merely accelerating reactions, it offers a nuanced approach to manage the complex sulfur conversion process, particularly at high current densities. Hua et al.[85] described how the selective catalysts optimize SRRs during fast charging by i) decelerating sulfur dissolution (the catalyst hinders the initial dissolution of sulfur into LiPSs, preventing excessive polysulfide buildup in the electrolyte, maintaining a balanced reaction environment) and ii) accelerating LiPSs

conversion (simultaneously, the catalyst expedites the LiPSs to solid Li_2S conversion minimizes the concentration of soluble polysulfides and thus mitigates the shuttle effect that plagues conventional LSBs). This dual action of selective catalysis tackles two fast-charging challenges in LSBs: a) Polysulfide shuttling mitigation, which improves the capacity retention and prolonged cycle life (Figure 3b), and b) Enhanced reaction kinetics for efficient (dis)charge without compromising energy efficiency. Figure 3c illustrates a schematic free-energy diagram for the key reactions involved in the conversion of elemental sulfur (S_8) to Li_2S at the cathode. The reaction from S_8 to Li_2S_8 is spontaneous, and the subsequent conversion from Li_2S_8 to Li_2S_6/Li_2S_4 is near thermodynamic equilibrium. However, the reduction of Li_2S_2 to Li_2S is the highest free-energy barrier, indicating the rate-limiting step in the sulfur redox process.[95] Catalysts help to lower the free energy difference, making the conversion more efficient.

3.6. Cathode Electrode Engineering: A Critical Enabler for Fast-Charging

Optimizing the cathode electrode design is crucial for fast-charging in LSBs. The performance of LSB electrodes is determined by factors such as porosity, pore size distribution, tortuosity, adhesion, and thickness. Besides current collector optimization and crack formation,[96] fine-tuning these parameters during the electrode fabrication process—including slurry preparation, coating, drying, and calendering—ensures mechanical integrity and ion transport of the electrodes.[31] This process is essential for achieving high power densities without sacrificing cycle stability.

Slurry Preparation: Proper control of solid content, binder selection, and conductive additives ensures optimal electronic and ionic conductivity. For instance, using a combination of CNTs and graphene in the slurry can create a highly conductive network.[63]

Coating: Precise coating thickness control ensures uniform active material distribution and consistent electrode wettability and tortuosity.

Drying and Calendering: Optimizing these processes controls pore formation, improves electrode and particle adhesion/cohesion, and enhances electrode performance during fast charging.[31]

To achieve fast-charging in LSBs, advanced cathode design emphasizes both enhanced conductivity and robust structural stability. Incorporating high-performance conductive materials significantly boosts both electrical and ionic conductivity, which is essential for rapid charge and discharge processes. For example, the use of highly conductive 3D structures made from 1D and 2D carbon components has shown excellent rate capability.[38] Additionally, cutting-edge fabrication techniques, including 3D printing and templating, allow for the development of sophisticated hierarchical cathode structures. These innovative designs maximize sulfur use and adapt to the volume changes during cycling, thereby maintaining high performance even at elevated charge rates. Porous and multi-layered architectures are particularly effective for creating optimized pathways for ion and electron flow, thereby facilitating efficient SRRs and sustaining high efficiency throughout the fast-charge/discharge process.[97]

The cathode particles are also pivotal in determining the efficiency and viability of fast-charging in LSBs. The cathode design directly impacts Li-ion and electron transport, sulfur accommodation, and LiPSs immobilization. The choice of materials, from sulfur-carbon composites[35] to advanced conductive frameworks,[98] plays a crucial role in determining the performance of the battery during fast charging. The primary challenge lies in maximizing sulfur utilization while maintaining structural stability and longevity, which is essential for achieving a long cycle life.

3.7. Interface Engineering for Enhanced Charge Transfer and Stability

Fast-charging LSBs face significant challenges related to interface instability and poor charge transfer between various components. Addressing these issues requires focused strategies for interface engineering:

Stable Interfaces: The interfaces between the cathode, electrolyte, and anode are prone to degradation, especially under fast-charging conditions. Engineering stable interfaces involve the use of protective coatings, surface modifications, and interfacial layers that prevent side reactions and maintain consistent performance. For instance, the use of artificial SEI layers on the lithium-metal anode, formed by electrolyte additives like $LiNO_3$,[66,67] can significantly enhance stability by suppressing lithium dendrite growth and reducing electrolyte decomposition.

Enhanced Charge Transfer: Improving charge transfer efficiency at the electrode-electrolyte interface is crucial for fast-charging. This can be achieved by integrating high-conductive interfacial layers, such as conductive polymers like PANI[99] and nanostructured coatings like MXenes,[98] which reduce charge transfer resistance and facilitate ion transport across the interface. These modifications help maintain low overpotentials and ensure efficient (dis)charge cycles even at elevated current densities.

Multi-Functional Interfacial Materials: Incorporating multifunctional interfacial materials having high conductivity, chemical stability, and catalytic activity is a promising approach to improve charge transfer while mitigating polysulfide shuttling and stabilizing electrode-electrolyte interfaces. For example, interlayers modified with metal-carbon composites that possess both high conductivity and the ability to catalyze polysulfide conversion can be effective.[100]

3.8. System-Level Optimizations and Practical Implementation: Beyond Core Challenges

Achieving practical fast-charging LSBs requires advancements not only in materials and electrodes, which are the main focus of this review paper, but also necessitate system-wide optimizations, including thermal management, battery management systems (BMS), module and pack level integration, scalability, and cost.

Thermal Management Solutions: Fast-charging generates substantial heat, which can negatively impact battery performance

and safety. To counter these thermal challenges, combining passive and active cooling methods is essential. Approaches like thermal management layers, phase-change materials, and liquid cooling work together to dissipate excess heat and maintain stable operation. These strategies ensure safe, efficient, and durable battery performance under high-power loads.

Battery Management Systems (BMS): Efficient BMS algorithms are essential for controlling charging rates, monitoring temperature, and managing safety during fast-charging. Advanced BMS solutions with real-time data analysis and predictive modeling can optimize charge protocols, prevent overcharging, and extend battery life. These systems also play a key role in mitigating risks such as thermal runaway and managing the dynamic behavior of LSBs under high power conditions.

Module and Pack-Level Integration: For commercial applications, integrating LSBs into modules and packs while preserving fast-charging capabilities is crucial. This involves optimizing cell arrangement, thermal interfaces, and electrical connections for consistent performance. Additionally, modular designs with flexible configurations can be tailored to specific applications, such as electric vehicles or grid storage, where fast-charging is a priority.

Scalability and Cost: For fast-charging LSBs to be commercially viable, scalable manufacturing processes are essential. From electrode fabrication to electrolyte formulation, each production step must be optimized for cost-effective mass production while ensuring consistent quality and performance.

3.9. Synergistic Approaches for Enhancing Fast-Charging in LSBs

Achieving optimal fast-charging performance in LSBs necessitates moving beyond optimizing individual components and embracing strategies that leverage synergies between different approaches. The inherent challenges of LSBs, particularly the polysulfide shuttle effect and sluggish reaction kinetics,[54] are often exacerbated at high current densities, requiring integrated solutions. This review highlights several instances where combining advancements in cathode engineering, catalyst integration, separator modification, and electrolyte formulation leads to performance greater than the sum of its parts.

A prominent synergistic strategy involves integrating highly active catalysts within engineered cathode architectures. For instance, combining 3D conductive frameworks (like CNT/graphene composites[63,64] or Nb_2O_5-x/CNTs[97]) with catalysts (e.g., metal oxides, sulfides, nitrides, or SACs) addresses multiple needs simultaneously: the framework ensures rapid electron/ion transport pathways crucial for high rates,[63,97] while the catalyst lowers activation energy barriers for SRRs and sulfur evolution reactions (SERs).[101] Heterostructures explicitly embody this synergy, using materials like Nb_2O_{5-x}/CNTs[97] or MXene composites[98] to provide high surface area, conductivity, polysulfide anchoring, and catalytic activity within a single electrode system. Wang et al.[83] demonstrated a synergistic combination where MoN acted as a catalyst for LiPS conversion and MoS_2 provided anchoring sites, both layered around CNTs for conductivity, achieving good performance even at 6C. Similarly, dual metallic single-atom pairs (Fe and Co) showed synergy where Fe facilitated Li_2S nucleation and Co aided its decomposition, boosting redox kinetics.[91]

Separator modifications also work synergistically with other components. Functional coatings containing conductive materials (e.g., carbon, MXenes) and catalysts (e.g., metal compounds, MOFs) not only physically block polysulfides but also provide active sites for their immobilization and rapid conversion. These modified separators, such as the lepidolite-coated separator facilitating Li-ion transport and polysulfide conversion[78] or metal-carbon heterostructures like MMT/rGO[100] and MCCoS/PP,[102] enhance the utilization of active material and maintain electrode integrity, especially under lean electrolyte conditions typical for high energy density. Some advanced separators also incorporate features to regulate Li-ion flux, synergistically mitigating Li-dendrite growth on the anode side,[103] a critical issue during fast charging. Furthermore, electrolyte formulation plays a synergistic role. Additives like $LiNO_3$ not only passivate the Li-metal anode but can work synergistically with dissolved polysulfides to form more stable SEI layers.[104] Homogeneous catalysts dissolved in the electrolyte can accelerate LiPS conversion throughout the electrolyte volume,[89] complementing heterogeneous catalysts fixed on cathodes or separators. The unique synergy between γ-monoclinic sulfur cathodes and carbonate electrolytes enables a direct solid-to-solid reaction pathway, bypassing polysulfide dissolution and enabling ultra-fast charging,[76] although challenges in sulfur loading remain.

These examples illustrate that future breakthroughs in fast-charging LSBs will likely rely on the intelligent combination of multiple strategies, targeting the complex interplay between electron transport, ion diffusion, reaction kinetics, and interfacial stability across all battery components. To consolidate the design principles and strategies discussed, the key challenges hindering fast charging in LSBs, their impact, and the corresponding enabling strategies covered in this section are summarized in **Table 2**.

By integrating fundamental scientific principles with innovative engineering techniques, we are advancing high-performance, fast-charging LSBs. The successful implementation of the material and electrode advancements discussed in this review will heavily rely on effective system-level optimizations. These developments promise to revolutionize electric vehicles and large-scale energy storage, bring us closer to fast, efficient, and sustainable energy storage solutions.

4. Cathode Engineering for Fast-Charging LSBs

The cathode is one of the key components in LSB, and significantly impacts battery performance, especially during fast charging. Comprising about 25 wt% of a pouch cell, it is the second heaviest component after the electrolyte[105] and requires careful design.

4.1. Cathode Overview

First of all, basic Li-ion storage and sulfur accommodation are of primary relevance in LSB cathodes.[106] Additionally, the way sulfur is embedded reduces the polysulfide shuttle effect, similar to

slow charging.[107] However, for fast-charging LSBs, high stresses act on the cathode weakening the mechanical integration of sulfur. The same applies to the immobilization of LiPS. Physical barriers, such as pores, and electrostatic attraction forces, e.g., polar functional groups, are the key aspects of previous research. The various storage possibilities are presented below. Particular emphasis is placed on hierarchical structures and nanoscale cages.

More importantly for fast-charging, due to the electrically insulating nature of sulfur, well-distributed conductive pathways are highly important for rapid S-conversion and activation of the entire mass loading.[108] At the same time, the cathode must have sufficient porosity to ensure fast Li diffusivity. The most relevant materials and strategies for fabricating an effective fast-charging cathode are discussed below.

Finally, more research has recently focused on converting sulfur to Li_2S, and catalyst-enhanced cathodes offering promising development potential for fast-charging LSBs.[109] Typically, catalytic materials possess good polarity and high conductivity. Besides metal compounds, SACs are also of increasing research interest. Beyond their inherent properties, the catalytic capabilities of these materials are often enhanced by introducing defects, such as controlling vacancies or doping them with other elements. Thus, catalyst additives contribute significantly to the battery performance for fast-charging LSBs.[110]

As already mentioned, the individual functions are not mutually exclusive. For example, a porous carbon structure serves both as a sulfur reservoir and an electrically conductive network. The functions and their interplay are largely determined by the choice of material for the cathode. In the following sections (4.2 and 4.3), we will classify the cathode materials. Section 4.2 covers carbon-based materials (from 1D to 3D), including dopants in carbon. Section 4.3 discusses non-carbon-based materials, further divided into polymers, metal compounds, SACs, and heterostructures. This classification will consider aspects such as electron transfer, ion diffusion, sulfur storage, and LiPS anchoring as well as conversion.

4.2. Carbon and Carbon Modifications

Carbon is an excellent cathode additive in LSBs, due to its large surface area, diversity of nanostructures, and high electrical conductivity. The carbon-based additives are mainly classified into 1D, 2D, and 3D carbon structures, followed by non-metal doping of carbons and carbonized polymers and biomass carbon.

4.2.1. 1D-Carbon Structure

As 1D material, CNTs are very common, as not only is their electrical conductivity between 10^6 and 10^7 S m^{-1}, but sulfur can also be stored in the tubes.[58,59] Thus, Fang et al.[111] produced a film using only single-wall CNTs. In order to improve the diffusion of Li-ions for fast-charging, the CNTs can be further processed. Chemical etching or physical heat treatment in an oxygen-containing atmosphere leads to defects in the tube walls in the form of holes and the formation of functional groups (see also 4.2.6 Non-metal doping of carbons), as was shown by Xiao et al.[112] with a treatment in a water vapor-containing environment at 850 °C. This treatment increased the capacity of LSB at 2C by around 55 %. The so-called porous CNTs can also be produced with CO_2 instead of oxygen. Their sp^3 hybridized defects have shorter Li-ion diffusion paths and a better overall distribution.[60] Not only single-wall CNTs, but also multi-wall CNTs can be porosified or partially unzipped, as reported by Jeong et al.[113] In this way, 590 mAh g^{-1} could be achieved after 200 cycles under 5C.

4.2.2. 2D-Carbon Structure

2D carbon materials such as graphene, graphene oxide (GO) and reduced graphene oxide (rGO) achieve an even higher electron conductivity of up to 10^8 S m^{-1} due to their additional dimensionality.[58,59] At the same time, their functional groups enable an increased electrostatic attraction with the polysulfides and thus trap LiPSs. The layers can either be placed around existing macroscopic structures to create a porous scaffold or formed directly through a hydrothermal reaction. Existing structures were utilized and covered with graphene by Zhou et al.[114] in 2014 using a Ni sponge. The formed graphene foam reached a capacity of 450 mAh g^{-1} with a relatively high loading of 3.3 mg cm^{-2} at 3.6C (6 A g^{-1}). Free-standing structures can be produced by hydrothermal reaction, in which the pore shape and size can be adjusted by the amount of graphene and the ambient conditions (like temperature, volume, autoclave shape). For example, Zhou et al.[115] and Sun et al.[116] produced N/S- and N/V- doped graphene networks with this method, respectively. With the high electron conductivity of the graphene in combination with the diffusion-favoring open structure, the latter reached a capacity of 701 mAh g^{-1} in the rate capability test at 3C, which corresponds to 2.1 mAh cm^{-2}, while still achieving 917 mAh g^{-1} after 200 cycles under 1C. Similar to CNTs, 2D carbons can also be further modified in their structure and porosity. Wang et al.[117] created holes in the GO in an aqueous H_2O_2 solution at an elevated temperature (100 °C) and could enlarge them as needed, which significantly increased the Li-ion transport and enhanced fast-charging. Even with a loading of 15.2 mAh cm^{-2}, the GO cathode still exhibited 81.5 % (581 mAh g^{-1}) capacity retention after 1500 cycles (at 2C).

4.2.3. 3D-Carbon Structure

Although 3D carbons such as carbon black (CB) or Ketjen black (KB) have a large surface area that can store sulfur well, e.g. by the hydrothermal infiltration of S into the porous carbon,[35] their electrical conductivity is lower compared to CNTs and graphene.[58,59] Therefore, 1D and 2D carbons are often combined in cathodes of fast-charging LSBs in order to obtain a highly conductive 3D framework that allows fast electron transfer over longer distances, while simultaneously being open-pored to ensure good Li-ion diffusion. Tang et al.[63] combined CNTs and graphene in the cathode, aligning N-doped CNTs across the graphene sheets decreasing the ion diffusion paths (770 mAh g^{-1} at 5C) (**Figure 4**a,b). Zhu et al.[64] also combined ultra-long CNTs with hollow graphene nanospheres by a dispersion-filtration approach. Here, the spheres acted simultaneously as sulfur hosts and electron conductors. The very electrically conductive network

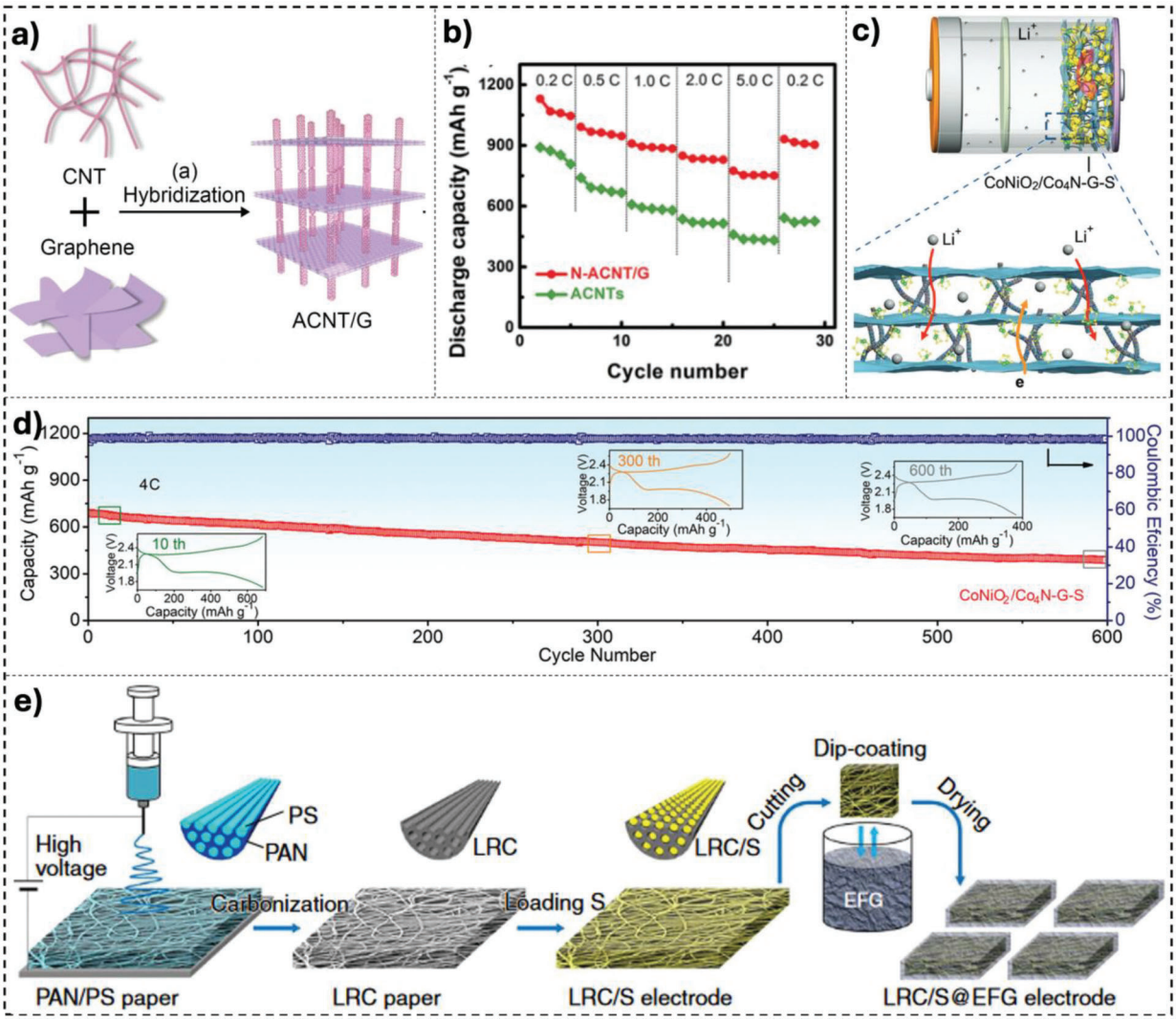

Figure 4. Highly electrically conductive 3D structures out of 1D (CNT) and 2D (graphene) components: a) schematic structure of graphene and CNTs, b) electrochemical rate capability test. Reproduced with permission.[63] Copyright 2014, John Wiley and Sons. c) Schematic representation of $CoNiO_2/Co_4N$ nanowires combined with graphene, d) cyclic stability at 4C. Reproduced with permission.[118] Copyright 2021, John Wiley and Sons. e) 3D framework synthesis out of carbonized polymer fibers made from electrospinning. Reproduced with permission.[122] Copyright 2015, Springer Nature.

created in this way was able to be charged with 10C for a short time without any further additives, reaching 535 mAh g^{-1}.

Uniquely, Jin et al.[38] combined CNTs with ultra-thin graphite sponges using CVD. This method created covalent C-C bonds between the CNTs and the graphite, thereby reducing scattering at the structural boundaries and improving the electron flow leading to 860 mAh g^{-1} at 12C. Pu et al.[118] used the combination of 2D graphene and 1D wires made of conductive $CoNiO_2/Co_4N$. In this way, excellent long-range conductivity could be achieved over several layers (Figure 4c,d), which was demonstrated in a 4C capacity of 618 mAh g^{-1}.

Gao et al.[119] first focused their research on the basic design of a 3D electrode. For this purpose, they used a finite element method (FEM) simulation to generate a binary descriptor value based on the Butler-Volmer equation, which takes into account both mass transport and charge transfer. The influence of the cathode on the Li deposition at the anode was also evaluated. It was shown that a high binary descriptor provides a homogeneous current density and thus leads to the most promising results. On this basis, a simple melamine formaldehyde sponge covered with CNTs was designed as a cathode, which has a capacity decay rate of 0.047 % after 800 cycles at 2C and delivers 738 mAh g^{-1} in the rate capability measurement.

4.2.4. Polymer Carbonization for Open-Pored Structures

The carbonization of open-pored structures enables the formation of conductive frameworks. A widely used method is the electrospinning of polymers (see Figure 4e) such as polyacrylonitrile (PAN),[120] poly(methyl methacrylate) (PMMA),[121] and polystyrene (PS).[122] The resulting carbon network fibers allow

rapid Li-ion transfer and can be further modified. Zhao et al.[28] used a mixture of poly(vinylpyrrolidone) (PVP) and PAN and added Fe-ZIF-8 nanocrystals (<100 nm) to the mixture before electrospinning, which resulted in an additional porosity within the carbon fibers. This cathode demonstrated remarkable performance, with a capacity retention of 78% when charged from 0.2C to 2C rates, and maintained a capacity of 791 mAh g^{-1} even when charged at the maximum rate of 5C.

Not only randomly produced carbon fiber structures can be used for sulfur cathodes. Aligned scaffolds, such as those used by Xu et al,[123] are also possible. They additionally coated 3D carbon cloth with CoS_2 nanoparticles. The interwoven carbon fibers and the CoS_2 film made it possible to achieve 823 mAh g^{-1} at 4C and still 610 mAh g^{-1} even after 1000 cycles at 4C with a load of 1.2 mg cm^{-2}.

4.2.5. Biomass Derived Carbon Structures

In general, besides technically engineered 3D structures produced in recent years, bio-derived scaffolds have also been frequently used. For example, Chen et al.[124] used the fibers of coconut shells as the basis, and after carbonization and further porosification with KOH for enhanced ion diffusion achieved a specific surface area of 2160 m^2 g^{-1} with micro- and mesopores, resulting in 700 mAh g^{-1} capacity at 5C. Zhou et al.[125] used tobacco stems as a porous carbon structure with Mn polar active sites and N-, O- and P-containing functional groups. The cathode reached 559 mAh g^{-1} even after 1500 cycles at 2C and thus had a very low capacity decay rate of 0.021 % per cycle. In addition, their cathode was characterized by particularly high volumetric and gravimetric energy densities (446 Wh L^{-1} and 422Wh kg^{-1}). Huang et al.[126] took a further step and grew their structures by a biological self-assembly method to Rhizopus hyphae balls, which grew up to 10 cm in diameter inside a Sabouraud dextrose broth nutrient solution. The 3D cross-linked organic network was first freeze-dried and then carbonized. The resulting hollow macrofibers were tightly interconnected and enabled a continuous electrically conductive network showing 663 mAh g^{-1} at 5C, which can be additionally modified by e.g., by metal ions (Cu, Ni, Fe, Co).

Given its simplicity, scalability, cost-effectiveness, environmental friendliness, and its virtually limitless structural potential, carbon-derived biochar continues to garner significant research interest.

4.2.6. Non-Metal Doping of Carbons

Besides the addition of metal compounds and polymers, the direct incorporation of non-metal elements such as O, N, S, and P in fast-charging sulfur cathodes is also widespread. They enhance the activity of each catalytic site by modifying the local electronic structures [84] and improving ionic diffusion and electronic conductivity by introducing defects that narrow band gaps and create additional energy levels. Moreover, defects in nonpolar materials can enhance surface polarization, thereby increasing the adsorption capability for LiPSs.[54] First examples are the porosification of CNTs and the production and use of GO, in which O-containing groups are integrated into the carbon (see section 4.1 Carbon and Carbon modifications). Apart from O, the second most important doping element is probably N, which is used especially for LiPS anchoring.[127] Among others, Zou et al.[128] and Deng et al.[129] each doped their honeycomb-like carbon structures, which they produced with templates from SiO_2 nanospheres. Zou additionally doped with N and O, achieving a capacity of 958 mAh g^{-1} under 3C,[128] and Deng added N as well as MoC to the structures, resulting in 0.049 % capacity decay rate per cycle at over 1000 cycles under 3C.[129] Not only because of the doping alone but also due to the 3D structure itself, both reached good battery performances. Similarly, Jin et al.[130] used N-doped carbon fibers, which were coated with V_2CT_x nanosheets (MXene) to further increase LiPS adsorption. Using this approach, an excellent cathode with 640 mAh g^{-1} at ultra-fast 15C and a capacity decay rate of 0.019 % per cycle after 1200 cycles (1C) with an initial capacity of 1165 mAh g^{-1} was obtained.

All doping elements have both the ability to retain LiPS and to change the conversion kinetics. However, not to the same extent, the O- and N-doping mainly improves LiPS adsorption, and S- and P-doping is used more as catalysts. Incorporation of doping elements into carbon (with the exception of O) is not as straightforward. Furthermore, doping in high concentrations can reduce electrical conductivity. Consequently, metal compounds and polymers are often preferred as sources in fast-charging LSB cathodes.[127] Nevertheless, P-doped carbons, for example, as used by Huang et al,[126] and S-doped carbons, such as described by Tong et al,[27] are also used, showing a capacity at 5C of 663 mAh g^{-1} and 689 mAh g^{-1}, respectively.

While carbon-based materials dominate, non-carbon materials like MOFs, COFs, and conductive polymers are also investigated for their potential in fast-charging LSB cathodes. The ideal cathode should possess a well-distributed conductive network for efficient electron transfer, sufficient porosity for rapid Li-ion diffusion, and strong LiPS anchoring to mitigate the shuttle effect. The ongoing research in this field focuses on developing innovative materials and strategies to overcome the challenges associated with fast-charging and enable the widespread adoption of LSBs for high-power applications. **Table 3** shows a comparison of carbon materials for fast-charging LSBs cathode composites, addressing challenges and leveraging advantages. **Table 4** summarizes the current fast-charging LSBs research in relation to carbon materials.

4.3. Non-Carbon Materials

Non-carbon-based frameworks, including polymers, metal compounds, metal-organic frameworks (MOFs), and covalent organic frameworks (COFs), are also widely explored in research. The key advantage of non-carbon materials over pure carbon is their superior ability to anchor LiPS. For example, MOFs and COFs allow particularly high Li-ion diffusion due to their open-pored and, at the same time, regular/ordered structure, while their electrical conductivity is lower. Polymers, on the other hand, can achieve high conductivity but with reduced Li-ion transport.[147]

Table 3. Characteristics of carbon-based cathode materials for fast-charging LSBs.

Material (source section(s))	Challenges (hindering fast-charging)	Impact (enabling fast-charging)
Carbon nanotubes (CNTs) (4.2.1, 4.2.3)	• Slow Li-ion diffusion along the tube length can limit charge/discharge rates without modifications like porosification.	• Provides high electrical conductivity for rapid electron transfer • Internal structure allows sulfur storage • Porosification/alignment can create defects/shorter paths improving Li-ion diffusion kinetics for high rates.
Graphene, graphene oxide (GO), reduced GO (rGO) (4.2.2)	• Layer restacking during processing or cycling can block pores, hindering rapid Li-ion diffusion needed for fast charging.	• Offers exceptionally high electron conductivity • Functional groups (GO/rGO) aid LiPS trapping, reducing shuttle effect during fast cycles • Can form porous scaffolds enhancing electrolyte access and ion transport pathways.
Carbon black (CB), Ketjen black (KB) (4.2.3)	• Lower intrinsic electrical conductivity compared to CNTs/graphene requires combination with more conductive materials for efficient long-range electron transport at high rates.	• Provides large surface area for sulfur storage • Often combined with 1D/2D carbons to create a 3D framework boosting overall conductivity for faster electron transport over distance within the cathode.
Carbon Derived From Polymer (4.2.4)	• Precise control over the final pore structure and size during synthesis can be difficult, potentially impacting optimal ion transport pathways for fast charging.	• Carbonization creates inherently conductive frameworks • Electrospinning allows tailored fiber networks (random or aligned) facilitating rapid Li-ion transfer • Can be doped/modified for porosity.
Carbon Derived From Biomass (4.2.5)	• Inherent structural variability of natural precursors can affect performance consistency • Optimization (e.g., activation) often needed for ideal fast-charging pore structure.	• Offers a sustainable and potentially cost-effective route to porous carbon structures (micro/mesopores) enabling good ion diffusion • Natural hierarchical structures can provide conductive networks.
Non-Metal Doped Carbons (O, N, S, P) (4.2.1, 4.2.2, 4.2.6)	• Balancing doping benefits (enhanced kinetics/adsorption) against potential reduction in electrical conductivity at high doping levels • Difficulty incorporating certain elements (S, P) and controlling uniformity/stability can hinder performance optimization.	• Introduces defects enhancing Li-ion diffusion and modifying electronic structure for better conductivity/kinetics • Increases surface polarity improving LiPS adsorption (esp. O, N) and potentially catalysis (esp. S, P).

4.3.1. Polymers

Several conductive polymers have been used so far in fast-charging LSBs. Polyacrylonitrile (PAN) and polyaniline (PANI) are widely used and serve as an electrically conductive network as well as holding sulfur and LiPS (PAN:[117,148–150], PANI: [26,99,151–154]). Most polymers are primarily used due to their functional groups for S-holding and reduction of the LiPS shuttle effect and are characterized by excellent interaction with LiPSs, so that the LiPSs are kept locally within the cathode structure.[155] These polymers often appear in the form of coatings, which simultaneously form a physical barrier that traps the LiPS molecules. For instance, Li et al.[152] coated PANI around S-C particles and thus created a core-shell structure, Wang et al.[156] covered nanosulfur with poly(3,4-ethylenedioxythiophene) (PEDOT), whose O and S atoms strongly interacted with LiPS and Li et al.[148] ball-milled and heated Te-doped S particles with PAN, resulting in 890 mAh g^{-1} under 6C with a loading of 2 mg cm^{-2}. The reason for the good LiPS anchoring is the N-containing amine/imine groups of PANI and nitrile groups of PAN. Razzaq et al.[149] electrospun PAN and CNT into nanofibers and vulcanized the composite in an S-containing atmosphere forming SPAN/CNT. The resulting porous and interwoven cathode material (**Figure 5**a,b) was highly flexible and showed outstanding battery performance in both the rate capability test (1000 mAh g^{-1} at 5C) and long-term stability (1106 mAh g^{-1} after 500 cycles at 1C with a capacity decay rate of 0.047 % per cycle) due to the interplay of SPAN and CNTs.

Also, the polar groups such as C═O and —NH_2 of PVP or PEI (polyethyleneimine) immobilize LiPS.[157] Polypyrrole (PPY) was used by Jiang et al.[147] to coat the MOF crystals and in this way not only physically prevents LiPS from shuttling but also holds it locally due to the N-containing functional groups. Due to the synergy of MOFs and PPY, the cathode was able to achieve 440 mAh g^{-1} in the end, even with a super-fast-charging rate of 10C over 1000 cycles according to a capacity decay of 0.03 % per cycle (Figure 5c,d). Kang et al.[158] chemically combined sulfur with the linker molecule tetra(allyloxy)-1,4-benzoquinone (TABQ) and achieved a capacity of 833 mAh g^{-1} even at 10C (Figure 5e-g). This high capacity is achieved not only by a good electron and Li-ion conducting network but also by the strong interactions of the polar keto groups.

Conjugated micro- and mesoporous polymers (CMPs) are an upcoming group of polymers characterized by their high porosity, variety of polar functional groups and electrical conductivity. Liu et al.[159] polymerized CMPs from squaric acid and 1,3,5-tris(4-aminophenyl)benzene around CNTs and obtained a cathode that delivered 631 mAh g^{-1} under 5C and retained 76.1 % of the initial capacity even after 500 cycles at 1C.

4.3.2. Metal compounds

As an additional LiPS anchor, metals and their compounds can also be used in sulfur cathodes, and most of them also possess

Table 4. Comparison of the electrochemical performance of fast-charging LSB regarding the cathode structure.

Structure	Material	Loading [mg cm^{-2}]	Ratio 2C/0.2C	Rate capability [mAh g^{-1}] /C-rate	Long-term cycling [mAh g^{-1}]/cycles/C-rate	Refs.
1D carbon	CNT alignment	N/A	80.6%	607/3C	486/400/5C	[131]
	CO_2 modified CNT	1.4	79.4%	460/5C	431/300/0.2C	[60]
	mesoporous CNT	N/A	71.9%	452/5C	560/100/0.1C	[132]
	MWCNT	2.07	69.8%[a)]	810/5C	1190/200/0.1C	[133]
	SWCNT network	2.4	68.5%[a)]	890/1C	1510/300/0.15C	[111]
	porous CNT	N/A	67.2%[a)]	100/15C	810/250/0.5C	[112]
	partially unzipped MWCNT	2	62.1%	520/5C	590/200/5C	[113]
2D carbon	rGO	3	64.8%	701/3C	917/200/1C	[116]
	graphene foam	3.3	64.7%[a)]	450/3.6C	448/1000/1C	[114]
	holey graphene	2	63.8%	494/5C	581/1500/2C	[117]
	graphene wrapped around MOFs	N/A	51.7%[a)]	500/3C	396/300/2.4C	[134]
	graphene sponge	4.6	37.2%	430/2C	670/200/0.5C	[115]
3D carbon or composites	CNT + graphite foam	2.6	87.0%[a)]	860/12C	761/400/2C	[38]
	porous carbon	0.5	83.0%[a)]	601/5C	642/200/2C	[135]
	carbon fibers + CNT	2.5	81.5%	839/4C	770/500/2C	[136]
	CNT + graphene	1	80.2%	770/5C	880/80/1C	[63]
	S-C composite	N/A	79.3%	200/100C	925/300/1C	[35]
	carbon sponge	1.5	77.7%	682/5C	627/500/2C	[137]
	CNT + hollow graphene	1.1	71.6%	535/10C	738/500/0.5C	[64]
	CNF + rGO	1.6	70.9%	821/2C	781/300/0.5C	[138]
	CNT/melamine formaldehyde sponge	1.5	70.9%	738/3C	500/800/2C	[119]
	carbon spheres	2.1	69.9%	615/10C	552/900/1C	[139]
	porous carbon spheres	1.2	68.8%	872/4C	908/500/1C	[140]
	CNT + graphene	1.5	68.2%	611/6C	659/1500/1C	[141]
	hollow MWCNT	0.9	68.1%[a)]	683/5C	855/200/1C	[142]
	S-CNT + graphene + Ni foam	1.6	67.9%[a)]	781/1C	660/250/2C	[143]
	Co_4N nanowires + graphene	1	63.9%	618/4C	389/600/4C	[118]
	3D porous graphene	1	44.8%[a)]	565/5C	310/1000/5C	[144]
Carbonization	coconut shell fibers	0.78	93.8%[a)]	700/5C	517/400/2C	[124]
	PVP/PAN nanofibers	1.7	78.9%	791/5C	654/500/2C	[28]
	carbon cloth	1.2	73.2%	823/4C	610/1000/4C	[123]
	PMMA/PAN nanofibers	2.2	71.2%	820/5C	990/300/0.2C	[121]
	tobacco stem	1.6	68.9%	719/2C	559/1500/2C	[125]
	PAN/PS nanofibers	3.6	25.8%[a)]	310/2C	803/100/0.1C	[122]
Non-metal	N + O	2	82.9%	958/3C	481/500/1C	[128]
doping of	N	4.5	77.9%	783/3C	738/600/1C	[145]
carbons	N + P	2	69.4%	663/5C	710/500/1C	[126]
	N + MoC	1.2	68.4%	646/3C	320/1000/3C	[129]
	N	1.2	66.3%[a)]	640/15C	927/1200/1C	[130]
	N + S	2	57.0%	689/5C	356/1000/5C	[27]
	N + O	2	54.6%[a)]	390/1.8C	671/200/0.12C	[146]

[a)] Deviation from common calculation, e.g., 2C/0.1C, due to missing data.

improved catalytic conversion. Metal catalysts are often oxides, chalcogenides and nitrides. Metal oxide compounds offer tunable electronic structures and stability within the operating potential window of LSB, reducing the activation potential of Li_2S, and leading to lower polarization and improved rate performance.[160] Iron oxides are used by Qiao et al.[77] in the form of Fe_3O_4 and Fe_2O_3. Moreover, Fe_3C was additionally used in their cathode. All showed strong interactions with LiPS (chemisorption) and catalytic ability. As a result, the cathode retained 76.1 % of its capacity when the charging rate was increased by a factor of ten (0.2C to 2C). The fastest measured charging rate of 5C resulted in 656 mAh g^{-1}, and even after 1000 cycles under 3C the cathode delivered 513 mAh g^{-1}. Other oxides used for LSBs include combination with titanium,[61,161,162] cobalt,[163,164]

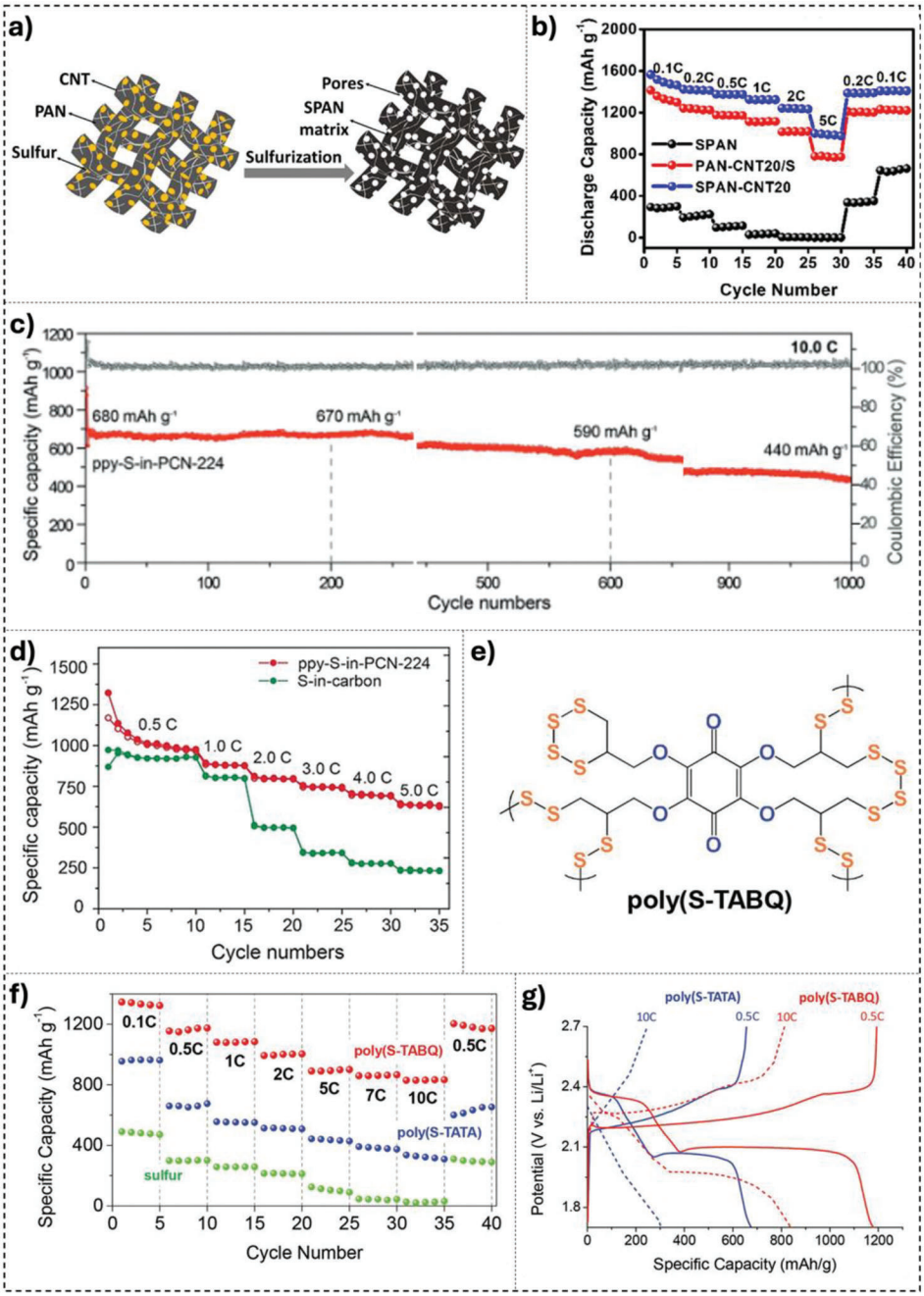

Figure 5. Polymers as LiPS immobilizer in combination with CNTs: a) Schematic illustration and b) rate capability of SPAN, PAN-CNT20/S, and SPAN-CNT20, respectively. Reproduced with permission.[149] Copyright 2019, Elsevier. c) Cycling stability of cathode composite out of PPY polymer and PCN-224 MOF at 10C over 1000 cycles and d) rate performance of ppy-S-in-PCN-224 and S-in-carbon from 0.5C to 5C. Reproduced and modified with permission.[147] Copyright 2018, John Wiley and Sons. e) Molecular structures of poly(S-TABQ) polymer, f) rate performance of Li cells based on poly(S-TABQ), poly(S-TATA) and elemental sulfur and g) galvanostatic (dis)charge voltage profiles of Li cells based on poly(S-TABQ) and poly(S-TATA), measured at 0.5C and 10C. Reproduced with permission.[158] Copyright 2018, John Wiley and Sons.

RuO_2 [81,165] and Nb_2O_5.[166] Zhou et al.[167] in turn, deposited ZrO_2 precisely at the ends of CNTs, making them permselective gateways for Li-ions resulting in 658 mAh g^{-1} at a very high rate of 20C. However, non-transition metal oxides are also used as efficient additives for LiPSs conversion and immobilization, such as In_2O_3.[85]

Metallic and multimetallic layered double hydroxides (LDH) are characterized by their electrocatalytic effect in addition to the storage capacity of sulfur and the suppression of the shuttle effect. Zhang et al.[168] used Ni-Fe-LDH as a coating for MOFs and achieved over 633 mAh g^{-1} at 2C even with an elevated S loading of 3 mg cm^{-2}. Furthermore, the capacity decay rate of

this cathode was 0.04 % per cycle in the long-term test. Also Mg-Al-LDH[169] and Ni-Co-LDH [170] variants also show the possibility of fast-charging. A special case is rare-earth metals. Liu et al.[171] grew layered yttrium hydroxide (LYH) in-situ on MWCNTs, which inhibits the aggregation of the 2D particles. The LYH exhibits a strong binding energy of 5.45 eV to Li_2S_4 and thus high LiPS immobilization and at the same time it shows a high catalytic effect. The combination of LYH and conductive CNTs thus enables a capacity of 730 mAh g^{-1} under 2C.

In recent years, metal chalcogenides, including metal sulfides, selenides, and tellurides, e.g. CoS_2,[123] TiS_2,[172] MoS_2,[83] FeS_2 [173] and NiS_2 [174] as well as $CoSe_2$,[175] $NbSe_2$ [176] and Bi_2Se_3,[177] have attracted much interest due to their unique catalytic properties. Compared to metal oxide catalysts, metal chalcogenides generally possess higher electrical conductivity, which facilitates faster electron transfer during the redox reactions of LSB. Moreover, metal chalcogenides are particularly sulfiphilic and by this they show strong polysulfide adsorption properties. Yuan et al.[82] were one of the first to demonstrate that sulfiphilic cobalt disulfide (CoS_2) serves as an effective catalyst for enhancing polysulfide redox reactions. Luo et al.[174] used NiS_2, and demonstrated that NiS_2 outperformed other sulfides (e.g., FeS_2,[173] Co/NiS_2 [178]), as it not only exhibits high LiPS anchoring and conversion ability, but can also be formed into smaller nanoparticles, generating a larger surface area. The particles can be distributed more homogeneously within the cathode, e.g., between the rGO layers, which effectively prevents their agglomeration. With a high sulfur loading of 5 mg cm^{-2}, 304 mAh g^{-1} was achieved at a charging rate of 4C. However, metal sulfides can also be further optimized. For example, Zheng et al.[179] tuned the d-orbital electronic structure of CoS_2 with the addition of Co atoms, which donated thier electrons and thus induced a negatively charged CoS_2 with an upshifted d-band center. Both the electron conductivity and the LiPS adsorption increases, resulting in 803 mAh g^{-1} at 3C.

Nitrides and N-containing metals have high catalytic activity in addition to a high LiPS binding capacity. Prominent representatives are TiN in the works of Zhou et al,[180] Hou et al.[181] or, as already mentioned in the Ma et al.[162] study. Wang et al.[29] combined highly catalytic Mo_3N_2 with Mo_2C, which as a metal carbide, can immobilize LiPS effectively even under fast-charging rates (512 mAh g^{-1}, 5C). MoN and MoS_2 were employed as layers around CNTs by Wang et al.[83] to combine LiPS conversion (MoN) and LiPS anchoring (MoS_2) while facilitating Li ion diffusion through its 2D structure (**Figure 6**). Even within a short charging time of 10 min (6C), 674 mAh g^{-1} was achieved in the rate capability test and after 1000 cycles at 1C, the capacity decay rate was as low as 0.039 % per cycle. At a higher charging rate of 2C, the cathode was also stable over 1000 cycles and reached 459 mAh g^{-1} (decay of 0.041 % per cycle).

Less often, metal phosphides are employed in past research; however, Liu et al.[182] recently introduced a bi-functional catalyst out of NiCoP and CoP, both selectively accelerating long-chain and short-chain polysulfide conversions by interacting strongly with the LiPSs (Li-P and Co/Ni-S). Similar interactions exist e.g., for FeP [183] and Ni_2P.[184] The latter was used by Cheng et al,[184] who created Ni_2P core-shell nanospheres by Ni-glycerol phosphorization a. The storage structure and material choice still enabled a capacity of 439 mAh g^{-1} at 10C.

4.3.3. Single-atom catalysts (SACs)

SACs maximize the surface area of active sites, enhance their utilization, and increase the catalytic activity due to their unique electron structure. An example is the single-atom copper (SA-Cu) catalyst, which endows Li_2S with an insulator-to-metal transition, improving electronic transport and catalytic efficiency. This catalyst enables the formation of 3D spherical Li_2S clusters, which improve the deposition capacity and catalytic efficiency.[90,185,186] With this concept, Zhang et al.[62] introduced Zn SACs positioned on highly ordered N-doped carbon (NC) nanotube arrays, serving as the sulfur host for rapid redox reactions (**Figure 7a,b**). With a uniform distribution of high-loading Zn SACs prepared by the pyrolysis method and a close atomic spacing under 1 nm, the cathode exhibited fast kinetic responses at 5C with more than 513 mAh g^{-1}. Xiao et al.[187] combined SACs with a 3D carbon nanofiber (CNF) matrix and introduced a novel N coordination method to develop free-standing single-atom Cu-decorated N-doped carbon fiber foam (SA-Cu@NCNF) as sulfur hosts. This technique led to the formation of 3D spherical clusters of electrodeposited Li_2S, a shift from the typical 2D lateral structures. This transformation is due to continuous 3D nucleation and growth. Additionally, the dissociation kinetics are improved through rapid charge transfer in Li_2S nanoparticles and the weakening of Li-S bonds. The batteries exhibit remarkable areal capacity, maintaining 1.6 mAh cm^{-2} at 5C over 500 cycles, with a low decay rate of 0.038 % per cycle. Tests with high sulfur loading (10 mg cm^{-2}), at low temperatures (−20 °C), and in Li-S pouch cells confirm the practicality of the SA-Cu@NCNF/S cathode.

The presence of double-active sites goes beyond merely doubling a single atom; they exhibit distinct catalytic properties. Additionally, there might be a synergistic effect that surpasses the theoretical limitations of SACs. Dong et al.[91] proposed a dual-solution method for implanting dual metallic single-atom pairs (Fe and Co) into carbon nanospheres (Figure 7c-e). The hollow C spheres provided a structure to mitigate volume expansion while improving the utilization of the Fe-Co single atoms. Fe atoms facilitated the nucleation of Li_2S, whereas Co atoms aided in its decomposition, thereby enhancing the redox kinetics of Li-S batteries. The batteries equipped with the S@Fe-CoNC cathode demonstrated stable performance, delivering a capacity of 618 mAh g^{-1} at 10C. Moreover, they showed durability over 2800 cycles with a minimal decay rate of 0.01 % per cycle at 2C. Recently, Dong et al.[188] designed a P, S co-coordinated single-atom Co catalyst (CoSA-N_3PS) with asymmetric coordination to regulate d–p orbital hybridization and accelerate polysulfide conversion. This structure enabled outstanding high-rate performance, delivering 619 mAh g^{-1} at 10C and an ultralow capacity fading rate of 0.027 % per cycle over 2000 cycles. Wang et al.[189] developed a Fe–Co single-atom-cluster catalyst (FeCo-SACC) supported on 3DOM carbon to synergistically enhance LiPS adsorption and sulfur redox kinetics. The catalyst exhibited stable cycling over 1000 cycles with only 0.038 % capacity fading per cycle

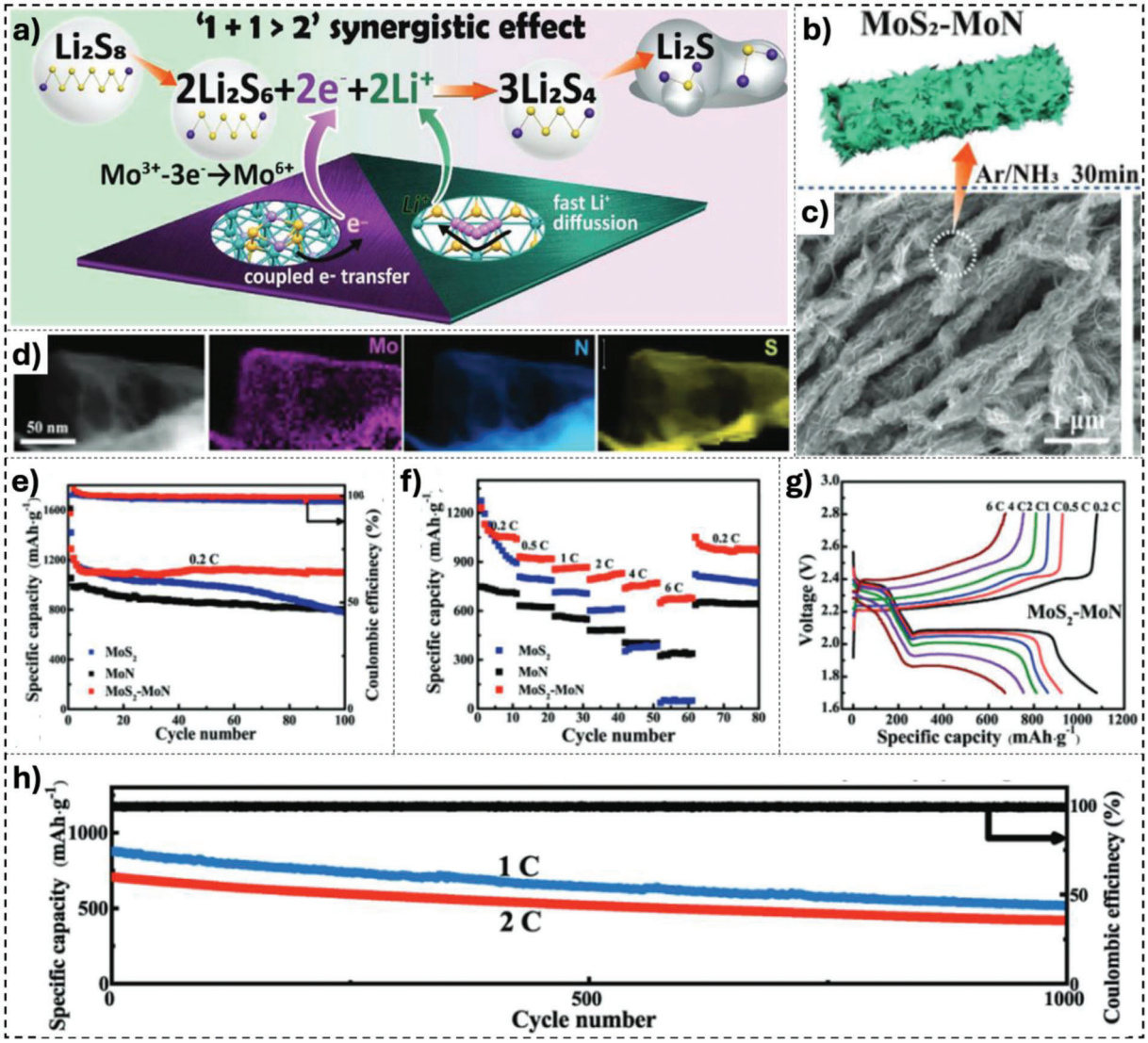

Figure 6. Combination of MnO and MoS_2 with different functions: a) Schematic illustration of synergistic catalytic conversion of LiPSs. b) Schematic illustration and c) SEM image of MoS_2–MoN nanosheets grown on NCNT vertically, d) STEM images and corresponding EELS mapping images. e) Cyclic performances at 0.2C for 100 cycles, f) rate performance at various current densities, g) galvanostatic (dis)charge curve. h) Long-term cycling performance at 1C and 2C of MoS_2–MoN/S. Reproduced with permission.[83] Copyright 2021, John Wiley and Sons.

and excellent rate capability up to 5C, even under high loading (15 mg cm^{-2}) and lean electrolyte (4.6 μL mg^{-1}) conditions.

4.3.4. Heterostructures

Heterostructures, such as core/shell structures, offer several significant advantages that enhance the overall performance of the LSB. This structure typically involves a combination of a core material with specific properties and a shell material that provides complementary benefits. In the following sections, we will discuss several heterostructures and show the results of the electrochemical performance in fast-charging LSBs.

Carbon materials with metal compounds: The combination of carbon materials, e.g. CNT, graphene, rGO, with metal compounds shows good high-rate performance in LSBs. A good example of the combination of different components can be found in the work of Wang et al.[97] Initially, PMMA spheres were used as a template for a mixture of niobium salt and CNTs. The calcination process removed the template, leaving an ordered micro-, meso- and macroporous structure that could effectively store sulfur and formed O-deficient niobium oxide (Nb_2O_{5-x}), which adsorbed LiPS (**Figure** 8a–c). The hierarchical sulfur cathode led to a high capacity of about 1475 mAh g^{-1} and 741 mAh g^{-1} under 0.2C and 5C, respectively, indicating good preservation of the active material even under high-stress conditions. Wang et al.[190] modulated the electronic states of Ti oxides and introduced defect-rich thin TiO_{2-x}-S nanosheets and CNTs. By placing reactive particles on electron-rich substances to create heterojunctions, catalyst activity is significantly improved

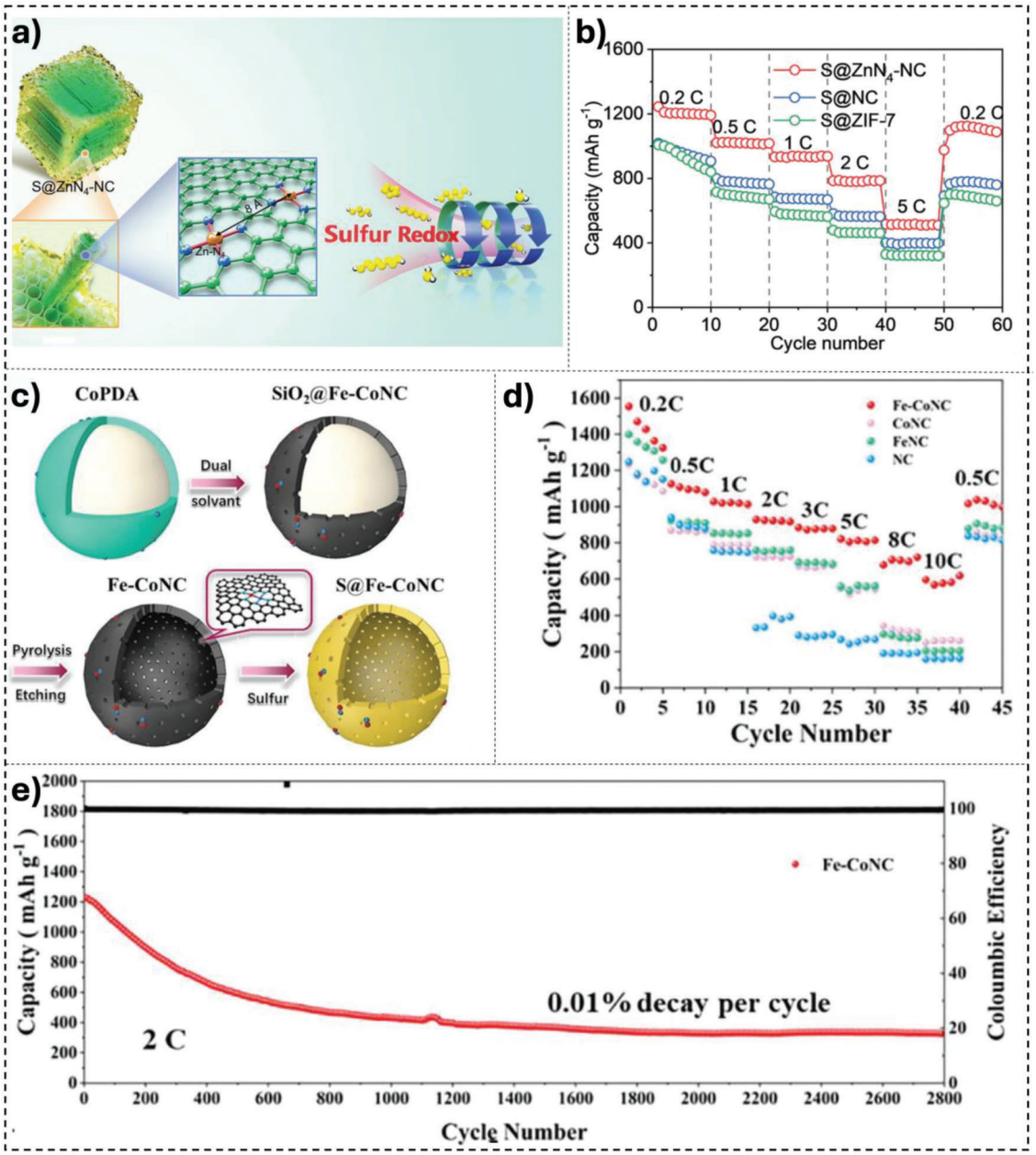

Figure 7. a) Schematic illustration of the ZnN_4-NC sample and b) Rate capabilities of S@ZnN_4-NC, S@NC, and S@ZIF-7 cathodes. Reproduced with permission.[62] Copyright 2022, John Wiley and Sons. c) S@Fe-Co N-doped carbon spheres (NC), d) the corresponding C-rate performance and e) long cyclic performance of S@Fe-CoNC electrode at 2C. Reproduced with permission.[91] Copyright 2023, John Wiley and Sons.

due to efficient electron flow at the heterojunction interface. The resulting CNT@TiO_{2-x}-S electrode demonstrated good cyclability up to 500 cycles at 1C (717 mAh g^{-1}) and rate capability up to 5C (399 mAh g^{-1}).

Higher-level structures with pores of various sizes were also shown by Li et al.,[191] who generated CO_2 bubbles in a melamine formaldehyde prepolymer solution and thus created micrometer-sized pores. The electrode achieved over 532 mAh g^{-1} at a high charging rate of 9C by subsequent carbonization and N-doping of the carbon.

MXene composites: Highly conductive MXenes with additional functional groups in their structure are another non-carbon material alternative to 2D carbons.[98,130,192] For example, Wang et al.[193] coated CNT spheres with $Ti_3C_2T_x$ MXene sheets and achieved a specific capacity of 557 mAh g^{-1} at 8C, significantly surpassing the samples without MXene sheets (around 200 mAh g^{-1}). The high conductivity and the functional groups of MXenes enhanced the long-term performance of the cathode, maintaining approximately 420 mAh g^{-1} after 700 cycles at a fast-charging rate of 6C.

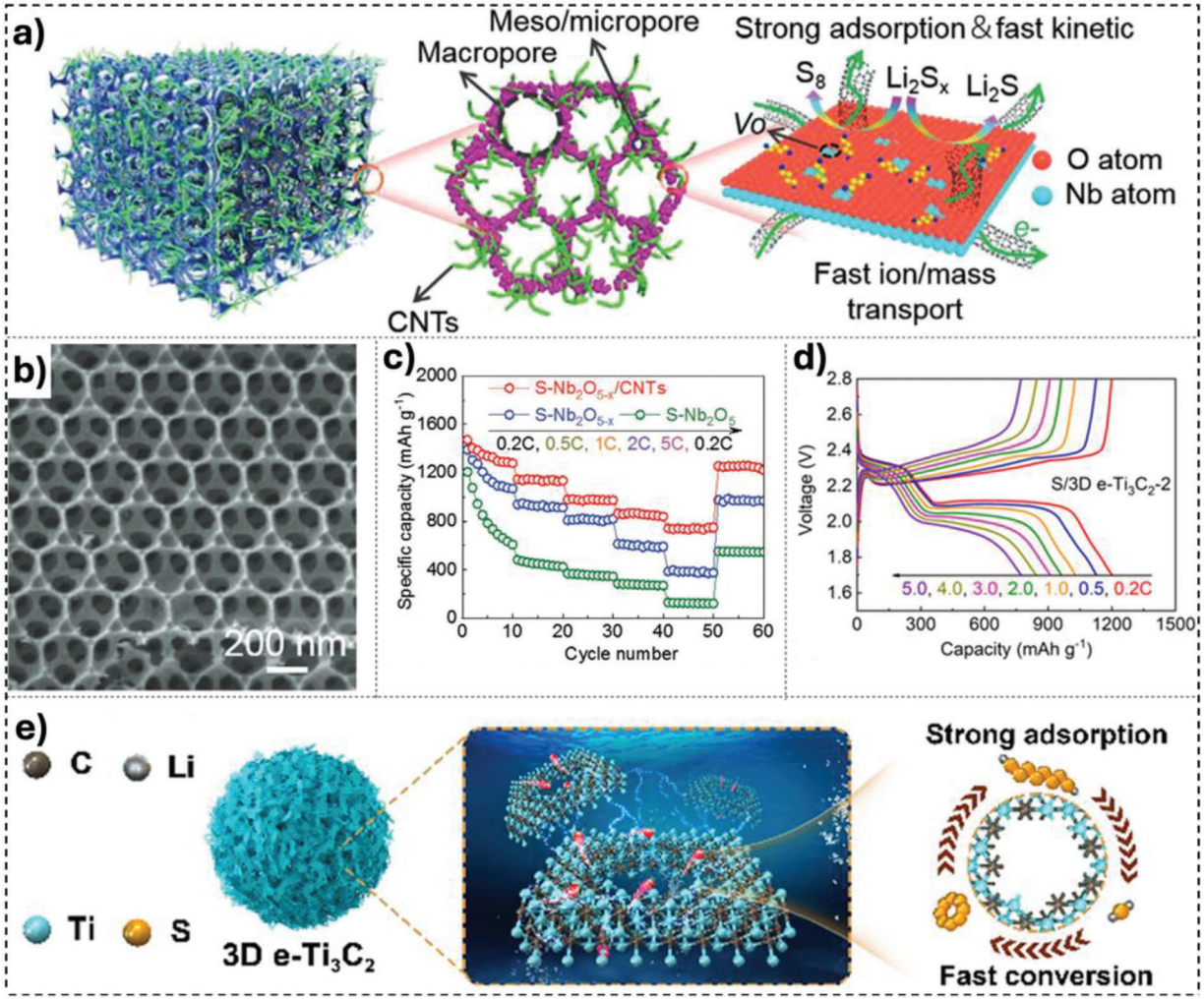

Figure 8. a) Schematic illustration of Nb_2O_{5-x}/CNTs, b) SEM image of porous and hierarchical 3D structure, c) rate performance. Reproduced with permission.[97] Copyright 2020, John Wiley and Sons. d) (Dis)Charge profiles of S/3D e-Ti_3C_2-2 cathode at different current rates and e) 3D e-Ti_3C_2 with active edges exhibits better polysulfide confinement capability and electrochemical performance. Reproduced with permission.[98] Copyright 2021, American Chemical Society.

Wang et al.[98] reported that MXene microspheres functioned as a versatile hierarchical sulfur storage and conversion system. The plentiful edges of the nanosheet-like Ti_3C_2 provide numerous catalytic sites and control the d-band center of Ti atoms due to the strong adsorption of LiPSs to inhibit the shuttle effect (Figure 8d,e). The S/3D e- Ti_3C_2 cathode achieves rate performance with capacities of 1202 and 772 mAh g^{-1} at 0.2 and 5C, with a high capacity ratio of 2C/0.2C of 80.1 %. Guan et al.[194] synthesized a multi-hierarchical cathode by first coating PMMA/$Co(acac)_2$ fiber network with $Ti_3C_2T_x$ MXenes. In a subsequent CVD step, CNTs were grown in-situ inside the hollow MXene tubes. With a loading of 1.2 mg cm^{-2}, the cathode achieved a specific capacity of 970 mAh g^{-1} at 2 C, retaining 81.6 % of the capacity measured at 0.2 C. Moreover, a high rate performance of 803 mAh g^{-1} at 7C was shown, which is attributed to the hierarchical structure and the MXene/CNT combination with Co doping.

MOF/COF and their nanosized cages: MOFs are highly porous materials consisting of transition metal atoms or clusters that are connected each other by organic linkers. Their versatile combination enables the creation of tailored 3D, 2D and 1D structures (**Figure 9**a–c). The fabricated MOFs serve dual functions: a) acting as catalyst materials by enhancing the redox kinetics of sulfur species and trapping LiPSs, and b) facilitating rapid ion diffusion and sulfur storage due to their high surface area and tunable pore structures. Various examples can be found in Zhu et al. (3D structure formed by ZIF-8)[195] or Jiang et al. (3D from PCN-224),[147] Wang et al. (2D from ZIF-7)[196] and Yang et al. (1D structure consisting of alternating Ni ions and 1,2,4,5-benzenetetramine tetrahydrochloride molecules).[197]

In addition to their structural characteristics with respect to ion diffusion, MOFs have strong catalytic properties. For instance, ZIF-67 (a 3D cobalt-based MOF) has shown improved

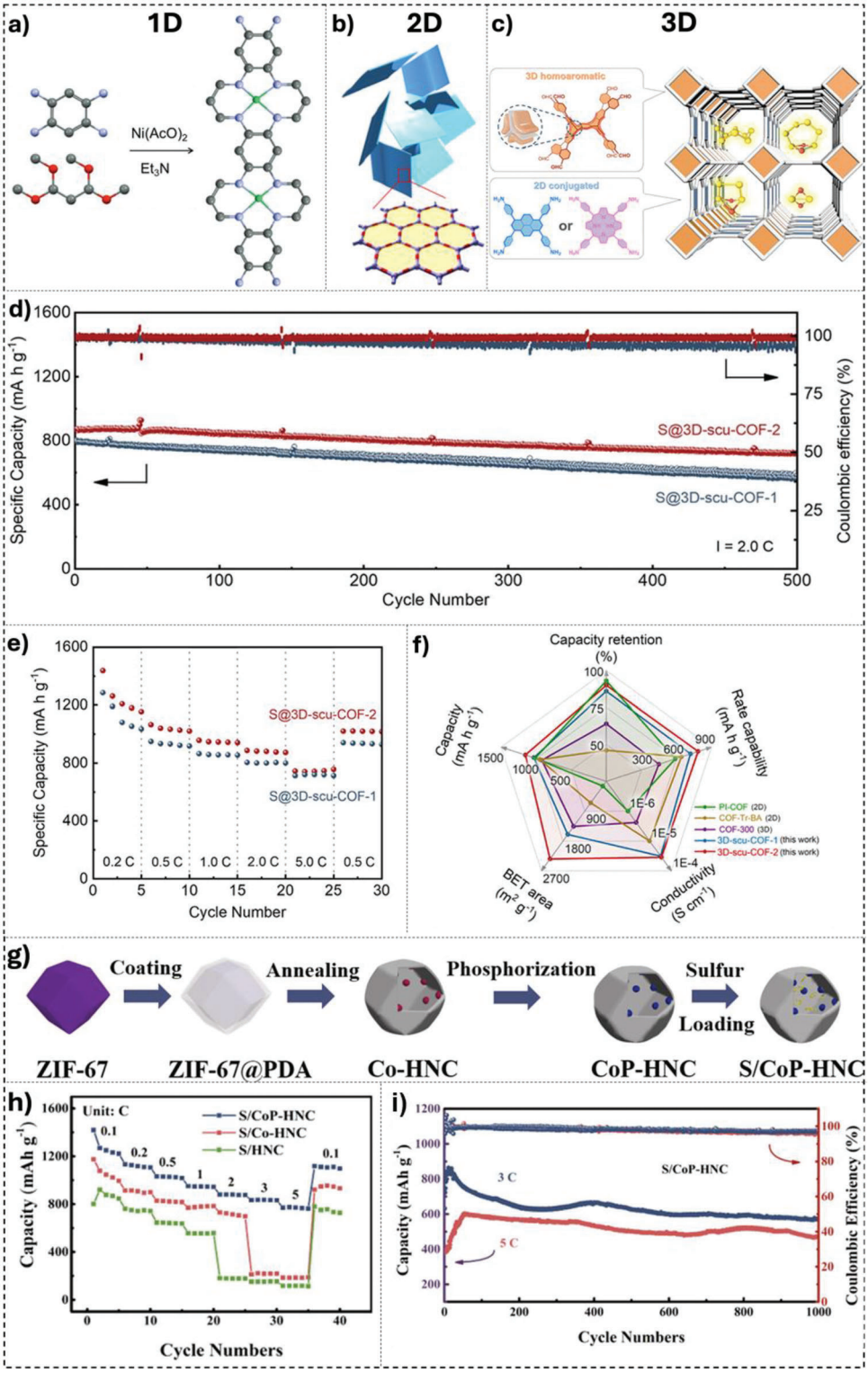

Figure 9. Structures of MOFs and COFs with different dimensions. a) 1D π–d conjugated Ni-MOF. Reproduced with permission.[197] Copyright 2022, John Wiley and Sons. b) 2D PI-COF Reproduced with permission.[201] Copyright 2021, American Chemical Society, c) Two different 3D scu-COFs which differ in their linking structure and their d) cycling stability at 2 Cover 500 cycles, e) rate capability, and f) comparison of the performance to other COF-based cathodes in LSBs. Reproduced with permission.[200] Copyright 2022, American Chemical Society. g) Schematic fabrication procedure making nanosized cages using MOFs as particle templates, h) rate performance, and i) cycling performance at 3C and 5C. Reproduced with permission.[65] Copyright 2021, Elsevier.

electrochemical performance of LSBs by providing a conducive environment for polysulfide conversion and reducing the shuttle effect. Additionally, as sulfur hosts, MOFs can achieve high sulfur loading and thus show improved cycling stability.[177]

COFs have a similar structure to MOFs, but instead of metal sites, they have light, non-metallic elements such as boron, carbon, nitrogen, silicon or oxygen and have strong covalent bonds to their organic neighbors.[198] It should be mentioned that only comparatively few COF structures are known (well over 600 compared to >100 000 MOF structures).[199] Two different highly crosslinked, porous 3D COFs were prepared by Liu et al.[200] using a traditional solvothermal reaction and differ in their linker molecules. Moreover, by choosing the building block molecule with delocalized π-electrons (DMOPTP), the entire COF scaffold became electrically conductive (up to $7.6 \bullet 10^{-5}$ S m^{-1}). This scaffold was used in the cathode composite, and demonstrating by the good battery performance of 757 mAh g^{-1} at 5C and 722 mAh g^{-1} after 500 cycles under 2C (Figure 9d-f). Duan et al.[201] used the inexpensive organic monomers pyromellitic dianhydride (PMDA) and melamine (MA) to initially produce three-dimensional polyimide COFs with a defined lamellar structure. In the second step, the individual layers could be separated from each other similarly to graphene, resulting in 2D nanosheets. The cathode fabricated with the 2D COFs delivered 620 mAh g^{-1} at 4C. Combinations of MOFs and COFs are also possible in cathode fabrication. For instance, Du et al.[202] utilized both ZIF-67 (MOF) and TpBD-Me2 (COF), although the latter only as an add-on layer on the dodecahedral ZIF-67, which reduced the LiPS shuttle effect. In combination with N-doping and Co-nanodots, this cathode reached a specific capacity of 636 mAh g^{-1} at 1C even after 500 cycles and maintained 80 % of the initial capacity, demonstrating the structural benefit of the MOFs/COFs in terms of Li-ion diffusion and LiPS anchoring.

In addition, the structural advantages of MOFs provide the opportunity to use them as templates for nanosized cages, which have shown to be very effective in terms of sulfur storage. Due to their high pore content, they can absorb a significant amount of sulfur, while the pores physically hold S and LiPS on the other due to their geometry. Zhang et al.[65] fabricated a cathode with N-doped carbon cages shaped from the dodecahedral MOF ZIF-67 and obtained 770 mAh g^{-1} at 5C (Figure 9g–i), holding the active mass even at this high charging rate inside the cages. Besides the widely used ZIF-67,[65,177,202–204] also other MOFs, such as ZIF-8,[205–208] MIL-88A[168] and MIL-125[162] were also employed. After removing the MOF template, all showed similar nanocages for S storage and preserved their active mass within the cathode even at increasing charge rates (capacity retention between 0.2C and 2C of more than 60 %). Lv et al.[209] synthesized a bifunctional Ni-coordinated covalent organic framework (NiS_4-TAPT COF) that simultaneously hosts sulfur and lithium, suppressing polysulfide shuttle and lithium dendrite growth. The full cell with NiS_4-TAPT achieved a high specific capacity of 966 mAh g^{-1} at 1C and maintained stable cycling with 0.055 % capacity fading per cycle, demonstrating strong potential for fast, stable Li–S systems.

Further Core–Shell Structures: Similar to nanosized cages derived from the shape of MOFs, further templates for core-shell materials are made from spheres, wires, and other particles, which are first coated and then removed. Spheres made of PS, for example, were used by Li et al,[210] which they coated these spheres with porphyrin organic frameworks, achieving 800 mAh g^{-1} under 4C. Nanowires made of MnO_2 were used as templates by Yao et al.[211] to coat them first with TiO_2 and then with N-doped carbon. His hollow double-shell nanotubes were stable over 5000 cycles, even under 5C, and achieved a capacity decay rate of 0.012 % per cycle (531 mAh g^{-1}) due to the combination of nanosized cages, LiPS anchoring, and electrically conductive and open-pored network made of 1D particles. Zhang et al.[212] used ferrous salt crystal particles of only 3–5 nm in size as a temporary template to obtain graphitic nanoshells within a graphene backbone (765 mAh g^{-1}, 5C). He et al.[213] also used metal oxides (Fe_2O_3); however, they did not etch them away completely after carbon coating. In this way, a small polar Fe_3O_4 core remained, which also held the LiPS electrostatically in the nanocage. Furthermore, the cathode loaded with 80 % sulfur reached a capacity of 1366 mAh g^{-1} and 773 mAh g^{-1} for 0.1C and 2C, respectively.

Template-free nanocages are also possible, as demonstrated by Luo et al.,[214] who synthesized a core-shell structure from Ni-Co oxide through a one-step hydrothermal method and subsequent annealing treatment in an oxygen atmosphere. The high capacity of 855 mAh g^{-1} (5C) is probably not only due to the spherical double-shell geometry but also to the high electrical conductivity caused by defects, such as oxygen vacancies, in the band gap of the metal oxide, which facilitates the formation of electron holes.

In addition to the various structural designs for heterogeneous catalysts, some homogeneous catalysts, such as metal complexes like Cu-2-T,[215] CuL,[216] Cu-ETL-INT,[217] and NiDME[89] have also been employed to suppress the LiPS shuttle effect, provide fixed active sites, and minimize electrochemical polarization. These catalysts further promote uniform Li_2S deposition, enhance both cathodic and anodic reaction kinetics, and reduce the activation energy required for SEI formation, collectively contributing to improved rate capability and cycling stability. For example, Yu et al.[216] developed a self-assembled macrocyclic Cu(II) complex (CuL) as a homogeneous catalyst for LSB, outperforming heterogeneous catalysts that are limited by surface contact area. CuL enhances liquid-solid conversion kinetics (Li_2S_4 to Li_2S_2) via steric and electronic effects, promoting 3D Li_2S deposition and improving sulfur utilization. At 5C, it delivers an initial capacity of 660 mAh g^{-1}, retaining 535 mAh g^{-1} after 500 cycles with a 0.04 % decay rate per cycle. Under high sulfur loading (10.4 mg cm^{-2}), it achieves 925 mAh g^{-1}.

4.4. Role of Cathode Design and Materials in Enabling Fast-Charging LSBs

The cathode's design and material choices significantly impact the battery's ability to handle high (dis)charge rates. The insulating nature of sulfur necessitates incorporating conductive additives and a porous structure in the cathode to enable rapid electron and Li-ion transport, which is crucial for fast-charging. Carbon-based materials, with their high conductivity and diverse nanostructures, are widely used as cathode additives. The modifications, such as porosification, controlled alignment, and heteroatom doping, aim to enhance Li-ion diffusion and electron transfer, leading to improved rate performance.

The primary focus of recent research in cathode design for fast-charging LSBs is on enhancing sulfur utilization and mitigating the polysulfide shuttle effect, both of which are crucial for achieving high-rate performance. The utilization of hierarchical structures, such as those formed by heterostructures and nanosized cages, for sulfur encapsulation has emerged as a key strategy. These structures offer physical confinement for sulfur and polysulfides, limiting their dissolution and diffusion into the electrolyte, while their multi-scale porosity facilitates rapid Li-ion diffusion and electron transport, enabling fast-(dis)charge rates. The incorporation of polar functional groups or metal compounds further enhances polysulfide anchoring through chemical and electrostatic interactions, further suppressing the shuttle effect and improving cycling stability. The use of catalysts, such as metal oxides, sulfides, nitrides, and SACs, is also being actively explored. These catalysts accelerate the redox kinetics of sulfur species, promoting the conversion of polysulfides to Li_2S during discharge and vice versa during charge, enabling faster (dis)charge rates and reducing polarization. The ideal cathode should effectively encapsulate sulfur, anchor polysulfides, and facilitate their rapid conversion, all while maintaining high electrical conductivity and Li-ion diffusivity. **Table 5** summarizes the key materials and strategies discussed in this section, highlighting their impact on fast-charging in LSBs. **Table 6** lists the fast-charging LSBs research in relation to non-carbon materials.

5. Separator Modification for Fast-Charging LSBs

As discussed, one of the main drawbacks of the practical application of LSBs is the dissolution of LiPSs from the cathode into the electrolytes and their subsequent deposition at the anode, resulting in irreversible capacity loss and the corrosion of the Li-anode. These issues become more severe when the sulfur loading is higher, and the LSB undergoes higher current densities. Moreover, the dissolution of LiPSs increases the viscosity of the electrolyte, which hampers the high-rate performance of the device. Apart from the modifications in the cathode and the utilization of catalysts, another strategy to mitigate LiPS dissolution is to modify separators that immobilize the LiPS and enhance their kinetic conversion. The pristine separator, which is an electronic insulator, provides Li-ion diffusion paths; however, it fails to retard the LiPS diffusion. Therefore, many strategies, including the utilization of separators modified with carbon coatings, metal oxide, and their hierarchal composites, have been developed to mitigate LiPS diffusion, enhancing polysulfide conversion, increasing Li-diffusion, and suppressing the Li-dendrite formation, which is explained in detail in the following section.

5.1. Carbon-Based Composites

Conductive carbon coating on the separator is one of the methods to improve the electrochemical performance of LSBs by blocking the dissolution and diffusion of soluble LiPSs, thereby avoiding the shuttle effect during cycling. Zhu et al.[68] utilized conductive carbon coating on glass fiber (CGF) as a separator for LSBs, showing an improved reversible capacity (417 mAh g^{-1}) compared to the pristine glass fiber (PGF, 4 mAh g^{-1}) at higher current rates of 4C. This improved performance is attributed to the increased contact offered by the carbon coating with the cathode material, which enhances sulfur utilization. Furthermore, the strong LiPS-absorbing nature of CGF reduces the polysulfide shuttle phenomenon and lithium surface corrosion, thereby maintaining the smooth surface of the Li-metal even after reaching higher current rates and extended cycles (showing a high CE of 97.6%, even after 200 cycles). Designing mesoporous channels and polysulfide adsorbing networks on the separator can enhance the electrochemical performance of LSBs by facilitating Li-diffusion and hindering LiPSs dissolution, respectively. For instance, Zeng et al.[78] developed a polypropylene (PP) separator modified with lepidolite (C-Lepidolite@PP) to mitigate polysulfide shuttling and expedite the conversion of LiPSs (**Figure 10a**). The strong Si–S bonds established by lepidolite weaken the S–S bonds of polysulfides, effectively confining them. Additionally, the ultralow Li-ion diffusion barrier (0.081 eV) of lepidolite (Figure 10b) facilitates the conversion of polysulfides from liquid Li_2S_8 to solid Li_2S, displaying high redox peaks with low polarization in the CV and lower semicircle in the EIS (Figure 10c) of C-Lepidolite-Li_2S_6 symmetrical cells compared to the C-Li_2S_6 cell. The reduction pathway of the LiPSs on the lepidolite surface simulated by AIMD shows the accelerated conversion of Li_2S_2 to Li_2S. The shortest pathway offered by the lepidolite surface for the conversion of LiPSs avoids their accumulation in the electrolytes and hence suppressing shuttling effects. The LSBs fabricated with the C-Lepidolite@PP separator delivered an ultrahigh rate capability of 703 mAh g^{-1} at 7C (Figure 10d) with good cycling stability. The utilization of materials with intrinsic point defects has been found to block the LiPSs effectively and, hence, improve the electrochemical performance of LSBs.

Phosphate catalysts effectively capture the polysulfides, inhibit the shuttling effect, and accelerate polysulfide conversions due to the strong surface polarity and superior electronic conductivity. Apart from the crystalline materials, the amorphous phase can be effectively used because of their intrinsic short-range local symmetry, unsaturated coordination atoms, and more abundant defects, which are expected to increase the number of active sites and induce a unique electronic structure. Zeng et al.[276] reported an amorphous Fe-Phytate to modify the PP separator (C-Fe-Phytate@PP), which is found to enhance the polysulfide conversion and suppress polysulfide shuttling. The lower charge transfer resistance and high exchange current density displayed by the C@Fe-Phytate-Li_2S_6 symmetric cell compared to the C-Li_2S_6 cell indicate excellent electrocatalytic activity of Fe-Phytate to accelerate LiPS conversion kinetics. Also, theoretical studies reveal that the polysulfide reduction process is more favorable on the Fe-Phytate surface (0.59 eV) compared to the carbon (0.90 eV) (Figure 10e). Additionally, the cell fabricated with the C-Fe-Phytate@PP separator exhibits higher discharge capacities of 690 mAh g^{-1} at 5C compared to PP (100 mAh g^{-1}) and carbon-coated PP (C@PP, 245 mAh g^{-1}) (Figure 10f). Wu et al.[277] decorated a thin molecular sieve film on the surface of an electrospun cellulose acetate (CA) membrane derived from recycled cigarette filters used as the separator, showing an enhanced LSB performance. The microporous truncated-cone structured-β cyclodextrin (β-CD) exhibited the "funnel effect", which promotes Li-ion transport and physically blocks and chemically traps polysulfides. The β-CD/CA/C cell displayed a high rate performance of

Table 5. Characteristics of advanced materials and structures for fast-charging LSB cathodes.

Material/strategy/structure (source setion(s))	Challenges (hindering fast-charging)	Advantages (enabling fast-charging)	Drawbacks/other considerations
Polymers with Polar Functional Groups (4.3.1)	• Strong LiPS binding might somewhat impede rapid Li-ion diffusion near binding sites.	• Strong LiPS anchoring via functional groups reduces the shuttle effect • Some polymers are conductive or form part of a conductive network • Can act as physical barriers.	• Can potentially reduce overall sulfur loading • May increase electrode resistance if non-conductive.
Catalysts: Metal Compounds (Oxides, Sulfides, Nitrides, etc.) (4.3.2)	• Non-uniform distribution/agglomeration can lead to inefficient catalysis/transport pathways.	• Enhance LiPS adsorption • Accelerate LiPS conversion kinetics, reducing polarization at high rates • Some possess good electrical conductivity (esp. sulfides, nitrides) improving electron transfer.	• Potential for increased electrode weight and cost • Synthesis required for specific nanostructures.
Single-Atom Catalysts (SACs) (4.3.3)	• Achieving high, stable single-atom loading without aggregation during synthesis/cycling is difficult.	• Maximize atom utilization for catalysis • Unique electronic structures boost catalytic activity and reaction kinetics • Can alter Li_2S deposition (e.g., 3D growth) potentially improving utilization at high rates.	• Synthesis and characterization complexity • Potential for atom deactivation over cycling.
Hierarchical Structures (e.g., multi-scale porosity) (4.3.4)	• Complex synthesis ensuring uniform sulfur infiltration across scales can be difficult.	• Accommodate high sulfur loading • Multi-scale pores facilitate both rapid Li-ion diffusion *and* electron transport pathways • Enhance physical confinement of LiPS within the structure.	• Potential for increased tortuosity or contact resistance impacting overall transport.
MXenes (4.3.4)	• Synthesis/processing control for desired structure/termination groups can be demanding.	• Possess high intrinsic electrical conductivity Surface functional groups aid LiPS anchoring • 2D structure suitable for layered composites facilitating ion transport pathways.	• Relatively new material class • Synthesis complexity and scalability challenges noted in text.
Metal–Organic Frameworks (MOFs) (4.3.4)	• Low intrinsic electrical conductivity often necessitates conductive additives, hindering direct electron transfer.	• Highly porous with tunable, regular pores enabling fast ion diffusion and high sulfur loading • Metal nodes/linkers can offer catalytic sites and LiPS anchoring.	• Low conductivity is a primary drawback for direct use without conductive support.
Covalent-Organic Frameworks (COFs) (4.3.4)	• Synthesis can be challenging • Fewer known structures compared to MOFs • Often low intrinsic conductivity.	• Similar high porosity/regularity to MOFs for ion diffusion/sulfur storage • Potentially lighter (all-organic) • Conductivity can be tuned by π-conjugated linker choice.	• Synthesis complexity and scalability challenges noted • Often require conductive additives.
Nanosized Cages/Core-Shell Structures (4.3.4)	• Achieving high sulfur loading without blocking pore access for ions/electrolyte is a balance.	• Provide excellent physical S/LiPS confinement, minimizing shuttle effect • Defined void space accommodates volume changes • Can integrate catalytic/conductive components in shell/core.	• May increase electrode resistance depending on shell material • Scalability of uniform synthesis challenging.

Table 6. Comparison of the electrochemical performance of fast-charging LSB regarding the LiPS holding strategy.

Structure	Material	Loading [mg cm^{-2}]	Ratio 2C/0.2C	Rate capability [mAh g^{-1}]/C-rate	Long-term cycling [mAh g^{-1}]/cycles/C-rate	Refs.
polymers	PAN	2	93.3% [a)]	890/6C	800/600/0.6C	[148]
	PAN	2.3	86.0%	605/8C	1077/1000/2C	[150]
	PAN	1.1	83.3%	1000/5C	1106/500/1C	[149]
	soft acid+hard base binder + PVP	2	81.7%	660/5C	790/300/1C	[218]
	PAN	4	81.5%	490/2.5C	580/400/1C	[219]
	PEDOT	1.8	80.5%	918/1C	815/1000/1C	[156]
	PVP + PEI	1.5	77.3%	717/2C	608/450/1C	[157]
	PAN	N/A	76.0%	420/4C	590/50/0.1C	[220]
	TTCA	0.8	73.7% [a)]	452/6C	886/300/0.5C	[221]
	PPY	1.4	73.1% [a)]	640/5C	440/1000/10C	[147]
	TABQ	2.5	72.9% [a)]	833/10C	791/500/1C	[158]
	TTCA	2	66.1%	645/5C	671/500/1C	[222]
	PANI around CNT	1.3	63.4%	504/5C	717/200/0.5C	[154]
	conjugated microporous polymer	1.5	61.6%	631/5C	737/500/1C	[159]
	ultra-thin PANI	1.5	61.2%	581/3C	640/500/2C	[99]
	conjugated microporous polymer	1	60.0%	610/4C	550/1000/2C	[223]
	iminated PANI	1.5	53.2%	532/5C	620/500/2C	[26]
	PANI	2	44.6%	462/3C	735/200/0.5C	[151]
	PANI	0.87	N/A	636/10C	420/200/3C	[152]
oxides	ZrO_2	N/A	91.0%	658/20C	878/200/0.5C	[167]
	$Ti_xO_y + Ti_3C_2$	1.2	81.7% [a)]	1025/5C	749/2000/0.5C	[224]
	Nb_2O_{5-x}	1.2	79.7%	899/5C	555/600/1C	[225]
	$Fe_3O_4 + Fe_2O_3 + Fe_3C$	1.6	76.1%	659/5C	513/1000/3C	[77]
	Co_3O_4 Hollow Nanoplates	3.8	76.1%	680/5C	990/500/1C	[226]
	TiO_2	2	75.0%	740/3C	980/500/1C	[61]
	$BaTiO_3$	1.5	74.7%	717/3C	737/500/1C	[227]
	Co_3O_4	2	72.8%	688/5C	780/500/2C	[175]
	Nb_2O_5	1.5	72.7%	684/3C	895/800/0.5C	[166]
	RuO_{2-x}	2	71.3%	779/3C	602/600/1C	[165]
	Co_3O_4	1	66.9%	569/3C	610/500/1C	[163]
	$BiVO_4$	2	66.6%	575/10C	820/1000/2C	[228]
	$Na_xTi_{0.5}Co_{0.5}O_2$	1	65.7%	615/5C	620/300/3C	[92]
	VO_x	1	64.5%	553/5C	577/400/2C	[229]
	MnO_2	1.4	61.9% [a)]	755/10C	409/900/10C	[230]
	Titanium dioxide nanospheres	5	61.8%	765/3C	985/500/1C	[231]
	CoO	2	61.5%	306/10C	1248/500/1C	[164]
	$NiCo_2O_4$	1.5	59.4%	435/5C	444/1000/2C	[185]
	Co—MnO	0.5	57.1%	707/4C	840/100/1C	[232]
	TiO_2 + CoS	1.1	55.5%	563/3C	736/300/1C	[233]
	TiO_2	0.6	51.9%	630/2C	690/1000/0.5C	[161]
hydroxides	Mg-Al-LDH	1.5	76.9% [a)]	580/5C	730/450/1C	[169]
	Ni-Co-LDH	1.5	70.9%	733/4C	910/1000/2C	[234]
	Ni-Fe-LDH	3	68.0%	633/2C	501/1000/1C	[168]
	FeOOH	0.4	65.9% [a)]	710/3C	733/500/2C	[235]
	Ni-Co-LDH	2	63.2%	713/2C	658/800/1C	[170]
	layered yttrium hydroxide	1.8	57.9%	730/2C	484/800/2C	[171]

(*Continued*)

Table 6. (Continued)

Structure	Material	Loading [mg cm^{-2}]	Ratio 2C/0.2C	Rate capability [mAh g^{-1}]/C-rate	Long-term cycling [mAh g^{-1}]/cycles/C-rate	Refs.
sulfides	Co_3S_4	1.7	82.2% [a)]	850/1.5C	700/200/1C	[120]
	Co_9S_8	1.5	81.8%	878/2C	1030/1000/1C	[88]
	CoS_2 + Co	1.2	76.5%	803/3C	675/500/1C	[179]
	MoS_2 + MoN	1.2	75.6%	674/6C	520/1000/1C	[83]
	$Co_{0.12}N_{i1.88}S_2$ + NiO	N/A	75.2%	741/4C	1056/1000/1C	[178]
	WS_2 + Co_9S_8	2.5	69.4%	655/4C	728/1000/2C	[236]
	MoS_2-B	1.5	69.3%	711/5C	710/1300/5C	[237]
	NiS_2 + $NiSe_2$	2	67.3%	539/5C	597/1000/3C	[238]
	FeS_2	1.6	62.8% [a)]	916/2C	485/900/1.5C	[173]
	$NiCo_2S_4$	1.5	50.8%	624/3C	543/500/2C	[239]
	TiS_2	12	N/A	959/0.2C	659/200/0.2C	[172]
	$LiInS_2$ + In_2O_3	1	48.5%	502/4C	920/1000/0.5C	[85]
selenides	$MoSe_2$ + MoC	1	82.1% [a)]	624/5C	500/500/1C	[240]
	Bi_2Se_3	1	68.1%	651/4C	910/1000/1C	[177]
	$Cu_{1.8}Se$	1	63.0% [a)]	588/5C	760/1000/3C	[87]
	$NiCo_2Se_4$	1.1	62.5%	626/5C	480/2000/3C	[241]
	$CoSe_2$	1	55.9%	681/2C	679/400/2C	[242]
tellurides	Co-Te alloy	1.5	77.9%	898/2C	865/1000/2C	[203]
	$Co_{0.9}Zn_{0.1}Te_2$	1	74.4% [a)]	1030/2C	893/2500/2C	[243]
	P-$NiTe_2$	1.8	68.2%	764/6C	840/1800/4C	[244]
	ZnTe + $CoTe_2$	5.4	65.9%	636/3C	890/500/1C	[245]
	DPDTe	1.2	57.4% [a)]	611/5C	1227/300/0.5C	[246]
nitrides	Co_2N + CoP	1.7	81.1%	972/4C	988/500/2C	[247]
	Mo_3N_2 + Mo_2C	N/A	68.7%	512/5C	983/1200/0.5C	[29]
	TiN-MXene	1.2	66.0%	593/5C	647/1000/5C	[248]
	NiS_2	5	41.9%	304/4C	601/300/1C	[174]
phosphides	NiCoP + CoP	1.1	64.3%	763/ 3	713/1000/ 1C	[182]
	FeP	1	60.7%	613/3C	673/400/1C	[183]
	CoP-Vp	1.8	58.3%	738/3C	804/300/2C	[249]
further	Mo-doped CoB	1.5	74.2% [a)]	668/10C	710/1000/5C	[36]
metals	Fe-Co	1.2	68.2%	688/5C	1001/1000/1C	[250]
	NbB_2-MXene	2	61.8%	678/2C	967/500/1C	[251]
SACs	Fe + Fe_2N	1.5	75.9%	904/4C	500/731/4C	[252]
	P+S co-coordination asymmetric configuration	4.4	75.6%	605/10C	800/2000/5C	[188]
	Cu	4	74.0% [a)]	711/5C	620/500/5C	[187]
	Fe-N-C	1.5	71.0%	760/5C	1053/500/1C	[253]
	Zn	1	70.5%	655/5C	932/800/1C	[254]
	Co—N_3X_1	3.3	65.5%	804/5C	1350/650/5C	[255]
	Fe-CoNC	2.2	64.8%	618/10C	1230/2800/2C	[91]
	Zn	2	64.0%	513/5C	935/500/1C	[62]
	Fe–Co bimetallic single-atom-cluster	3	61.5%	701/10C	810/ 1000/2C	[189]
	Ru Single Atom Dispersed on MoS_2/MXene	0.95	60.7%	684/6C	808/1000/2C	[256]
	RuO_x Quantum Dots	5.5	53.1%	638/5C	680/250/5C	[257]
	polyoxometalate nanodots	1.5	81.3%	573/5C	895/1000/3C	[258]

(*Continued*)

Table 6. (Continued)

Structure	Material	Loading [mg cm^{-2}]	Ratio 2C/0.2C	Rate capability [mAh g^{-1}]/C-rate	Long-term cycling [mAh g^{-1}]/cycles/C-rate	Refs.
Carbon–metal heterostructures	porous CaO graphene	2	84.4%	656/5C	700/150/0.5C	[259]
	TiO_{2-x} + CNT	2.2	63.2%	399/5C	717/500/1C	[190]
	CO_2 bubble template	1.3	65.3%	532/9C	712/300/0.5C	[191]
	Mo_2C–MoS_2	6	62.5%	642/5C	642/1000/5C	[260]
	porous CNT microspheres	2	60.8%	785/3C	830/500/1C	[261]
	CNT in Nb_2O_{5-x} skeleton	2	58.3%	741/5C	847/500/1C	[97]
	Zinc Telluride	3.5	56.3%	639/3C	850/500/1C	[262]
	GC-uNiCoP@NPC	5.8	48.0%	750/1C	1260/200/0.1C	[94]
MXene	MXene tubes + CNT	1.2	81.6%	803/7C	725/500/1C	[194]
	porous Ti_3C_2 MXene	N/A	80.0%	772/5C	1028/500/1C	[98]
	$Ti_3C_2T_x$@AlF_3 /$Ni(OH)_2$	1.2	71.0%	635/4C	435/1000/1C	[192]
	MXene + carbon fibers	1.2	66.3% [a]	640/15C	910/1200/1C	[130]
	S-microcrystal on MXene	2	65.1%	800/2C	786/700/1C	[263]
	ultra-thin MXene shell	1.2	61.2% [a]	557/8C	420/700/6C	[193]
Organic frameworks	ZIF-8/N-doped C	1	83.9% [a]	693/3C	923/100/0.18C	[208]
	CMK-3	1	80.1% [a]	1096/1.2C	990/500/0.3C	[264]
	ZIF-8/CNT + CoP	1.1	79.3%	528/3C	630/300/0.2C	[207]
	ZIF-67/N-doped C + CoP	2	77.7%	770/5C	569/1000/3C	[65]
	3D building block + 2D conjugated linker	1.2	75.6%	757/5C	722/500/2C	[200]
	Ni-MOF (1D)	1.2	67.4%	575/8C	588/1000/3C	[197]
	γ-cyclodextrin MOF	1.5	67.4%	589 /5C	615/1200/2C	[265]
	MOF-Co_4N	1	66.7%	729/3C	745/400/1C	[266]
	ZIF-8/N-doped C + ZnO	N/A	66.1%	767/3C	740/500/1C	[205]
	ZIF-7 (2D)	1.8	65.3%	511/5C	679/500/1C	[196]
	ZIF-67/CNT + Co_3O_4	1.2	64.6%	702/5C	752/500/1C	[204]
	polyimide COF (2D)	N/A	64.2%	620/4C	900/500/1C	[201]
	ZIF-8/N-doped C + ZnSe	1	62.4%	542/3C	480/800/3C	[206]
	ZIF-8	1.6	60.5%	552/2C	688/300/0.5C	[195]
	Mg-reduced ZIF-8	2	60.4%	703/5C	577/1000/5C	[267]
	ZIF-67 + TpBD-Me2	1.3	60.4%	543/5C	636/500/1C	[202]
	MIL-125/C + TiN/Ti_4O_7	1	59.8%	616/4C	720/1000/1C	[162]
	MIL-53	1.5	59.2%	505/5C	755/300/1C	[268]
	Bi-MOF	1.5	59.0%	720/3C	799/1000/1C	[269]
	Metal-coordinated covalent organic frameworks	2	57.1%	620/4C	750/400/1C	[209]
Further core–shell structures	MgO nanoflakes/graphene + CNT	2.3	95.0% [a]	750/5C	892/50/1C	[270]
	CNT network	1	85.0%	841/5C	565/500/5C	[271]
	Ferrous salt crystals/graphene	N/A	82.9% [a]	765/5C	706/1000/1C	[212]
	Li-MMT silicate	1.2	83.0% [a]	345/9C	405/350/4.8C	[272]
	Polystyrene/POF	1.1	77.6%	800/4C	773/200/0.5C	[210]
	porous carbon spheres	1	75.4%	855/5C	781/800/0.2C	[214]
	MnO_2/C + TiO_2	1.6	73.5%	675/8C	531/3000/5C	[211]
	Fe_2O_3/C + Fe_3O_4	2.2	60.4%	773/2C	1165/200/0.1C	[213]
	In_2O_3 spheres + C	2.1	60.9% [a]	392//3.2C	440/1000/1C	[273]
	SiO_2 NiO/C	1.2	59.5%	698/2C	568/300/1C	[274]
	Ni_2P spheres + core	N/A	57.0% [a]	439/10C	575/500/2C	[184]
	SiO_2 + NiS/C	1	56.2%	674/2C	695/300/0.5C	[275]

[a] Deviation from common calculation, e.g., 2C/0.1C, due to missing data.

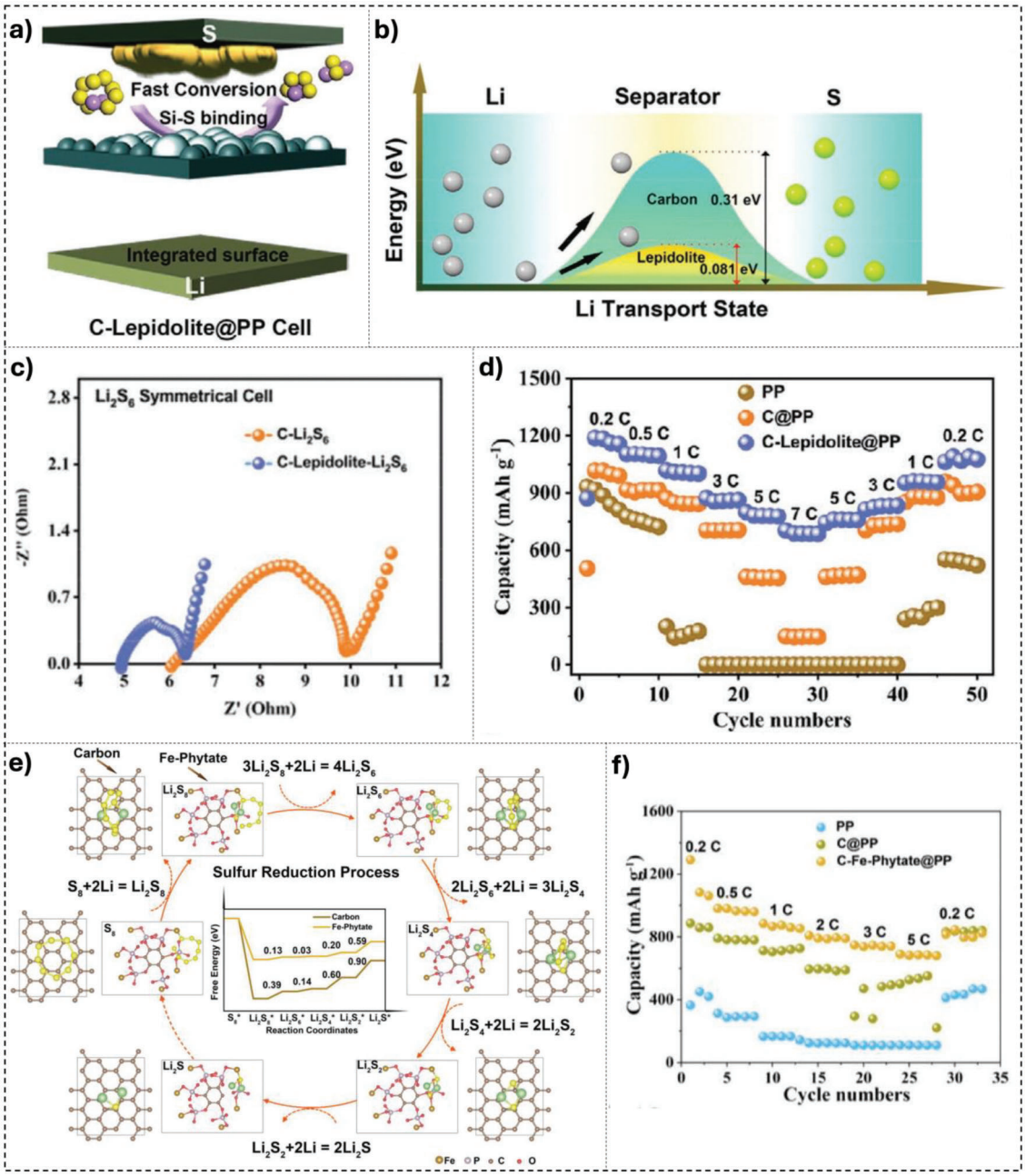

Figure 10. a) Schematics representation of polysulfide absorption and conversion on C-Lepidolite@PP separator, b) graph comparing the Li diffusion energy barriers on (6 × 6) carbon layer and lepidolite (0 0 1) surface, c) Nyquist plots display less resistance in C-Lepidolite-Li_2S_6 compared to C-Li_2S_6, symmetrical cell, d) Rate performance of LSBs based on various separators with sulfur loading of 1.66 mg cm^{-2}. Reproduced with permission.[78] Copyright 2021, John Wiley and Sons. e) Energy profiles displaying the reduction process of S and LiPSs on the carbon and Fe-Phytate surfaces, f) Comparison of the rate performances of the PP, C@PP, and C-Fe-Phytate@PP based LSBs. Reproduced with permission.[276] Copyright 2023, John Wiley and Sons.

565 mAh g^{-1} at a high current rate of 5C, which is about twice that of the PP separator (274 mAh g^{-1}), and also showed long cycling stability by maintaining a specific capacity of 863 mAh g^{-1} after 1000 cycles at 0.2C, which is three times more than that of the PP separator after 500 cycles.

Zue et al.[278] investigated the impact of the electronic structure of a FeCoNi alloy catalyst on sulfur conversion. The electronic structure is regulated and optimized, thereby defining sulfur adsorption and catalytic conversion. The FeCoNi-modified separator demonstrates enhanced initial capacity (753 mAh g^{-1}) compared to CB alone (less than 400 mAh g^{-1}) at 3C and good anti-self-discharge performance. Recently, Liu et al.[279] demonstrated the dual functionality of a natural Spidroin-coated carbon nanotube (SN-CNT) separator, which effectively captures lithium polysulfides (LiPSs) and regulates Li^+ flux, thereby enhancing the electrochemical performance of LSBs. The LSB

equipped with the SN-CNT-modified separator facilitates the Li_2S_2 to Li_2S conversion reaction, delivering a high rate-specific capacity of 744 mAh g^{-1} at 5C, along with an impressive areal capacity of 7.5 mAh cm^{-2} under lean electrolyte conditions (E/S = 6 µL mg_S^{-1}), making it suitable for practical applications. Overall, the strategic architecture of carbon-based materials, balancing porosity and conductivity, can significantly boost LSB performance by suppressing polysulfide dissolution and accelerating redox kinetics.

5.2. Metal-Based Composites

Various types of metal-based composite modified separators, including MoS_2/Celgard separator,[280] CeO_2-decorated porous carbon nanostructure (CeO_2/KB/PP),[69] hierarchical crumpled MXene/MoS_2 (CM/MoS_2),[281] lepidolite modified separator,[78] $Bi_2Te_{2.7}Se_{0.3}$ (BTS) coated on PP separator,[282] FeOOH coated on PP separator [283] etc., improved the high-rate capability of LSBs. Ghazi et al.[280] demonstrated that the MoS_2-modified separator effectively suppresses the polysulfide shuttling and also facilitates the Li-ion diffusion across the separator, which is attributed to the high Li-ion density on the surface of MoS_2. Wei et al.[283] utilized a conductive FeOOH nanorod interlayer as an effective trapper of polysulfides and suppresses the LiPS shuttling. This is attributed to the Lewis acid effect between the LiPSs and the Fe atoms in FeOOH. Besides, the FeOOH acted as an excellent electrocatalyst to expedite the LiPS conversion and also reduced the charging potential barrier, thus enhancing the Li_2S decomposition for fast redox kinetics. Moreover, the hydroxyl and oxygen functional groups also chemically bonded the LiPSs through polar–polar effect and confined them on the surface, and also mediated the Li-ions to improve the ionic conductivity. Thus, the use of FeOOH/PP modified separator enhances the electrochemical performance of LSBs, and achieves a high rate capability of 449 mAh g^{-1} at 2C.

Cai et al.[284] proposed a metal-semiconductor (Mo and MoO_2) hollow microsphere heterostructure-modified separator designed to physically confine the polysulfide species and catalytically accelerate both liquid-solid and solid-liquid conversions. The hollow microsphere traps the LiPSs, avoids their shuttling, and buffers the volume during (dis)charging. Moreover, the Mott-Schottky heterojunction created at the Mo/MoO_2 interface generates the built-in electric field that redistributes the charge density, enhancing ion/electron-transfer rates, which facilitates the polysulfides redox kinetics. The fast bi-directional conversion kinetics and the efficient trapping of LiPS improve the electrochemical performance of LSBs, showing an impressive specific capacity of 630 mAh g^{-1} at a high current density of 4C. He et al.[282] demonstrated that the ultrathin and lightweight $Bi_2Te_{2.7}Se_{0.3}$ (BTS) interlayers with high-density antisite defects deposited on the PP separator surface by the magnetron sputtering method (BTS/PP) effectively block LiPSs diffusion. This is attributed to the intrinsic point defect in BTS, especially at the antisite defect Bi'_{Te} (−2.97 eV), showing more negative adsorption energy of Li_2S_6 compared to $V^{\cdot\cdot}_{Te}$ (−2.36 eV). This leads to better trapping of soluble polysulfides than in perfect BTS (−0.65 eV), enhancing the electrochemical performance of LSBs, especially during fast-charging. At a higher current rate of 2C, the BTS/PP modified separator-based LSBs exhibit a discharge capacity of 756 mAh g^{-1} approximately five times higher than the pristine PP separator-based LSBs (≈150 mAh g^{-1}), which shows the promise of using defect engineering in separators to improve high-power performance of LSBs. Recently, Ma et al.[81] introduced a novel α-MnO_2/RuO_2 heterostructure-modified polypropylene separator designed to enhance the electrochemical performance of LSBs. The α-MnO_2/RuO_2 heterostructure (MRO), prepared through the hydrothermal method, regulates the energy barrier for LiPS transformation, improving both reduction and oxidation kinetics. The large active sites in this unique heterostructure facilitate the LiPS transformation and provide high electrical and Li+-conductivity. The α-MnO_2 component confines the LiPSs, while RuO_2 enhances electrical conductivity and catalyzes LiPS transformation. Additionally, the RuO_2 effectively shifts the rate-determining step (RDS) to reactions that reduce the formation of soluble LiPSs, thereby mitigating the shuttle effect. The LSBs fabricated with the α-MnO_2/RuO_2 heterostructure modified separator (MRO-8) exhibited an enhanced specific discharge capacity of 668 mAh g^{-1} at a high rate of 4C, which is ≈9.7 times higher than the discharge capacity of 69 mAh g^{-1} achieved with only α-MnO_2. This indicates that the adoption of suitable metal-based heterostructures can adsorb the polysulfides and catalyze the LiPS transformation process, which results in excellent high-rate electrochemical performance of LSBs.

5.3. Metal-Carbon-Based Composites

Even though carbon materials, metal oxides, sulfates, and nitrides can effectively adsorb LiPSs, their poor conductivity reduces the conversion kinetics of LiPSs.[285–287] Utilization of composite structures by the incorporation of conductive materials improves stability, enhances adsorption and catalytic capabilities, and hence boosts high-rate capability.[288,289] Long et al.[100] designed a 2D heterostructure with fast ion/electron transport bi-pathways by integrating monolayer lithium-montmorillonite (MMT) and N-doped rGO; this heterostructure was coated onto one side of commercial PP membrane (Celgard 2500) to create an efficient separator. The 2D MMT/rGO heterostructure provides ion/electron pathways for high-efficiency LiPS conversion and effective suppression of the polysulfide shuttle. The MMT monolayers exhibit robust chemisorption towards LiPSs due to their abundance of Lewis polar sites, facilitating rapid lithium-ion transport by minimizing diffusion energy barriers. On the other hand, the rGO monolayers, characterized by their expansive lateral size, establish a highly conductive electronic network, thereby enabling swift electron transport pathways for immediate conversion of adsorbed LiPSs. The density functional theory (DFT) simulations confirm that both MMT and the N-doped carbon network in rGO strongly adsorb LiPSs. To evaluate the rapidness of polysulfide conversion kinetics, the potentiostatic measurement conducted displayed higher Li_2S nucleation capacity (341 mAh g^{-1}) with earlier peaks response time (3917 s) for MMT/RGO coated on carbon fiber papers, using Li_2S_8 as the active material at 2.05 V, compared to RGO (201 mAh g^{-1} and 3967 s) and MMT-based electrodes (which showed no nucleation capacity). This represents the lowest overpotential and fastest Li_2S precipitation kinetics on the surface of MMT/RGO. Besides,

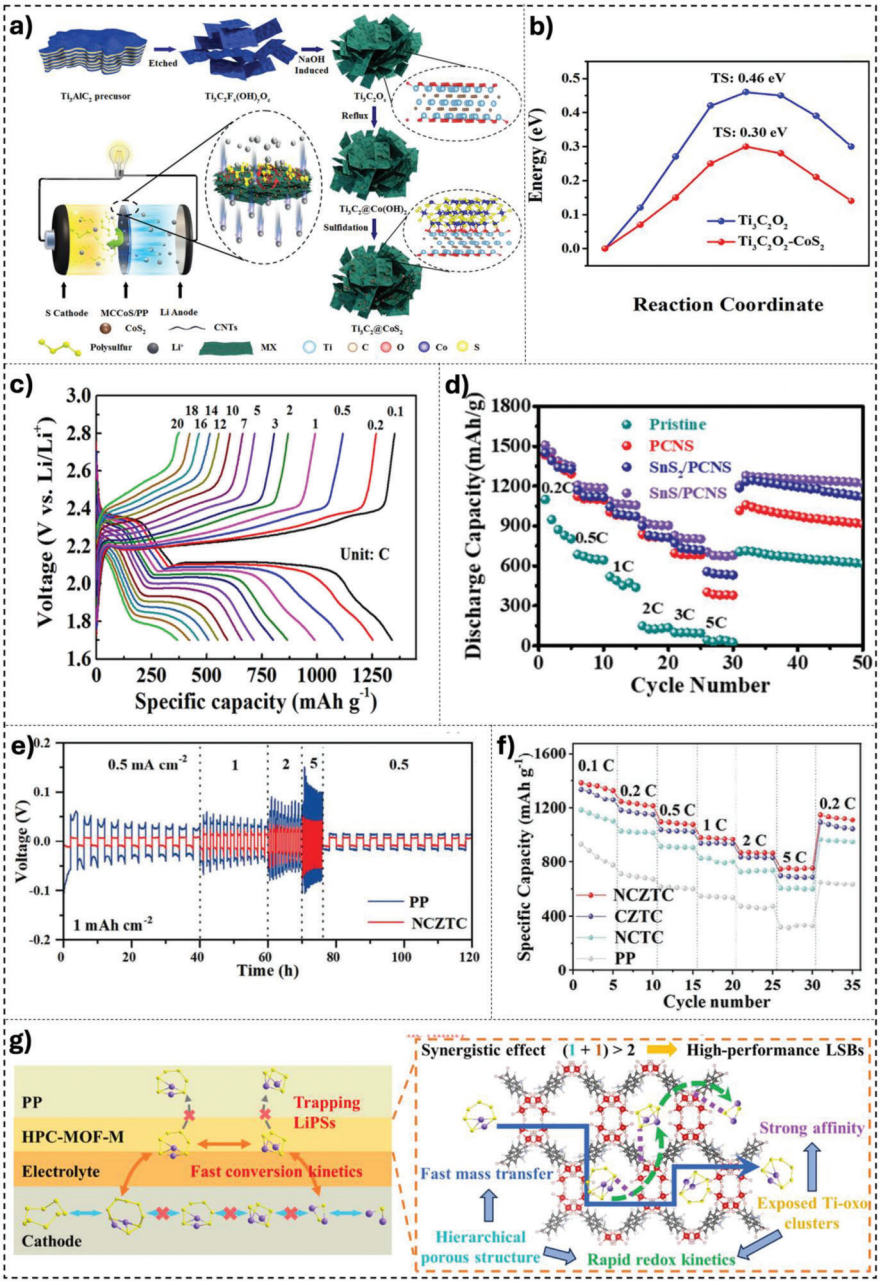

Figure 11. a) Schematic illustration of the synthesis of MCCoS/PP multidimensional composite framework for the LSB application, and b) the Li_2S decomposition energy profile on $Ti_3C_2O_2$-CoS_2 and $Ti_3C_2O_2$, c) the voltage profile at different current densities of the MCCoS/PP modified separator-based LSB. Reproduced with permission.[102] Copyright 2022, Springer. d) Rate capability of SnS/PCNS modified separator-based LSB at different current densities. Reproduced with permission.[290] Copyright 2020, John Wiley and Sons. e) Galvanostatic (dis)charge profile of Li || Li symmetric cells showing enhanced rate capability with NCZTC compared to PP separators, f) Rate performance of LSBs with different separators, Reproduced and modified with permission.[103] Copyright 2024, John Wiley and Sons. g) Schematic representation of the working mechanism of the HPC-MOF-M interlayer for LSBs. Reproduced with permission.[297] Copyright 2024, American Chemical Society.

the higher oxidation current density (3.470 mA) with earlier rinsing time (226 s) of MMT/RGO indicates favorable dissolution kinetics of Li_2S, further showing the synergistic effect of the composition. The cell fabricated with the 2D MMT/rGO heterostructure modified separator showed a high initial specific capacity of 1317 mAh g^{-1} at 0.2C, a good rate capability of 848 mAh g^{-1} even at 3C, and a low-capacity decay rate of 0.067% per cycle at 2C over 600 cycles. Tian et al.[102] developed a multi-dimensional composite frame (MCCoS/PP) for LSB separators, combining MXenes (Ti_3C_2) and CoS_2 with CNTs through suction filtration (**Figure 11a**). This MCCoS/PP frame demonstrates bifunctional catalytic activity by effectively blocking LiPS diffusion, facilitating liquid-solid conversion during reduction, and accelerating Li_2S decomposition by lowering the oxidation barrier. This

enhanced effect of the MCCoS/PP frame is due to the synergetic effect of CoS_2 on the Ti_3C_2 MXenes, where the high binding energy between the MX@CoS_2 and LiPSs increases the adsorption of LiPSs, while the increased density of states at the Fermi level in the MX@CoS_2 composite reduces the Gibbs free energy transformation of Li_2S_6 to Li_2S_2 and Li_2S, thus improving the catalytic conversion of polysulfides (Figure 11b). Furthermore, the enhanced charge transfer process on the MX@CoS_2 composite interface facilitates the decomposition of Li_2S by lowering the decomposition barrier in the oxidation process. Besides, the CNTs act as supporting layers, provide active surface area, and promote channels for the rapid transport of Li-ions. Thus, the LSB cell with a multi-dimensional composite frame separator (MCCoS/PP) achieved a specific capacity of 368 mAh g^{-1} at a very high C-rate of 20C and displayed a very low-capacity decay rate of only 0.033 % per cycle over 1000 cycles at 7C (Figure 11c). The LSB fabricated by the SnS-modified porous carbon nanosheet (SnS/PCNS) coated on the celgard separator reported by Li et al.[290] displayed both cycling stability and high-rate capability, showing a specific capacity of 452 mAh g^{-1} at 5C even after 800 cycles with a low average capacity attenuation rate (0.048 % in each cycle). Here, the SnS in SnS/PCNS shows strong adsorption of polysulfides, having more negative adsorption energy for Li_2S_4 (−1.0908 eV), which is attributed to the inherent S vacancy of SnS, and the ion diffusion channels provided by the PCNS improve the rate performance (Figure 11d).

Similarly, the strong physiochemical adsorption and catalytic effect of the N and P co-doped CNFs uniformly anchored with TiC nanoparticles (NPCNFT) coated on the PP separator improve the LSB electrochemical performance, achieving a specific capacity of 737 mAh g^{-1} at a higher rate of 5C with the slow capacity-fading rate (0.06 % per cycle over 500 cycles).[291] By introducing the NiO nanosheet network on a thin carbon layer porous membrane separator Wang et al.[292] demonstrated the high-rate performance of LSB cells, achieving a high specific capacity of 696 mAh g^{-1} at 5C. This high-rate performance is due to the mesoporous channels in the NiO network and the NiO-S interaction, which hinders LiPS dissolution. The composition of Co_3Fe_7 alloy and the N-doped hollow carbon sphere composite (CoFe/NHCS)-modified separators developed by Gu et al,[293] exhibit a high-rate capacity of 1029 mAh g^{-1} at 2C with good cycling stability (644 mAh g^{-1} at 1C after 500 cycles). The synergetic effect of CoFe/NHCS, including the strong chemisorption and superior electrocatalytic conversion of LiPSs by the Co_3Fe_7, along with the polysulfides shuttling suppression and the Li^+/electron transportation facilitated by the N-doped carbon hollow spheres, improves the high-rate performance and stability of LSB. Zeng et al.[37] utilized Ni_3Fe@hierarchical porous carbon-carbon nanotube (Ni_3Fe@HPC–CNT) modified separators to improve the electrochemical performance of LSBs, achieving a superior rate performance of 645 mAh g^{-1} at a very high rate of 15C. The Ni–Ni (Fe) bond length in Ni_3Fe increases due to alloying metallic Ni with Fe and reduces the coordination number of Ni, which uplifts the d-band center towards the Fermi level. Thus, the Ni_3Fe surface accelerates the interconversion between LiPSs and Li_2S and facilitates Li^+ diffusion due to the lowest diffusion barrier, significantly mitigating the shuttle effect.

Apart from the shuttling of polysulfide intermediates and the sluggish reaction kinetics, the uncontrollable growth of Li-dendrite growth is also a concern for LSBs, particularly for high-rate applications. To address the S-cathode and the Li-anode problems simultaneously Wu et al.[103] put forward a strategy for developing defects-rich (both N-doping and Te vacancies) bimetallic (zinc-cobalt) telluride electrocatalysts with dense heterointerfaces embedded in hollow carbon polyhedron bunches (N⊂$CoTe_{1-x}$/$ZnTe_{1-y}$@NC, NCZTC). The developed NCZTC composites exhibit large electrical conductivity (due to the N-doping at Te vacancies), a high polysulfide adsorption capability, and the accelerated bi-directional catalytic conversion of sulfur species showing a Li_2S precipitation capacity of 459mAh g^{-1} with an earliest Li_2S nucleation response time of 1350 s, and high Li_2S dissolution capacity of 545 mAh g^{-1} with a dissolution time of 1367 s. Additionally, the Li || Li symmetric cells with NCZTC-modified separator maintain a low and stable overpotential even at a higher current rate of 5 mA cm^{-2} (46.2 mV, Figure 11e) and also exhibit reduced nucleation overpotential (12.7 mV) in Li||Cu with NCZTC-modified separator compared to the PP-separator (77.5 mV). This indicates the lithiophilicity and the ionic sieving property of the NCZTC, which is favorable for uniform distribution of Li^+ flux during Li plating/stripping by decreasing the local current density. The superior catalytic activity and the Li dendrite suppression offered by the NCZTC composites enhance the electrochemical performance of the LSBs with NCZTC-modified separators demonstrating a high-rate performance of 748 mAh g^{-1} at 5C (Figure 11f), and outperforming other reported LSBs with modified separators in many categories including high rate, and cycling stability. Liang et al.[101] recently introduced a multifunctional separator with C_3N_4-$CoSe_2$ heterostructure that accelerates SRRs and improves lithium deposition. The C_3N_4-$CoSe_2$ has a large number of chemisorption sites that can form strong chemical bonds with LiPSs, effectively confining them and reducing their diffusion to the anode. Due to metal-like conductivity and high catalytic activity, the $CoSe_2$ lowers the energy barriers in transforming LiPSs, facilitating faster conversion reactions essential for rapid charging. Moreover, the use of C_3N_4-$CoSe_2$ heterostructure formed an internal electric field, which accelerates the charge flow at the interface and facilitates the bi-directional sulfur conversion. At the same time, the lithiophilic nature of C_3N_4-$CoSe_2$ induces uniform distribution of Li-ions, thus avoiding the dendrite formation. As a result, the LSB based on the C_3N_4-$CoSe_2$ functionalized membrane achieved a significantly higher discharge-specific capacity of 804 mAh g^{-1} at 2C. This shows that the synergetic effect of such functional heterostructures can improve the charge transfer efficiency, reduce battery polarization, and ensure stable cycling at high current rates, which is essential for fast-charging LSBs.

5.4. MOF-Based Composites

The separators modified with MOFs are also found to be a feasible method to improve the electrochemical performance of LSBs by mitigating the LiPSs diffusion and accelerating the catalytic conversions. Bai et al.[70] demonstrated that the MOF@GO separator acts as an ionic sieve and efficiently mitigates the polysulfide migration towards the anode while preserving

Li-ion transfer, thereby improving cycling stability. Kim et al.[294] developed a functional separator with sulfonated MOF/Nafion hybrids coated on polyethylene, which enhances redox kinetics and rate capability, achieving a specific capacity of 785 mAh g^{-1} at 3C. Furthermore, this separator also suppresses polysulfide diffusion through molecular sieving and electrostatic repulsion, hence improving the stability of the device. Chen et al.[295] designed a pore network rearranged MOF (FJU-90) separator with large pore size and surface area, showing a synergetic effect of both accelerating Li^+ ion conduction and inhibiting the polysulfide shuttle, exhibiting an excellent high-rate specific capacity of 827 mAh g^{-1} at a C-rate of 5C. Amorphous MOFs with ligand deficiency also show higher electrical conductivity and fast Li-ion transfer through different pores, which can be utilized to modify the separator to improve the performance of LSBs. Zhang et al.[296] fabricated LSBs with an amorphous MOF (aMIL-88B), which is synthesized through the ligand competition strategy, exhibiting enormous active sites to facilitate catalytic conversion and mitigate polysulfide shuttling, achieving a high-rate capacity of 610 mAh g^{-1} at 5C with higher stability. Xie et al.[297] synthesized hierarchical porous catalytic MOFs (HPC-MOFs) containing both micro- and macropores, exhibiting high catalytic sites with enhanced catalytic efficiency (Figure 11g). The HPC-MOFs mitigate the shuttle effect by adsorbing the polysulfides exposed at the Ti-oxo sites within the pores, and the LSB device fabricated with the modified HPC-MOFs separator enhances the electrochemical performance to achieve a high C-rate of 3C. Zuo et al.[298] designed Co-HMCF hieratical structures by combining the N-doping, and Co nanoparticles loading onto the Zeolitic Imidazolate Framework-8 (ZIF-8) to obtain Co-ZIF-8@Glu-g-C_3N_4, which is annealed at high temperature. The Co-HMCF having hollow and porous N-doped carbon frameworks with evenly embedded Co NPs in the MoF framework coated on the Celgard 2400 PP separator improves the redox kinetics, achieving an excellent rate capability of 582 mAh g^{-1} at 5C. This high redox kinetics is attributed to the uniformly distributed Co NPs in the ZIF-8 pores which accelerate the fast conversion of soluble LiPSs to solid Li_2S. Furthermore, the N-doping and the abundant pore structures in carbon framework reduce the attenuation due to the enhanced chemisorption and confinement effect toward LiPSs, exhibiting an extremely low rate of 0.047 % capacity decay per cycle for 800 cycles at 1C. Similarly, various types of MOF-based modified separators have been explored (Table 8) to enhance redox kinetics and mitigate polysulfide dissolution by leveraging their porous structure, which can accommodate catalysts.

5.5. Achieving Separator Modifications

To conclude, modifying the separator is one of the strategies to improve the stability and rate performance of LSBs by effectively mitigating the polysulfide shuttling, and facilitating the catalytic conversion, respectively. This can be achieved by coating the separator with different materials, including conductive carbon, metal oxides, or hybrid composites. Polar metal compounds, such as oxides, phosphates, and sulfides, offer abundant active sites that can adsorb LiPSs and improve catalytic conversion towards lower sulfides; however, their poor conductivity hampers Li-ion transport, leading to LiPS accumulation. Combining conductive carbon with the polar metal compounds improves the ionic conductivity, which accelerates the redox kinetics of LiPSs by facilitating Li^+ diffusion, hence providing high-rate performance to the LSBs. The MOF-based compounds coating on the separator is found to be an efficient method for mitigating polysulfide diffusion and accelerating Li-ion diffusion due to the presence of both metal ion nodes and organic ligands, which provide more active sites and catalytic centers and improve the electrochemical performance of LSBs. Additionally, tuning the thickness and increasing the homogeneity of the coating are different methods to improve the high-rate performance.

Generally, fast-charging capabilities are augmented by separator modifications in several ways:

Enhanced Polysulfide Trapping: Carbon-based materials, metal oxides, and MOFs with high surface areas and strong chemical interactions effectively immobilize polysulfides, minimizing the shuttle effect and improving capacity retention during rapid (dis)charge cycles.

Accelerated Redox Kinetics: Conductive carbon coatings, metal catalysts, and heterojunctions facilitate electron transfer, enabling faster conversion of polysulfides to Li_2S during charging and vice versa during discharging. This is crucial for fast-charging applications.

Improved Li-Ion Diffusion: Mesoporous channels and materials with intrinsic point defects expedite Li-ion transport across the separator, minimizing concentration polarization and enhancing rate performance.

Despite these advantages, some drawbacks persist: The additional layer on the separator can increase internal resistance, impacting overall battery efficiency. Moreover, ensuring the long-term stability of these modifications under high current densities remains a challenge. **Table 7** demonstrates separator types, challenges, advantages, and their impact on fast-charging LSBs. Besides two primary challenges applicable across all listed separator types, namely, i) increased internal resistance and ii) ensuring long-term stability under high current densities, the table specifies the unique challenges pertinent to each individual modification described. **Table 8** lists the fast-charging LSBs research in relation to separator modifications. Future research should focus on developing multifunctional separators that not only address polysulfide shuttling and reaction kinetics but also mitigate lithium dendrite formation, thereby enhancing the safety and cycle life of fast-charging LSBs. The integration of advanced materials and novel separator architectures holds the key to unlocking the full potential of LSBs for high-power applications.

6. Electrolyte Advancements for Fast-Charging LSBs

Electrolytes play a key role in the high-power electrochemical performance of LSBs, where the rate capability is highly dependent on the Li-ion diffusivity, and the speed of redox-reactions facilitated by the electrolytes. Additionally, the ability of electrolytes to prevent polysulfide dissolution and LiPS shuttling, form a uniform SEI layer on the lithium metal surface, and create robust electrode/electrolyte interfaces are essential for achieving high cycling stability and extended shelf-life in LSBs.[326,327] Moreover, the amount of electrolyte has a strong impact on the high-power electrochemical performance of LSBs. Brückner et al.[328] showed

Table 7. Separator modifications for fast-charging LSBs.

Separator type (source section(s))	Challenges (hindering fast-charging)	Advantages (enabling fast-charging)
Carbon-based Composites (5.1, 5.5)	• Basic carbon coatings may have limited catalytic activity/adsorption compared to functionalized materials	• Good electrical conductivity (facilitating electron transfer for faster redox reactions) • Blocks LiPS diffusion • Improves cathode contact/sulfur utilization
Metal-based Composites (5.2, 5.5)	• Some polar metal compounds (e.g., oxides) exhibit poor conductivity alone, potentially hindering efficient Li-ion/electron transport	• Strong chemical interaction/adsorption with polysulfides • Catalytic activity for redox reactions (catalyzing the conversion of polysulfides) • Can facilitate Li-ion diffusion (e.g., MoS_2, lepidolite)
Metal/Carbon-based Composites (5.3, 5.5)	• Requires balancing multiple components and optimizing interfaces for synergy	• Synergistic effect (e.g., overcomes poor conductivity of metals) • Improved overall conductivity and stability • Enhanced adsorption and catalytic capabilities (ensuring both efficient electron and ion transport)
MOF-based Composites (5.4, 5.5)	• Ensuring good electrical integration if MOF is intrinsically insulating	• High porosity and surface area. • Tunable pore structure/functionality • Molecular/ionic sieving effect (allowing selective passage of Li-ions while blocking larger polysulfide species) • Can provide catalytic sites

the influence of a high amount of electrolytes with lower sulfur loading (high E/S) resulting in low capacity degradation at high current rates. However, this approach limits energy density due to the excess electrolyte and underutilization of sulfur. Therefore, from a practical perspective, the use of a low E/S ratio is an important parameter for the fabrication of LSBs. However, operating under lean electrolyte conditions can lead to cell failure as the cell dries out, primarily due to the instability of solvent molecules with lithium metal, causing degradation. This degradation is exacerbated at higher current rates, which also pronounces dendrite formation. Zhang et al.[329] argue that the rate capability of LSBs under lean electrolyte conditions during discharge is mainly limited by the mass transfer rather than the charge transfer. At high discharge rates, restricted Li^+ transport to the cathode leads to increased polysulfide migration at the separator, lowering the discharge capacity.[330] Furthermore, the distribution of LiPSs in Li/S electrolytes has been observed to exhibit a significant dependency on both the specific composition of the electrolyte and the type of electrolyte utilized in various studies. Therefore, careful attention must be given to electrolyte design under lean conditions to achieve high-power LSBs without significantly sacrificing energy density, optimizing electrolyte composition, ensuring reversible electrochemistry, and improving redox conversions. In the following subsections, we will discuss the challenges faced by electrolytes for high-power LSBs and different strategies to improve electrochemical performance.

6.1. Electrolyte Types and Their Challenges in Fast-Charging LSBs

Highly solvating electrolytes (HSE) [331] and sparingly solvating electrolytes (SSE)[332] are the two types of electrolytes used in the practical lean-electrolyte LSBs working in opposite approaches towards the dissolution of polysulfides. HSEs exhibit high polysulfide solvation ability, improving the oxidation kinetics of Li_2S; however, they compromise long-term cycling stability due to polysulfide shuttling and Li-metal instability. The HSE electrolytes, which include the high-donor electrolyte solvents such as dimethyl sulfoxide (DMSO), N,N-dimethylacetamide (DMA), etc., show high polysulfide solvation ability, improve the oxidation kinetics of Li_2S from slow solid $Li_2S \leftrightarrow$ solid S_8 to fast liquid solvated $Li_2S \leftrightarrow$ liquid solvated polysulfides. However, the long-term cycling stability of LSBs is compromised by polysulfide shuttling and the instability of Li-metal due to continuous side reactions. With the use of electrolyte additives such as $LiNO_3$, NH_4NO_3, etc., the Li-metal can be protected and hence improve the cycling stability without deteriorating the power performance under lean-electrolyte conditions.[333,334] On the other hand, SSEs such as hydrofluoric ethers, ionic liquids, etc. inhibit polysulfide dissolution, working in the mode of quasi-solid-state reactions severely affects the high-rate performance of LSBs. Therefore, different approaches need to be implemented to surpass the technical challenges of utilizing both electrolytes for the development of high-rate LSBs.[332,335–337]

6.2. Ether-Based Electrolytes and the Need for Optimization

Ether-based electrolytes are the state-of-the-art non-aqueous organic liquid electrolytes used for LSBs.[73,338,339] The preference for LSB towards ether-based electrolytes is due to their capability to form soluble polysulfides (Li_2S_n, $2 < n \leq 8$). These polysulfides serve as redox mediators, converting the slow surface-based solid-solid reaction ($S \leftrightarrow Li_2S$) into a faster solution-based solid-liquid-solid reaction ($S \leftrightarrow Li_2S_n \leftrightarrow Li_2S$),[340,341] and hence preventing the passivation due to Li_2S/Li_2S_2 precipitation at the electrode. However, more optimization is required to utilize ether-based electrolytes for fast-charging applications, and the key challenges include:

i. Polysulfide shuttle effect: The unwanted polysulfide shuttle effect in ether-based electrolytes leads to capacity loss, exacerbates self-discharging, and reduces efficiency. Furthermore,

Table 8. Comparison of the electrochemical performance of fast-charging LSB classified based on the separator modifications.

Classifications	Separator modification	Loading [mg cm^{-2}]	Ratio 2C/0.2C	Rate capability [mAh g^{-1}]/C-rate	Long-term cycling [mAh g^{-1}]/cycles/C-rate	Refs.
Carbon-based composites	C-Lepidolite@PP	1.66	73.4%	703/7C	785/450/1C	[78]
	g-DCN/Celgard/g-C3N5	3	72.6%	471/4C	471/400/4C	[299]
	g-C_3N_4/CNT@PP	1.4	72.9%	755/2C	785/500/1C	[300]
	Ge+N-doped C skeleton	1.5	68.8%	871/2C	755/300/1C	[301]
	Spidroin (SN CNT)	1	67.0%	744/5C	851/300/ 1C	[279]
	C-Fe-Phytate@PP	2.8	62.2%	690/5C	631/800/1C	[276]
	β-CD/CA/C	1.73	58.1%	565/5C	863/1000/0.2C	[277]
	Gra/DTT	0.49	51.3%	712/5C	301/1100/5C	[302]
	carbon-coated GF (CGF)	1	N/A	496 /4C	993/200 /0.2C	[68]
	SNP/Celgard	N/A	N/A	692/10C	809/300/1C	[303]
	MCNT@PEG-Celgard	1.6	N/A	657/5C	490/500/1C	[304]
Metal-based composites	$Bi_2Te_{2.7}Se_{0.3}$ (BTS/PP)	4	71.3%	756/2C	560/300/2C	[282]
	CM/MoS_2	2	68.8%	652/3C	773/500/1C	[281]
	LCL-TCL (Janus type)	2	68.4%	680/4C	400/2000/1C	[305]
	p-Fe_3O_4-NSs	1.5	65.9%	878/2C	195/2176/1C	[306]
	Mo/MoO_2	1	61.7%	630/4C	580/500/1C	[284]
	FeOOH/PP	1.1	39.4%	449/2C	714/500/1C	[283]
	MoS_2/Celgard	N/A	N/A	550/1C	401/600/0.5C	[280]
Metal-carbon-based composites	MCCoS/PP	1.5	67.7%	368/20C	375/1000/7C	[102]
	MMT/RGO-PP	1.5	62.9%	848/3C	520/600/2C	[100]
	Mo_2C-Mo_2N/C@PP	1.5	62.2%	660/4C	575/1000/1C	[307]
	MoS_2-SnS/NC	0.9	68.6%	690/4C	435/400/4C	[308]
	CeO_2/KB/PP	1.3	N/A	627/3C	310/1000/2C	[69]
	PhIO@CNT	1	76.0%	686/3C	463/1000/2C	[309]
	Co-MoP/PCNFs	2.2	74.7%	826/5C	632/500/2C	[310]
	G-mSnO_2/$SnSe_2$	1.8	69.7%	794/8C	648/2000/5C	[311]
	Mo_2C@HGr	2	74.5%	836/5C	900/500/2C	[312]
	NbN@NC/PP	1.5	73.4%	604/10C	847/400/1C	[313]
	ZnSe@$CoSe_2$/C@CC	1.2	68.2%	340/10C	509/550/5C	[314]
	Ni_2P@NPG/PP	1	69.0%	731/2C	735/400/1C	[315]]
	V_2C/V_2O_5/CNTs	2	75.8%	607/5C	871/500/1C	[316]
	SnS_2@HCNF	1.2	69.1%	694/3C	675/500/1C	[317]
	Ni_3Fe@HPC–CNT	1.5	73.9%	645/15C	650/800/2C	[37]
	CoFe/NHCS	1	74.0%	1029/2C	644/500/1C	[293]
	SnS/PCNS	1.5	75.0%	700/5C	452/800/5C	[290]
	(N/P co-doped CNF@TiC) NPCNFT	1.5	75.2%	737/5C	505/500/5C	[291]
	NcCoTe1-x/ZnTe1-y@NC, NCZTC	3.5	69.8%	748/5C	527/1000/1C	[103]
	NiO network + C porous membrane separator	2.18	65.1%	696/5C	682/300/2C	[292]
	BNNs@CNFs + CNTs/rGO@Ru SAs	1.2	54.0%	450/5C	505/800/1C	[318]
	CACNM@PP		66.0%	614/5C	613.5/1500/5C	[319]
	FeCoNi	N/A	78.0%	753/3C	361/1000/3C	[278]

(*Continued*)

Table 8. (Continued)

Classifications	Separator modification	Loading [mg cm^{-2}]	Ratio 2C/0.2C	Rate capability [mAh g^{-1}]/C-rate	Long-term cycling [mAh g^{-1}]/cycles/C-rate	Refs.
MOF-based composites	HPC-MOF-M	1.5	72.0%	857/3C	850/500/1C	[297]
	UiO-66-S/Nafion	1.7	78.4%	785/3C	655/1000/1C	[294]
	SVO/AB	2	78.6%	793/2C	550/500/1C	[320]
	Ultrathin In/Zr-BTB@PP	N/A	68.9%	637/5C	679/500/2C	[321]
	FJU-90 MOF	1	66.8%	827/5C	826/500/1C	[295]
	Co-HMCF@PP interlayer	2.5	65.0%	582/5C	675/800/1C	[298]
	CON/CNT	4	64.7%	625/5C	625/1000/5C	[322]
	NSMX in Celgard 2400 separator	1.2	60.5%	595/5C	715/300/1C	[323]
	Amorphous aMIL-88B	1.8	60.2%	610/5C	740/500/1C	[296]
	Au–COF/rGO @PP interlayer	0.5	53.0%	568/4C	490/1000/1C	[324]
	MOF@GO	N/A	50.1%	488/3C	855/1500/1C	[70]
	Co-C@separator	2	32.1%	260/1.8C	401/600/0.6C	[325]
	Au–COF/rGO/PP	0.5	N/A	568/4C	600/1000/1C	[324]

the shuttling under lean electrolyte conditions and at higher current rates induces overpotential.

ii. Hindrance in ionic transport: The high polysulfide dissolution in ether-based electrolytes increases the polysulfide concentration in the electrolyte, which inhibits the mass transport and hence increases the viscosity and lowers the ionic conductivity. This is more pronounced under low E/S ratio and at higher current rates.

iii. Stability and Safety: The deposition of polysulfides at the anode over cycling deteriorates the Li-metal, and reduces the cycling stability. Moreover, due to the lower flash point, the use of ether-based electrolytes increases the concern of catching fire.

Therefore, much attention is required to avoid the dissolution of the formed polysulfides, their shuttle towards the anode, and their reactivity with the Li-metal, particularly under practical lean-electrolyte conditions and at high current rates. Various research activities on ether-based electrolytes are conducted focusing on mitigating polysulfide dissolution and shuttling, improving the conductivity of the electrolyte, stability, and efficiency of the device. For instance, Kong et al.[338] reported the tetrahydrofuran (THF) and di-isopropyl ether (DIPE) based novel dual salt high concentration ether electrolyte for LSBs showing enhanced performance by inhibiting the LiPSs dissolution and the side reactions at the Li-metal. The LiFSI salt used in the dual salt formulation increases the ionic conductivity and hence achieves a high-power performance of 280 mAh g^{-1} specific capacity at a high C-rate of 7.5C (5 A g^{-1}) in an electrolyte combination of L1L2TD-0482 (LiTFSI:LiFSI:THF:DIPE = 0:4:8:2, molar ratio). This is due to the lower coordination affinity of Li^+ toward FSI^- over $TFSI^-$, which increases the Li^+ self-diffusion coefficient in the LiFSI solution. In contrast, the dual salt formulation L1L2TD-1382 electrolyte (LiTFSI:LiFSI:THF = 1:3:8:2, molar ratio) exhibits higher cycling stability and greater CE than the L1L2TD-0482 electrolyte. This inferior cycling stability of LSBs in the L1L2TD-0482 electrolyte is because of the failure of pure LiFSI salt to create a robust SEI layer at the Li-metal, which creates a rough surface on the Li-metal anode after cycling.

6.3. Carbonate-Based Electrolytes and a Novel Approach for High-Power LSBs

The carbonate-based electrolytes, commonly investigated in LIBs, are generally not suitable for LSBs due to the side reactions.[342] However, recent reports demonstrated stable and reversible capacity with carbonate-based electrolytes by utilizing some unique nano-confinement of the sulfur cathode. The rationale behind the confinement of short-chain sulfur molecules is to convert directly to Li_2S without the intermediate polysulfide formation, enabling solid-to-solid reactions [133,343–346] in carbonate electrolyte-based LSBs using monoclinic γ-sulfur within CNFs, resulting in exceptionally high performance even at high power rates. Pai et al.[76] reported a striking discovery concerning solid-to-solid reaction in carbonate electrolyte-based LSBs by using γ-sulfur phase within CNF cathodes (γS-CNFs), resulting in an exceptionally high-performance device. The fabricated LSB exhibited a specific capacity of 400 mAh g^{-1} at a very high power rate of 40C, which corresponds to the (dis)charge time of about 30 s (**Figure 12**). This exceptional behavior is attributed to the synergetic effect of the γ-monoclinic sulfur phase incorporated in the CNF cathode with the carbonate electrolyte, forming only one (dis)discharge plateau in contrast to the two-plateau behavior of sulfur phases in ether electrolytes. This work explores the use of confirmed γ-monoclinic sulfur deposition in host materials and their compatibility with carbonate electrolytes, forming a direct high-rate conversion of γ-monoclinic sulfur to Li_2S without intermediate polysulfides. This approach avoids irreversible side reactions, resulting in highly stable devices, which facilitates the commercialization of LSBs. Nevertheless, this method limits the use of high sulfur loading, which will seriously affect the cycling stability, and the complicated cathode architecture design hinders the real application.

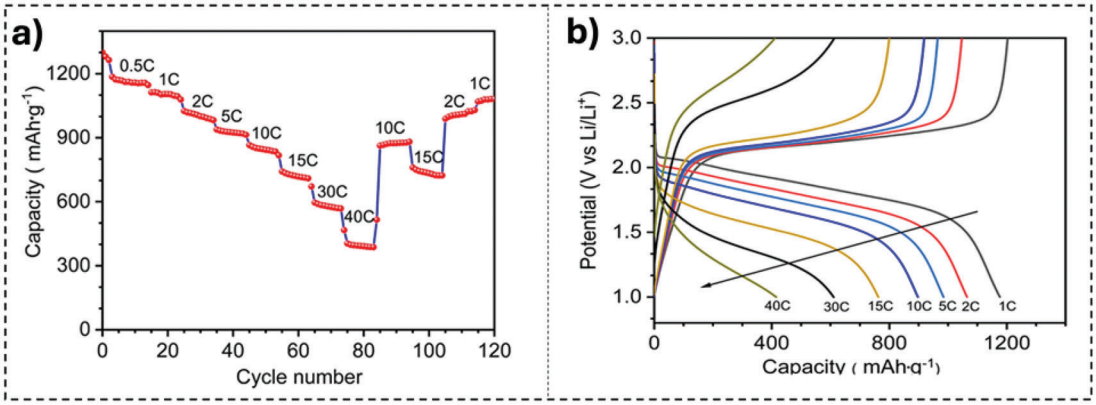

Figure 12. a) Rate performance and b) voltage profile of γS-CNFs in carbonate electrolyte at various C rates. Reproduced with permission.[76] Copyright 2022, Springer Nature.

6.4. Electrolyte Additives for Enhanced Performance

Electrolyte additives are one of the cost-effective strategies to enhance the electrochemical performance of LSBs by inhibiting the polysulfide shuttling, mitigating the uncontrolled dendrite formation at the Li-metal, and improving the safety of the device.[73] By utilizing different types of electrolyte additives, it is possible to engineer highly robust SEI layers at the Li-metal and suppress LiPSs shuttling. $LiNO_3$ is one of the most explored electrolyte additives in LSBs. The reduction of $LiNO_3$ creates nitrogen-containing groups based on a stable SEI layer on the Li-metal, which suppresses the reaction between polysulfides and the Li-metal, and thus improves the stability of the LSBs.[66,67] Additionally, the addition of LiPSs along with $LiNO_3$ is found to be synergistically suppressing the electrolyte decomposition and the dendrite formation at the Li-metal, even at the higher current density of 2 mA cm^{-2}.[104] Different functional additives such as phosphorus pentasulfide (P_2S_5),[347] alkaline ions (Cs^+ and Rb^+),[348] NO_3^--containing salts ($ZrO(NO_3)_2$ [349]), lithium iodide,[350] lithium azide,[351] organic lithium salts (Lithium oxalyl difluoroborate (LiODFB),[352] lithium bis(oxalato)borate (LiBOB) [353]), etc. based electrolyte additives are primarily focusing on suppressing the shuttling of LiPSs physically, thereby improving cycling stability. However, they do not facilitate catalytic polysulfide conversions, which are essential for the high-power performance of LSBs. The use of homogeneous catalysts and electrolyte-soluble organic additives offers another approach to suppress LiPSs by capturing them and facilitating their catalytic conversion. Luo et al.[89] reported a fundamental methodology to suppress the LiPSs shuttling by using nickel chloride dimethoxyethane (NiDME) as organometallic-based homogeneous catalyst additives, which accelerated LiPS conversion and reduced the polysulfide accumulation in a lean electrolyte condition (5 $\mu L_{(electrolyte)}$ $mg^{-1}_{(sulfur)}$). The 0.5 wt% of NiDME electrolyte additive improved the rate performance of LSBs to 635 mAh g^{-1} at 3C compared to the additive-free electrolyte (<500 mAh g^{-1}) and also exhibited a high cycling stability of 784 mAh g^{-1} at 1C after 500 cycles. This increased performance is attributed to the reduced activation energy (E_a) for the LiPS conversion due to the NiDME additives compared to the non-additive electrolyte. The energies associated with the reaction step in the transformation from S_8 to LiPSs to Li_2S are calculated from the DFT calculations, showing that the activation energy drop is more in the Li_2S_n-to-Li_2S conversion step, indicating the increased deposition of Li_2S at the cathode. Thus, the use of NiDME catalyst additives enhances LiPS suppression due to the stronger interaction between LiPS and NiDME additives, and the rapid LiPS conversion leads to the high-power performance of LSBs.

6.5. Alternative Electrolyte Compositions and the Importance of Solid Electrolytes

Beyond HSEs, SSEs, and carbonate- and ether-based electrolytes, alternative electrolyte compositions such as ionic liquids (IL),[354,355] high salt concentration electrolytes,[79] dual-salt electrolytes,[356] quasi-solid electrolyte,[357–359] solid polymer electrolytes[74] glassy electrolytes,[360] and combinations of electrolytes are also employed to improve the electrochemical performance of LSBs, by mitigating the polysulfide shuttle effect, improving the electrochemical stability window, increasing cycling stability, and enhancing the safety of the device. However, these highly viscous alternative electrolytes suffer from low ionic conductivity, which negatively affects the high-power performance of the device.[74,80,354,355,357,358,361–363] Moreover, high electrode/electrolyte interfacial resistance, complex manufacturing processes, and high production cost are further difficulties that need to be resolved, particularly for commercial applications. Therefore, challenges in ionic conductivity, interfacial stability, and manufacturing scalability must be addressed to fully unlock the potential of solid-state LSBs for high-power applications.

6.6. Key Considerations for Electrolyte Design of Fast-Charging LSBs

The choice of electrolyte and its additives significantly impacts the performance of LSBs, particularly under lean-electrolyte conditions and high-current rates. Balancing polysulfide solvation, Li-metal stability, and fast-charge transfer kinetics is crucial. The development of novel electrolyte formulations, including those

Table 9. Electrolyte design considerations for fast-charging LSBs.

Electrolyte type/property (source section(s))	Challenges (hindering fast-charging)	Advantages (enabling fast-charging)
Highly solvating electrolytes (HSEs) (6.1, 6.2)	• Increased polysulfide shuttling, especially at high currents, leads to capacity fade and overpotential, hindering sustained fast-charging • Li-metal instability (due to side reactions/shuttling) limits high-current cycling and long-term performance	• High polysulfide solubility and improved Li_2S oxidation kinetics facilitate faster liquid-phase redox reactions necessary for high rates
Sparingly solvating electrolytes (SSEs) (6.1, 6.2)	• Quasi-solid-state reaction mechanism results in slow ion transport and charge transfer kinetics, directly limiting the achievable fast-charging rate • Slower intrinsic reaction kinetics compared to HSEs inherently limits power capability	• Reduced polysulfide shuttling minimizes active material loss and side reactions, improving stability during cycling, including at potentially higher rates
Electrolyte additives (6.4)	• Need to carefully select additives or combinations to balance multiple functions (shuttle suppression, SEI formation, catalysis) for optimal fast-charging • Some additives primarily block shuttling physically and may not actively promote fast LiPS conversion kinetics, thus limiting ultimate rate performance	• Can enhance Li-metal stability (via robust SEI formation) and suppress polysulfide shuttling (by trapping/catalysis), enabling more stable high-current cycling (by stabilizing interfaces and suppressing side reactions)
Carbonate-based electrolytes (6.3)	• Generally incompatible due to side reactions with intermediate LiPSs, leading to cell failure, especially exacerbated at high currents • Requires specific cathode architectures (e.g., confined γ-S); challenges with achieving high practical sulfur loading limit energy density and applicability	• Direct solid-to-solid reaction mechanism (when using specific S phases/hosts) avoids soluble LiPSs, potentially enabling extremely high charging rates (e.g., 40C)
Alternative electrolytes (ILs, solid electrolytes, HCEs, etc.) (6.5)	• Often exhibit lower intrinsic ionic conductivity compared to conventional liquid electrolytes, limiting maximum achievable charge/discharge rates • High electrode/electrolyte interfacial resistance can hinder fast charge transfer • Manufacturing complexity and cost can be significant.	• Can offer improved thermal stability and safety, potentially enabling operation at higher currents/temperatures; may suppress shuttling and dendrites

based on solid electrolytes and innovative cathode architectures, holds the key to unlocking the full potential of LSBs for high-power applications. The following are key considerations for electrolytes of fast-charging LSBs:

i. Balancing solvation and stability: Electrolytes must balance polysulfide solvation (for fast kinetics) with effective suppression of shuttling (to prevent capacity loss at high currents).
ii. Stable interfaces: A robust SEI on the Li-metal anode is crucial to prevent dendrite formation and ensure stable performance during fast-charging.
iii. Catalytic conversion: Promoting rapid LiPS conversion, either through electrolyte additives or cathode design, is essential for high-power performance.
iv. Ionic conductivity and mass transport: High ionic conductivity and efficient mass transport are critical for fast-charge transfer, especially in lean-electrolyte conditions.
v. Material compatibility: Electrolyte components must be compatible with both electrodes and function effectively under high-current conditions.

Addressing these key considerations will be crucial in developing electrolytes that enable fast and stable charging in LSBs, bringing them closer to practical applications. **Table 9** shows electrolyte strategies for high-power LSBs.

In addition to these considerations, the design of electrolytes for high-power LSBs must also take into account the specific requirements of the intended application. For example, electrolytes for electric vehicles may require high thermal stability and wide operating temperature ranges, while electrolytes for portable electronics may prioritize high energy density and long cycle life. Developing advanced electrolytes that address these challenges will be crucial for unlocking the full potential of LSBs and enabling their widespread adoption in various applications. Future research efforts should explore novel electrolyte compositions, additives, and interfacial engineering strategies to achieve high performance, safety, and cost-effectiveness.

7. Safety Considerations and Strategies for Fast-Charging LSBs

Although LSBs offer significant advantages in energy density, their practical application, especially with the implementation of fast-charging capabilities, necessitates a thorough examination and mitigation of inherent safety concerns. The pursuit of rapid charging in LSBs can exacerbate several existing challenges, demanding robust safety strategies. As summarized in **Figure 13**, key safety concerns during the fast charging of LSBs include the formation of lithium dendrites at the anode due to high current densities promoting non-uniform plating,[66,67] which can lead to internal short circuits and thermal runaway. The polysulfide shuttle effect,[20–22] characteristic of LSB chemistry and often intensified during fast charging, can also contribute significantly to safety risks through anode corrosion, detrimental electrolyte decomposition, SEI degradation, and parasitic heat generation. Furthermore, the common reliance on volatile and flammable

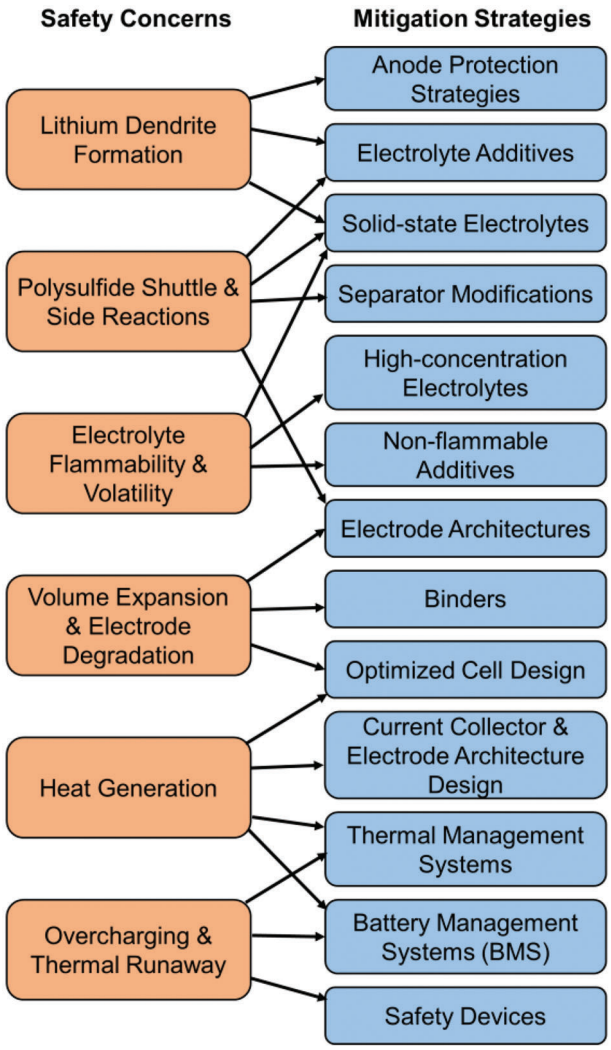

Figure 13. Summary of safety concerns and mitigation strategies for fast-charging LSBs.

ether-based electrolytes,[73,338,339] coupled with the substantial volume fluctuations of the sulfur cathode during cycling[6,13–19] (potentially impacting electrode integrity), increases the potential for thermal events and structural failures, particularly under the elevated temperatures resulting from increased ohmic and kinetic heat generation during fast charging.[96]

Addressing these multifaceted safety challenges in fast-charging LSBs requires a comprehensive approach involving modifications at the material, component, and system levels. As detailed in Figure 13, various strategies are under intense investigation. Electrolyte modifications, such as the incorporation of additives like $LiNO_3$[66,67,104] to promote stable SEI formation, and developing inherently safer alternatives like SSEs[74,80] (which can act as physical barriers but currently face interfacial resistance and scalability challenges) and high-concentration electrolytes (aimed at suppressing shuttling, potentially with viscosity/conductivity trade-offs), are crucial. Separator modifications[68,78] involving functional coatings or interlayers[125–127,146] play a vital role in physically or chemically trapping polysulfides and can help regulate ion flux to prevent dendrite penetration. Anode protection strategies, including the creation of artificial SEI layers[66,67] or using structured/lithiophilic interfaces, aim to stabilize the reactive lithium metal interface. Furthermore, effective thermal management is essential for dissipating the increased heat generated during rapid charging and preventing thermal runaway. Coupled electrochemical–thermal models[364] offer accurate heat generation predictions to guide battery design and cooling optimization. Specific strategies often involve combining passive methods, such as utilizing phase change materials[365] to effectively buffer temperature rise or employing multifunctional separators that integrate ionic conduction with thermal blocking functions,[366] with active approaches like liquid cooling systems. These combined thermal management techniques work to maintain stable operation under high-power loads. Finally, optimized cell designs that can accommodate volume changes and prevent internal faults, along with sophisticated BMS that continuously monitor and control battery parameters to mitigate risks, are indispensable for ensuring the safe and reliable operation of high-performance fast-charging LSBs.

8. Challenges in Scaling LSBs for Fast-Charging

LSBs have garnered significant attention for their potential to offer higher energy densities, both gravimetrically and volumetrically, compared to conventional LIBs. However, translating this potential into commercial-level performance, especially when combined with fast-charging capabilities, presents substantial technical challenges. Achieving high practical energy density necessitates specific cell design choices (primarily high sulfur loading, optimized electrode structures, and low electrolyte volumes), which often conflict with the requirements for fast charging (rapid kinetics and transport). Key challenges include optimizing energy density under high-rate conditions, managing transport limitations within electrodes, ensuring efficient catalysis, mitigating the polysulfide shuttle, ensuring component stability, and developing cost-effective manufacturing processes. These issues and potential solutions are summarized in **Figure 14**, and will also be explained in the following paragraphs.

The energy density dilemma: A primary challenge lies in maximizing practical energy density (both gravimetric and volumetric) under fast-charging constraints. This fundamentally requires:

1) Electrolyte/sulfur ratio (E/S ratio): Minimizing inactive electrolyte volume is crucial for both high gravimetric and volumetric energy density, ideally with E/S ratios below 3 µL mg^{-1}. However, such lean electrolyte conditions severely restrict ion transport pathways, increase cell resistance, and can lead to poor electrode wetting and premature cell dry-out, particularly during fast-charging. This limits both rate capability and cycle life under practical energy-dense configurations.
2) High sulfur loading and utilization: Achieving competitive energy density necessitates high areal sulfur loadings (> 5 mg cm^{-2}). However, the resulting thick electrodes amplify challenges related to poor intrinsic electronic/ionic conductivity and sluggish SRR kinetics. These factors

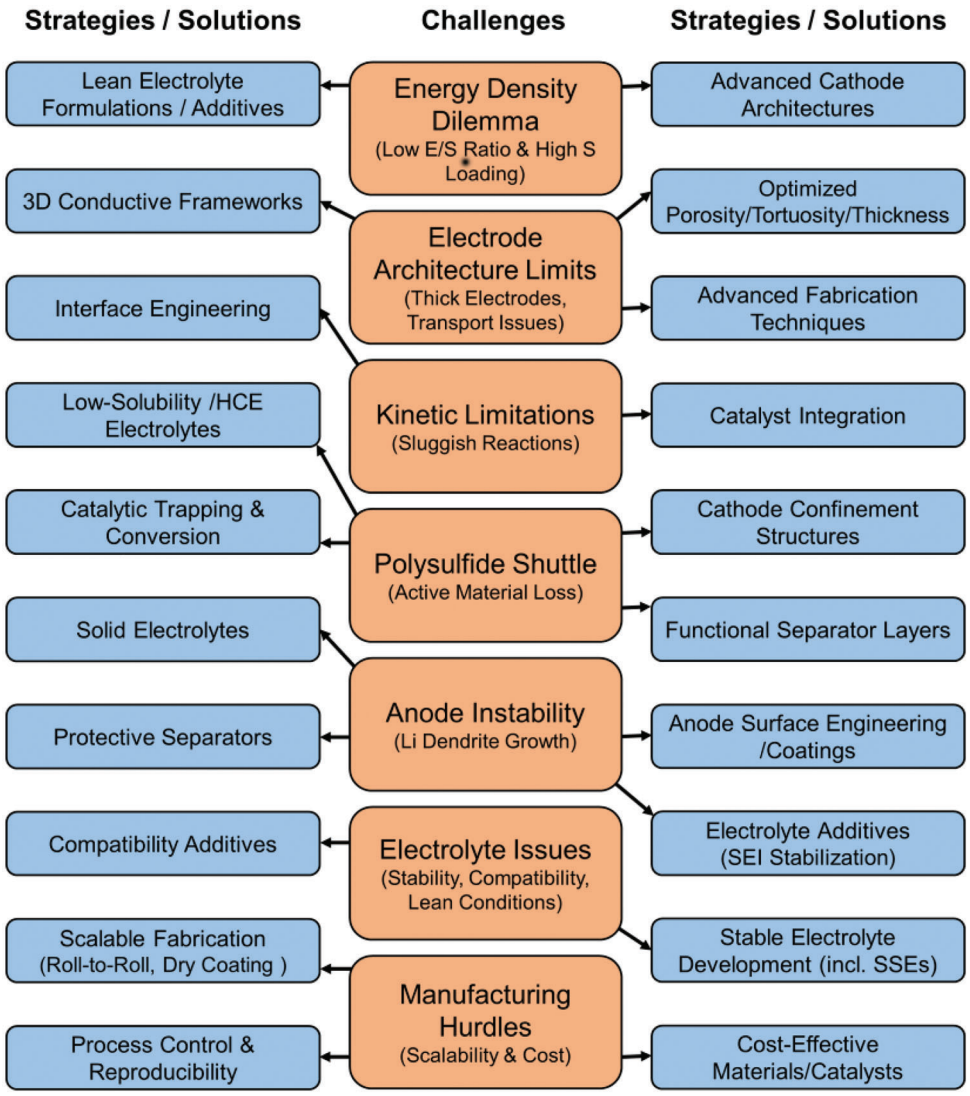

Figure 14. Primary challenges and solutions for fast-charging, high-energy-density LSBs.

hinder efficient active material utilization, limiting the practical energy density achievable, especially at high current densities.

3) Electrode architecture (balancing thickness, porosity, and tortuosity): Beyond simply loading sulfur, the physical architecture of the cathode is critical. There is an inherent trade-off between electrode thickness (required for high sulfur loading and energy density) and the porosity/tortuosity needed for efficient ion transport. Thick, dense electrodes maximize volumetric energy density but create long, convoluted pathways for Li^+ ions, hindering fast charging. Conversely, highly porous structures facilitate rapid ion transport but reduce volumetric capacity and can compromise mechanical integrity. Engineering optimal electrode structures requires precise control over porosity, pore size distribution, tortuosity, and particle/binder adhesion during fabrication (slurry preparation, coating, drying, calendering) to ensure efficient ion/electron transport throughout the thick electrode without sacrificing sulfur loading or structural stability under high-rate cycling.
4) Kinetic limitations and the role of catalysis: Even with optimized electrode structures and sufficient transport pathways, the intrinsic kinetics of the multi-step SRRs and SERs can be a bottleneck, particularly the solid-state conversions involving Li_2S_2/Li_2S. These sluggish kinetics contribute significantly to polarization and limit sulfur utilization at high (dis)charge rates. Integrating effective catalysts within the cathode or on the separator is therefore crucial. Catalysts lower the activation energy barriers for these reactions, promoting faster and more complete conversion of sulfur species. This enhanced kinetic activity directly benefits the practical energy density achievable at high rates by improving sulfur utilization, potentially compensating for some limitations imposed by high loading or lean electrolyte conditions. Finding cost-effective, stable, and highly active catalysts remains a key area of research for enabling energy-dense, fast-charging LSBs.

Table 10. Summary of key approaches and future directions for fast-charging LSBs.

Approach	Advancements	Challenges (hindering fast-charging)	Future directions
Cathode/electrode design	• Optimized hierarchical/conductive structures enhance utilization, ion transport, stability.	• Balancing high S loading/capacity with integrity, stability at high currents.	• Scalable fabrication of advanced microstructures for enhanced ion transport and high S loading.
Catalytic materials	• Advanced catalysts improve SRR/SER kinetics and reduce shuttle effect.	• Cost-effective synthesis, scalability, and long-term stability under operating conditions.	• Designing efficient, durable, affordable catalysts for large-scale use.
Separator modifications	• Functional coatings/layers trap LiPS, regulate ion transport, reduce dendrites, improve stability.	• Stable, cost-effective, scalable modifications without significant resistance increase.	• Refining techniques/materials for multi-functionality (trapping, ion transport, anti-dendrite) and long cycle life.
Electrolyte optimization	• Diverse formulations (Ether+additives, HCEs, SSEs, etc.) explored for high-rate/lean conditions and stability.	• Balancing high ionic conductivity with Li-metal stability and shuttle suppression.	• Novel formulations (incl. additives, solid/hybrid) for improved safety, compatibility, operating window and cost.
Anode stabilization	• Strategies developed (artificial SEI, composites, coatings, 3D structures) for anode protection.	• Preventing dendrites and maintaining high CE during sustained high-rate cycling.	• Developing robust, scalable, cost-effective anode protection methods.
Novel chemistries/pathways	• Monoclinic γ-sulfur enables direct solid-state conversion (potentially avoids LiPS shuttle, allows high rates).	• Integrating novel chemistries (like γ-S) with practical, high-loading, scalable designs.	• Optimization and validation of direct conversion pathways and compatible architectures.
AI/ML applications	• Accelerating materials discovery, optimizing charging protocols, performance prediction/analysis.	• Effective R&D integration, data handling, model accuracy/reliability.	• Wider adoption for streamlined development, adaptive BMS, improved lifetime management.
Scalability and manufacturing	• Exploration of potentially scalable processes.	• Cost-effective, high-volume manufacturing of advanced components; Quality control and reproducibility.	• Developing cost-effective materials synthesis and scalable, precise manufacturing for commercialization.

Polysulfide Shuttle Effect and Anode Instability: The migration of soluble LiPS intermediates (polysulfide shuttle) remains a major impediment, causing loss of active material (reducing practical energy density and cycle life), low CE, and corrosion/passivation of the lithium metal anode. Fast-charging can exacerbate this issue due to higher concentration gradients and potential temperature increases. The resulting continuous loss of active sulfur directly reduces the battery's energy storage capacity over time. Furthermore, high current densities promote non-uniform Li plating and dendrite growth on the anode, creating significant safety risks and further degrading performance.

Electrolyte Stability and Compatibility: Fast-charging places extreme demands on the electrolyte. It must possess high ionic conductivity, remain chemically stable during rapid cycling, and be compatible with both electrodes under high-current, potentially elevated-temperature conditions. Traditional electrolytes often suffer from decomposition and parasitic reactions, which are accelerated during fast-charging. Developing electrolytes (including advanced liquid formulations, additives, or solid-state systems) that facilitate rapid Li^+ transport while preventing dendrite growth, and maintaining stability under lean (low E/S) conditions is critical for achieving safe, long-lasting, and energy-dense fast-charging LSBs.

Cost-Effective and Scalable Manufacturing: Finally, scaling up LSB technology requires addressing manufacturing challenges. Fabricating electrodes with optimized architectures (high loading, controlled porosity/thickness) demands precise and potentially costly techniques. Integrating advanced materials like catalysts or functional separator coatings must be scalable and reproducible. Transitioning from lab-scale proof-of-concepts to high-volume, cost-effective manufacturing while ensuring consistent quality and performance is a crucial hurdle for the commercial viability of fast-charging, high-energy-density LSBs.

9. Conclusions and Future Perspectives

The progress in fast-charging LSBs has been impressive in recent years, driven by advancements across multiple battery components, including cathodes, catalyst integration, separators, and electrolytes. These innovations aim to address the inherent challenges of sulfur redox chemistry, polysulfide shuttling, and lithium metal anode instability, which are crucial to achieving high-rate performance. **Table 10** overviews key strategies and future directions for fast-charging LSBs. A brief summary of key findings on cathode, electrolytes, separator, and catalysts can be found below:

Engineering Cathode Materials: Effective cathode design is imperative for enhancing the storage and utilization of sulfur. High-performance cathodes should be highly porous, conductive, and provide robust sulfur immobilization. Hierarchical structure carbons and bio-derived composites have shown promise in holding sulfur efficiently while promoting fast ion diffusion. Modifying cathodes with defect sites in CNTs or nanocages enhances LiPS

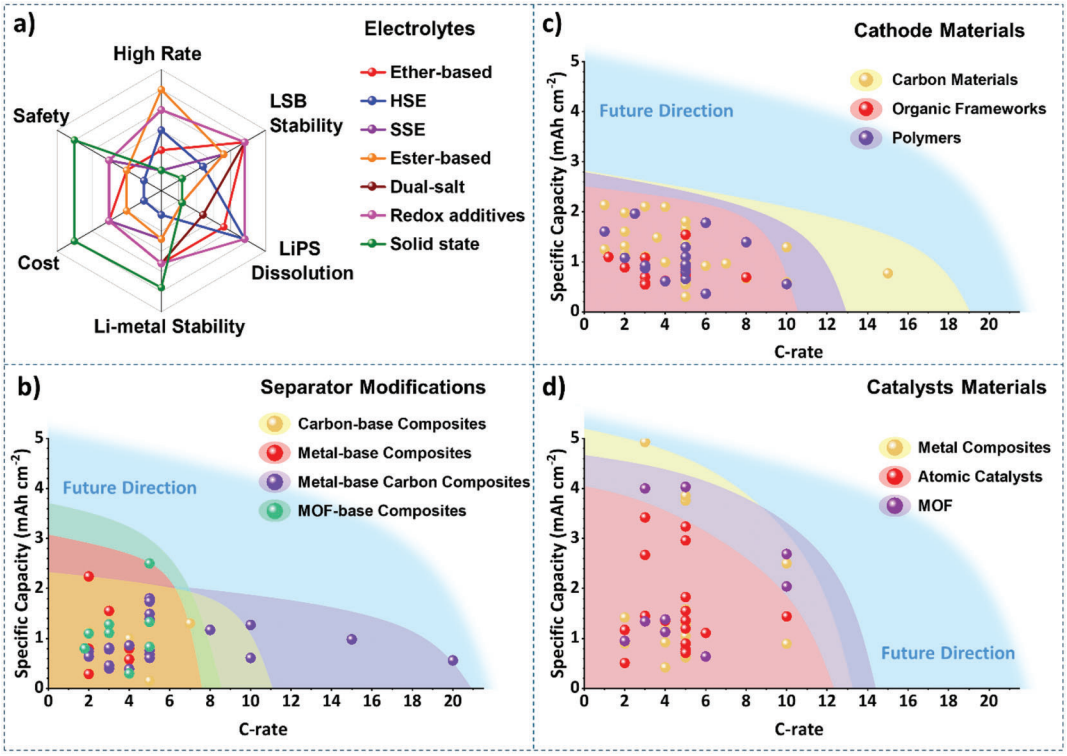

Figure 15. Comparison of strategies for enhancing high-rate LSBs. a) Qualitative spider chart comparing key attributes of state-of-the-art electrolyte systems. Panels (b–d) show capacity vs C-rate performance for LSBs utilizing different (b) modified separators, (c) structural cathode materials, and (d) catalyst materials. Data presented in Tables 4, 6, and 8 were used to generate the graphs.

retention and minimizes the polysulfide shuttle effect, reducing anode passivation and prolonging battery life.

Separator Modifications: Separators act as both a physical barrier and functional layer that immobilize LiPSs and reduce dendrite formation. Modifications involving carbon-metal hybrids, MOF-based materials, and coatings of polar metal-carbon composites have been shown to anchor LiPSs, enhance sulfur utilization, and improve Li-ion transport. These enhanced separators effectively prevent polysulfide migration, thus stabilizing long-term cycling performance even at high (dis)charge rates.

Electrolyte Selection: Electrolyte engineering is essential for fast-charging LSBs, affecting LiPS dissolution, Li-metal stability, and safety. Ether-based electrolytes with tailored additives control polysulfide formation and enhance dendrite suppression. Ester-based electrolytes, though traditionally inactive in LSBs, have recently demonstrated a breakthrough when used with monoclinic γ-sulfur, enabling direct high-rate conversion to Li_2S without intermediate LiPS formation. SSEs could also offer safe, high-rate charging potential, although challenges like cost and ionic conductivity remain barriers.

Incorporation of Catalysts: Catalysts play a pivotal role in expediting the conversion of LiPSs, reducing the energy barriers for SRR and SER. This enhancement not only improves the rapid activation of sulfur but also mitigates the polysulfide shuttling effect that leads to capacity loss. Catalysts such as metal oxides, chalcogenides, and heterostructures have effectively driven the rapid conversion of S_8 to Li_2S. The introduction of novel SACs and metal-organic frameworks (MOFs) has further optimized the catalytic performance, leading to better cycling stability and rate capability. Among the catalysts reviewed, metal oxides are the most established, showing excellent high C-rate performance and specific capacity. SACs excel in C-rate performance, and heterostructures demonstrate impressive areal capacity.

Figure 15 provides a comparative analysis of strategies aimed at enhancing the high-rate performance of LSBs, summarizing key developments and their associated performance trade-offs. Figure 15a utilizes a spider chart to qualitatively compare various state-of-the-art electrolyte systems across multiple parameters. Regarding high-rate capability, the data suggests that ester-based electrolytes and the incorporation of redox additives tend to offer enhanced performance compared to other systems like ether-based or solid-state electrolytes, although trade-offs concerning LSB/Li-metal stability, safety, and polysulfide dissolution are evident. Subsequently, Figure 15b–d presents scatter plots illustrating the relationship between areal capacity (mAh cm^{-2}) and C-rate for LSBs employing different strategies. These plots universally demonstrate the inverse correlation between achievable capacity and applied C-rate, highlighting the kinetic challenges in LSBs. However, a trend emerges when comparing these approaches: the implementation of catalysts (Figure 15d), encompassing metal composites, atomic catalysts, and MOFs, generally allows for operation at higher C-rates while maintaining moderate areal capacity, seemingly more effective in pushing towards higher rate capabilities than advancements focusing solely on separator modifications (Figure 15b) or cathode architectures (Figure 15c). Despite these advancements, current strategies

individually often fall short of the desired "Future Direction" zone, which requires both high capacity and high-rate capability. Collectively, these comparisons underscore that overcoming the kinetic barriers for practical fast-charging LSBs remains a significant challenge, likely necessitating synergistic approaches that combine optimized catalysts with advanced separator and cathode designs.

9.1. Breakthroughs in Next-Generation LSBs for Fast-Charging

Significant progress has been made in developing innovative solutions to enable fast-charging LSBs at scale. Next-generation LSBs incorporate advances in materials science, electrolyte engineering, and cell design that address key bottlenecks, paving the way for commercial adoption:

High-Loading, High-Performance Cathodes: Recent advancements focus on designing advanced cathodes that support high sulfur loading and rapid (dis)charge cycles. Hybrid designs, combining hierarchical carbon networks with metal oxides and sulfides, improve sulfur utilization and reduce polysulfide shuttle. Materials like CNFs and defect-engineered graphene enhance electronic conductivity and structural integrity, ensuring stable performance at high current densities. These cathodes offer an enhanced surface area for sulfur confinement and better electron/ion transport, making them suitable for fast-charging applications.

Single-Atom and Multifunctional Catalysts: The introduction of SACs has revolutionized the kinetics of SRRs in LSBs, by accelerating the conversion of LiPSs to Li_2S, even at high charge rates. Multifunctional catalysts with catalytic activity, electronic conductivity, and LiPS trapping capabilities further enhance fast-charging performance, by mitigating the shuttle effect and enhance fast-charging performance. The utilization of SACs and multifunctional catalysts enables LSBs to achieve high sulfur utilization under demanding operating conditions.

Low E/S Ratio Electrolytes with Fast Kinetics: To achieve high energy density and fast-charging, next-generation electrolytes are being designed for low E/S ratios. High-concentration and localized high-concentration electrolytes offer enhanced ionic conductivity and reduce LiPS solubility. Additionally, ester-based electrolytes and ionic liquids are being explored for their ability to stabilize the lithium anode and suppress side reactions. SSEs are also gaining attention due to their potential to eliminate the polysulfide shuttle and enhance safety. While SSEs face challenges in achieving fast ion transport, they offer a promising pathway to high-rate LSBs.

Advanced Separator Designs for Fast-Charging: Innovative separator designs are key to enabling fast-charging LSBs. Separators coated with functional layers, such as carbon-metal composites, MOFs, and polymeric materials, can selectively block polysulfides while allowing rapid lithium-ion transport, mitigating the shuttle effect and improving cycling stability. Moreover, they enhance the mechanical strength and thermal stability of the battery, making it more resilient during high-rate operations.

Anode Protection and Stabilization Strategies: Stabilizing the lithium anode is crucial for fast-charging LSBs. Techniques such as artificial SEI layers, lithium-metal composites, and protective coatings are being developed to prevent dendrite formation and maintain high CE, thereby improving compatibility between the lithium anode and the electrolyte, reducing side reactions, and enhancing long-term stability. Advanced 3D lithium anode architectures and alloying strategies are also being explored to improve ion distribution and support high-rate performance.

Monoclinic Sulfur and Direct Conversion Technologies: A breakthrough approach involves using monoclinic γ-sulfur, which undergoes a direct conversion to Li_2S without forming intermediate polysulfides. This simplifies the reaction pathway, reduces the risk of polysulfide shuttle, and enhances sulfur utilization at high charge rates. Research into integrating γ-sulfur with scalable cathode designs is ongoing, offering the potential to revolutionize LSB technology by delivering high energy density and fast-charging in a single platform.

Hybrid and Multi-Functional Electrolytes: Hybrid electrolyte systems that combine the benefits of liquid, gel, and solid-state components are emerging as a solution to the limitations of conventional electrolytes. These systems can maintain high ionic conductivity, suppress LiPS migration, and offer better compatibility with fast-charging profiles. Multifunctional additives are introduced to enhance electrolyte stability, improve lithium-ion transport, and prevent side reactions to achieve high-rate LSBs with a long cycle life.

AI Driven Advancements for Fast-Charging LSBs: Artificial intelligence (AI) and machine learning (ML) are poised to play a transformative role in overcoming the challenges of fast-charging LSBs, accelerating development from materials discovery to operational management.

i. AI for Accelerated Materials Discovery: AI/ML techniques offer powerful tools to expedite the design and identification of novel materials tailored for the demands of fast-charging. By analyzing vast datasets from computational simulations and experiments, AI can predict material properties, and screen potential candidates for cathodes, electrolytes, separators, and catalysts much faster than traditional methods. This includes identifying promising material combinations with enhanced ionic/electronic conductivity, improved electrochemical stability, superior catalytic activity for SRRs, and better LiPS anchoring capabilities, ultimately streamlining the development cycle for next-generation LSB components suitable for high-rate operation.
ii. AI for Optimization of Fast-Charging Protocols: Beyond materials, AI is crucial for developing dynamic and adaptive fast-charging protocols. Advanced algorithms integrated into BMS can move beyond static charging curves. AI can enable real-time optimization of charging current and voltage profiles based on the battery's instantaneous state (temperature, state-of-charge, impedance, estimated state-of-health). By predicting battery behavior and identifying conditions conducive to degradation (like lithium plating or excessive heat), AI-driven BMS can dynamically adjust the charging strategy to maximize speed while minimizing damage and ensuring safety. Techniques like reinforcement learning are being explored to allow the BMS to learn and refine optimal charging strategies over the battery's lifetime, potentially tailored to individual user patterns and extending cycle life under demanding fast-charge regimes.

iii. AI for Data Analysis and Performance Prediction: The complexity of LSB operation, especially under fast-charging, generates vast amounts of data. AI/ML excels at analyzing these large datasets to identify subtle correlations, degradation patterns, and key factors influencing performance. This data-driven insight can inform better cell designs and operational strategies. Furthermore, AI models can be developed to predict the long-term performance and remaining useful life of LSBs under various fast-charging scenarios, enabling more accurate lifetime estimations and informing predictive maintenance schedules. Cloud-based AI platforms could further enhance these capabilities by leveraging collective data and performing complex simulations without overburdening the vehicle's onboard systems.

9.2. Future Outlook and Directions

Novel Materials and Architectures: Discovery of next-generation materials is crucial for unlocking higher performance. Research will focus on new catalysts, separators, and electrolytes for better conductivity, sulfur retention, and safety. AI models and simulations will accelerate material design by predicting properties and optimizing combinations for specific charging profiles. Specifically addressing the challenge of achieving extreme fast-charging rates (≥ 20C), certain strategies reviewed herein show particular promise and warrant focused future investigation. The direct solid-to-solid conversion pathway enabled by γ-monoclinic sulfur cathodes in carbonate-based electrolytes stands out, having demonstrated exceptional capability up to 40C,[76] although challenges in achieving high sulfur loading currently limit practical application. For cathode materials within more conventional electrolyte systems, specific modifications like ZrO_2 permselective gateways on CNTs have enabled performance at 20C,[167] suggesting that precisely engineered ionic pathways are critical. Furthermore, advanced separator/interlayer designs, such as the multi-dimensional MCCoS/PP composite frame, have also demonstrated potential by maintaining significant capacity at 20C through synergistic catalytic activity and LiPS blocking.[102] Furthermore, catalytic materials such as Fe-CoNC SACs[91] significantly accelerate redox kinetics. While preliminary data for some specialized composites like sulfur-carbon even suggest potential up to 100C under specific lab conditions,[35] realizing practical performance at these extreme rates will require significant further research focusing on optimizing material stability, electrode architecture for high mass loading, electrolyte compatibility, and thermal management under such demanding conditions.

Robustness Under Harsh Conditions: Furthermore, ensuring reliable fast-charging performance under harsh working conditions is paramount for the widespread adoption of LSBs in demanding applications like electric vehicles or aerospace. Future research must systematically address the impact of environmental stressors beyond standard laboratory settings, including extreme temperatures (both high and low), and potentially high pressure, humidity, or mechanical stress (vibrations, shocks) depending on the target application. Extreme temperatures pose significant hurdles: low temperatures severely impede electrochemical kinetics and increase lithium plating risks during fast-charging, while high temperatures accelerate material degradation and heighten safety concerns. Although some materials show promise under specific non-standard conditions, achieving robust fast-charging across a wide temperature spectrum remains a key challenge. Similarly, the effects of other stressors like pressure and mechanical loads on fast-charging LSBs require dedicated investigation. Consequently, a critical future direction involves not only systematic performance evaluation (capacity retention, charge times, stability) under relevant harsh conditions but also the development of targeted mitigation strategies. This includes designing robust electrolytes with wider operating windows, implementing advanced thermal management systems, and engineering mechanically resilient cell architectures capable of withstanding diverse operational demands.

High Sulfur Loading and Low E/S Ratio: To achieve high gravimetric and volumetric capacities, higher sulfur content and lower electrolyte volume are needed. Future research should focus on cathode architectures and electrolytes that operate efficiently in lean electrolyte conditions. Integration of hierarchical cathode designs with γ-monoclinic sulfur phases is expected to enhance direct sulfur conversion and reduce side reactions.

Solid-State LSBs: SSEs offer a promising solution for enhancing the safety of fast-charging LSBs by preventing polysulfide migration and dendrite growth. Ongoing research aims to improve ion transport and interface compatibility of LSBs for high-rate applications.

Anode-Free: Anode-free metal batteries represent a promising avenue for achieving even higher energy densities and faster charging capabilities.[367–371] By eliminating the anode, these batteries offer the potential for simplified fabrication and reduced weight. However, challenges such as dendrite formation and electrolyte instability must be addressed to ensure their safe and efficient operation at high charge rates. Further research on novel electrolyte formulations, protective coatings, current collector optimization, and lithium deposition control strategies are crucial to unlocking the full potential of anode-free LSBs for fast-charging applications.

Electrode Dry Coating: Dry coating technologies provide a promising path to enhance the performance of fast-charging LSBs.[372] By enabling the precise deposition of active materials on the current collector, dry coating methods could improve electrode stability, reduce interfacial resistance, and enhance ion transport by engineering electrode properties. As dry coating techniques evolve, they offer a scalable and environmentally friendly approach to manufacturing high-performance LSB electrodes for a wide range of applications.

Advanced Characterization Techniques: Deeper insights into the complex reactions during fast-charging can be obtained using in-situ spectroscopy and microscopy analysis. Understanding the real-time dynamics of LiPSs and interfacial phenomena is crucial for optimizing fast-charging LSBs with liquid electrolytes and guiding future material innovations.

Scalable Manufacturing Processes: Transitioning from lab-scale prototypes to commercial products will require advances in 3D printing, roll-to-roll processing, and binder-free electrode fabrication. These methods provide precise control over material distribution and electrode architecture, enabling consistent production of high-performance LSBs at scale.

Safety and Sustainability: The future of fast-charging LSBs will emphasize non-flammable electrolytes, improved thermal management strategies, and sustainable recycling processes. As these technologies mature, LSBs are expected to have a lower environmental impact because of using abundant materials like sulfur and more efficient energy storage.

High-Energy-Density Configurations: Combining high energy density with fast-charging capabilities remains a critical goal. Innovations in high-loading cathodes, lean electrolytes, and lightweight current collectors will be pivotal in making LSBs competitive with traditional LIBs for electric vehicles and portable electronics applications.

Overall, despite challenges in materials, design, and manufacturing, ongoing research and innovations could unlock the full potential of scaling fast-charging LSBs, offering a sustainable, high-capacity, and rapid-charging alternative to current battery technologies.

Acknowledgements

This work was supported by the financial support of the German Federal Ministry for Education and Research (BMBF) for the funding of the research project of SiLiNE (Reference No. 03XP0419B), and also the project "SuSiBaby" – Sulfur-Silicon Batteries (LPW-E/3.1.1/1801) funded by the EUSH and the European Regional Development Fund of the European Union in Schleswig-Holstein, Germany. Furthermore, this project received support from the German Research Foundation (DFG) through the German-Taiwan Collaborative Project (AD 183/35-1). SN and BB would gratefully acknowledge Shiv Nadar Institution of Eminence, India, for providing necessary academic resources and the fund provided by Anusandhan National Research Foundation, ANRF (SERB)-SRG (File No: SRG/2023/000084), India, during manuscript preparation. This work was also supported by the National Science and Technology Council, Taiwan, R.O.C. through (NSTC 113-2221-E-033-008), Department of Chemical Engineering at Chung Yuan Christian University.

Open access funding enabled and organized by Projekt DEAL.

Conflict of Interest

The authors declare no conflict of interest.

Keywords

catalyst integration, cell design, electrode engineering, fast-charging, material design, lithium-sulfur batteries

Received: September 23, 2024
Revised: April 11, 2025
Published online: June 13, 2025

[1] Z. Yang, J. Zhang, M. C. W. Kintner-Meyer, X. Lu, D. Choi, J. P. Lemmon, J. Liu, *Chem. Rev.* **2011**, *111*, 3577.
[2] B. Dunn, H. Kamath, J.-M. Tarascon, *Science* **2011**, *334*, 928.
[3] S. Orangi, N. Manjong, D. P. Clos, L. Usai, O. S. Burheim, A. H. Strømman, *J. Energy Storage* **2024**, *76*, 109800.
[4] B. Babu, *Batter. Supercaps* **2024**, *7*, 202300537.
[5] M. Winter, J. O. Besenhard, M. E. Spahr, P. Novák, *Adv. Mater.* **1998**, *10*, 725.
[6] M. Zhao, B.-Q. Li, X.-Q. Zhang, J.-Q. Huang, Q. Zhang, *ACS Cent. Sci.* **2020**, *6*, 1095.
[7] A. Manthiram, *ACS Cent. Sci.* **2017**, *3*, 1063.
[8] S. H. Yu, X. Feng, N. Zhang, J. Seok, H. D. Abruña, *Acc. Chem. Res.* **2018**, *51*, 273.
[9] M. Balaish, A. Kraytsberg, Y. Ein-Eli, *Phys. Chem. Chem. Phys.* **2014**, *16*, 2801.
[10] W. J. Kwak, N. Rosy, D. Sharon, C. Xia, H. Kim, L. R. Johnson, P. G. Bruce, L. F. Nazar, Y. K. Sun, A. A. Frimer, M. Noked, S. A. Freunberger, D. Aurbach, *Chem. Rev.* **2020**, *120*, 6626.
[11] C. Xia, C. Y. Kwok, L. F. Nazar, *Science* **2018**, *361*, 777.
[12] P. G. Bruce, S. A. Freunberger, L. J. Hardwick, J.-M. Tarascon, *Nat. Mater.* **2012**, *11*, 19.
[13] A. Manthiram, Y. Fu, S. H. Chung, C. Zu, Y. S. Su, *Chem. Rev.* **2014**, *114*, 11751.
[14] M. Abdollahifar, P. Molaiyan, U. Lassi, N. L. L. Wu, A. Kwade, *Renew. Sustain. Energy Rev.* **2022**, *169*, 112948.
[15] Y. X. Yin, S. Xin, Y. G. Guo, L. J. Wan, *Angew. Chem., Int. Ed.* **2013**, *52*, 13186.
[16] X. Ji, L. F. Nazar, *J. Mater. Chem.* **2010**, *20*, 9821.
[17] M. Wild, L. O'Neill, T. Zhang, R. Purkayastha, G. Minton, M. Marinescu, G. J. Offer, *Energy Environ. Sci.* **2015**, *8*, 3477.
[18] H. J. Peng, J. Q. Huang, X. B. Cheng, Q. Zhang, Review on High-Loading and High-Energy Lithium–Sulfur Batteries, Wiley-VCH Verlag, **2017**.
[19] G. Zhou, H. Chen, Y. Cui, *Nat. Energy* **2022**, *7*, 312.
[20] A. Kim, S. H. Oh, A. Adhikari, B. R. Sathe, S. Kumar, R. Patel, *J. Mater. Chem. A* **2023**, *11*, 7833.
[21] Y. W. Song, L. Shen, N. Yao, X. Y. Li, C. X. Bi, Z. Li, M. Y. Zhou, X. Q. Zhang, X. Chen, B. Q. Li, J. Q. Huang, Q. Zhang, *Chem* **2022**, *8*, 3031.
[22] Z. Han, S. Li, Y. Wu, C. Yu, S. Cheng, J. Xie, *J. Mater. Chem. A* **2021**, *9*, 24215.
[23] X. Liang, C. Hart, Q. Pang, A. Garsuch, T. Weiss, L. F. Nazar, *Nat. Commun.* **2015**, *6*, 5682.
[24] A. Manthiram, Y. Fu, Y. S. Su, *Acc. Chem. Res.* **2013**, *46*, 1125.
[25] J. He, A. Manthiram, *Energy Storage Mater.* **2019**, *20*, 55.
[26] M. Li, H. Chen, C. Guo, S. Qian, H. Li, Z. Wu, C. Xing, P. Xue, S. Zhang, *Adv. Energy Mater.* **2023**, *13*, 2300646.
[27] Z. Tong, L. Huang, J. Guo, Y. Gao, H. Zhang, Q. Jia, D. Luo, W. Lei, S. Zhang, *Carbon* **2022**, *187*, 451.
[28] G. Zhao, Q. Chen, L. Wang, T. Yan, H. Li, C. Yuan, J. Mao, X. Feng, D. Sun, L. Zhang, *J. Mater. Chem. A* **2022**, *10*, 19893.
[29] Y. Wang, D. Zhang, J. Han, Y. Yang, Y. Guo, Z. Bai, J. Cheng, P. K. Chu, H. Pang, Y. Luo, *Chem. Eng. J.* **2022**, *433*, 133629.
[30] C. Zu, A. Manthiram, *Adv. Energy Mater.* **2013**, *3*, 1008.
[31] M. Abdollahifar, H. Cavers, S. Scheffler, A. Diener, M. Lippke, A. Kwade, *Adv. Energy Mater.* **2023**, *13*, 2300973.
[32] S. S. Zhang, *J. Power Sources* **2013**, *231*, 153.
[33] J. T. Lee, K. Eom, F. Wu, H. Kim, D. C. Lee, B. Zdyrko, G. Yushin, *ACS Energy Lett.* **2016**, *1*, 373.
[34] G. Liu, Q. Sun, Q. Li, J. Zhang, J. Ming, *Energy and Fuels* **2021**, *35*, 10405.
[35] Y. T. Weng, H. Wang, R. C. Lee, C. Y. Huang, S. S. Huang, M. Abdollahifar, L. M. Kuo, B. J. Hwang, C. L. Kuo, Y. Cui, N. L. Wu, *J. Power Sources* **2020**, *450*, 227676.
[36] T. Feng, T. Zhao, N. Zhang, Y. Duan, L. Li, F. Wu, R. Chen, *Adv. Funct. Mater.* **2022**, *32*, 2202766.
[37] P. Zeng, C. Liu, C. Cheng, C. Yuan, K. Dai, J. Mao, L. Zheng, J. Zhang, L. Y. Chang, S. C. Haw, T. S. Chan, H. Lin, L. Zhang, *J. Mater. Chem. A* **2021**, *9*, 18526.
[38] S. Jin, S. Xin, L. Wang, Z. Du, L. Cao, J. Chen, X. Kong, M. Gong, J. Lu, Y. Zhu, H. Ji, R. S. Ruoff, *Adv. Mater.* **2016**, *28*, 9094.
[39] X. Yang, X. Li, K. Adair, H. Zhang, X. Sun, *Electrochem. Energy Rev.* **2018**, *1*, 239.

[40] T. Li, X. Bai, U. Gulzar, Y. J. Bai, C. Capiglia, W. Deng, X. Zhou, Z. Liu, Z. Feng, R. P Zaccaria, *Adv. Funct. Mater.* **2019**, *39*, 1901730.
[41] A. Karton, *Chem. Phys. Impact* **2021**, *3*, 100047.
[42] Sungjemmenla, C. B. S, S. K. Vineeth, V. Kumar, *Adv. Energy Sustain. Res.* **2022**, *3*, 2100157.
[43] W. J. Chung, J. J. Griebel, E. T. Kim, H. Yoon, A. G. Simmonds, H. J. Ji, P. T. Dirlam, R. S. Glass, J. J. Wie, N. A. Nguyen, B. W. Guralnick, J. Park, Á. Somogyi, P. Theato, M. E. Mackay, Y.-E. Sung, K. Char, J. Pyun, *Nat. Chem.* **2013**, *5*, 518.
[44] C. Barchasz, F. Molton, C. Duboc, J. C. Leprêtre, S. Patoux, F. Alloin, *Anal. Chem.* **2012**, *84*, 3973.
[45] J. Yan, X. Liu, B. Li, J. Yan, B. Li, X. Liu, *Adv. Sci.* **2016**, *3*, 1600101.
[46] D. W. Wang, Q. Zeng, G. Zhou, L. Yin, F. Li, H. M. Cheng, I. R. Gentle, G. Q. M. Lu, *J. Mater. Chem. A* **2013**, *1*, 9382.
[47] K. Kumaresan, Y. Mikhaylik, R. E. White, *J. Electrochem. Soc.* **2008**, *155*, A576.
[48] Y. Li, S. Guo, *Matter* **2021**, *4*, 1142.
[49] H. Pan, Z. Cheng, P. He, H. Zhou, *Energy Fuels* **2020**, *34*, 11942.
[50] Q. Wang, J. Zheng, E. Walter, H. Pan, D. Lv, P. Zuo, H. Chen, Z. D. Deng, B. Y. Liaw, X. Yu, X. Yang, J.-G. Zhang, J. Liu, J. Xiao, *J. Electrochem. Soc.* **2015**, *162*, A474.
[51] S. Zhang, K. Ueno, K. Dokko, M. Watanabe, *Adv. Energy Mater.* **2015**, *5*, 201500117.
[52] Y. V. Mikhaylik, J. R. Akridge, *J. Electrochem. Soc.* **2004**, *151*, A1969.
[53] B. Li, H. Xu, Y. Ma, S. Yang, *Nanoscale Horiz.* **2019**, *4*, 77.
[54] H. Chen, Z. Wu, M. Zheng, T. Liu, C. Yan, J. Lu, S. Zhang, *Mater. Today* **2022**, *52*, 364.
[55] Y. S. Su, Y. Fu, T. Cochell, A. Manthiram, *Nat. Commun.* **2013**, *4*, 1.
[56] J. Ming, M. Li, P. Kumar, A. Y. Lu, W. Wahyudi, L. J. Li, *ACS Energy Lett.* **2016**, *1*, 529.
[57] Y. Zhao, Z. Wang, X. Zhao, X. Wang, K. H. Lam, F. Chen, L. Zhao, S. Wang, X. Hou, *Energy and Fuels* **2020**, *34*, 10188.
[58] Y. Wang, G. J. Weng, in *Micromechanics Nanomechanics Compos. Solids*, Springer International Publishing, Cham **2018**, pp. 123–156.
[59] B. Marinho, M. Ghislandi, E. Tkalya, C. E. Koning, G. de With, *Powder Technol.* **2012**, *221*, 351.
[60] D. Wang, K. Wang, H. Wu, Y. Luo, L. Sun, Y. Zhao, J. Wang, L. Jia, K. Jiang, Q. Li, S. Fan, J. Wang, *Carbon* **2018**, *132*, 370.
[61] Q. Zeng, L. Xu, G. Li, Q. Zhang, S. Guo, H. Lu, L. Xie, J. Yang, J. Weng, C. Zheng, S. Huang, *Adv. Funct. Mater.* **2023**, *33*, 2304619.
[62] X. Zhang, T. Yang, Y. Zhang, X. Wang, J. Wang, Y. Li, A. Yu, X. Wang, Z. Chen, *Adv. Mater.* **2023**, *35*, 2208470.
[63] C. Tang, Q. Zhang, M. Q. Zhao, J. Q. Huang, X. B. Cheng, G. L. Tian, H. J. Peng, F. Wei, *Adv. Mater.* **2014**, *26*, 6100.
[64] L. Zhu, H. J. Peng, J. Liang, J. Q. Huang, C. M. Chen, X. Guo, W. Zhu, P. Li, Q. Zhang, *Nano Energy* **2015**, *11*, 746.
[65] H. Zhang, S. Xin, J. Li, H. Cui, Y. Liu, Y. Yang, M. Wang, *Nano Energy* **2021**, *85*, 106011.
[66] L. Zhang, M. Ling, J. Feng, L. Mai, G. Liu, J. Guo, *Energy Storage Mater.* **2018**, *11*, 24.
[67] M. Baloch, D. Shanmukaraj, O. Bondarchuk, E. Bekaert, T. Rojo, M. Armand, *Energy Storage Mater.* **2017**, *9*, 141.
[68] J. Zhu, Y. Ge, D. Kim, Y. Lu, C. Chen, M. Jiang, X. Zhang, *Nano Energy* **2016**, *20*, 176.
[69] L. Peng, M. Zhang, L. Zheng, Q. Yuan, Z. Yu, J. Shen, Y. Chang, Y. Wang, A. Li, *Small Methods* **2022**, *6*, 2200332.
[70] S. Bai, X. Liu, K. Zhu, S. Wu, H. Zhou, *Nat. Energy* **2016**, *1*, 16094.
[71] J. Liu, Y. Zhou, T. Yan, X. P. Gao, *Adv. Funct. Mater.* **2024**, *34*, 2309625.
[72] Z. Shi, Z. Tian, D. Guo, Y. Wang, Z. Bayhan, A. S. Alzahrani, H. N. Alshareef, *ACS Energy Lett.* **2023**, *8*, 3054.
[73] Y. Lin, S. Huang, L. Zhong, S. Wang, D. Han, S. Ren, M. Xiao, Y. Meng, *Energy Storage Mater.* **2021**, *34*, 128.
[74] D. Wang, L.-J. Jhang, R. Kou, M. Liao, S. Zheng, H. Jiang, P. Shi, G.-X. Li, K. Meng, D. Wang, *Nat. Commun.* **2023**, *14*, 1895.
[75] A. Rafie, J. W. Kim, K. K. Sarode, V. Kalra, *Energy Storage Mater.* **2022**, *50*, 197.
[76] R. Pai, A. Singh, M. H. Tang, V. Kalra, *Commun. Chem.* **2022**, *5*, 17.
[77] Z. Qiao, Y. Zhang, Z. Meng, Q. Xie, L. Lin, H. Zheng, B. Sa, J. Lin, L. Wang, D. L. Peng, *Adv. Funct. Mater.* **2021**, *31*, 2100970.
[78] G. Zeng, Y. Liu, D. Chen, C. Zhen, Y. Han, W. He, *Adv. Energy Mater.* **2021**, *11*, 2102058.
[79] Y. Peng, R. Badam, T. P. Jayakumar, W. Wannapakdee, C. Changtong, N. Matsumi, *J. Electrochem. Soc.* **2022**, *169*, 050515.
[80] X. Cai, B. Cui, B. Ye, W. Wang, J. Ding, G. Wang, *ACS Appl. Mater. Interfaces* **2019**, *11*, 38136.
[81] Z. Ma, Z. Qi, G. Song, S. Huang, Z. Du, J. Dong, C. Guan, P. Luo, P. Gan, B. Yu, B. Guo, J. Chen, M. Wang, J. Zhang, X. Li, J. Zhang, F. Li, *Adv. Funct. Mater.* **2024**, *34*, 2403101.
[82] Z. Yuan, H. J. Peng, T. Z. Hou, J. Q. Huang, C. M. Chen, D. W. Wang, X. B. Cheng, F. Wei, Q. Zhang, *Nano Lett.* **2016**, *16*, 519.
[83] S. Wang, S. Feng, J. Liang, Q. Su, F. Zhao, H. Song, M. Zheng, Q. Sun, Z. Song, X. Jia, J. Yang, Y. Li, J. Liao, R. Li, X. Sun, *Adv. Energy Mater.* **2021**, *11*, 2003314.
[84] F. Shi, L. Zhai, Q. Liu, J. Yu, S. P. Lau, B. Y. Xia, Z. L. Xu, *J. Energy Chem.* **2023**, *76*, 127.
[85] W. Hua, H. Li, C. Pei, J. Xia, Y. Sun, C. Zhang, W. Lv, Y. Tao, Y. Jiao, B. Zhang, S. Z. Qiao, Y. Wan, Q. H. Yang, *Adv. Mater.* **2021**, *33*, 2101006.
[86] Z. Ye, H. Sun, H. Gao, L. Sun, J. Guo, Y. Jiang, C. Wu, S. Zheng, *Energy Storage Mater.* **2023**, *60*, 102855.
[87] D. Yang, M. Li, X. Zheng, X. Han, C. Zhang, J. Jacas Biendicho, J. Llorca, J. Wang, H. Hao, J. Li, G. Henkelman, J. Arbiol, J. R. Morante, D. Mitlin, S. Chou, A. Cabot, *ACS Nano* **2022**, *16*, 11102.
[88] H. J. Li, Y. H. Song, K. Xi, W. Wang, S. Liu, G. R. Li, X. P. Gao, *J. Mater. Chem. A* **2021**, *9*, 10704.
[89] C. Luo, X. Liang, Y. Y. Sun, W. Lv, Y. Y. Sun, Z. Lu, W. Hua, H. Yang, R. Wang, C. Yan, J. Li, Y. Wan, Q.-H. H. Yang, *Energy Storage Mater.* **2020**, *33*, 290.
[90] M. Zhao, X. Chen, X. Y. Li, B. Q. Li, J. Q. Huang, *Adv. Mater.* **2021**, *33*, 2170100.
[91] C. Dong, C. Zhou, M. Wu, Y. Yu, K. Yu, K. Yan, C. Shen, J. Gu, M. Yan, C. Sun, L. Mai, X. Xu, *Adv. Energy Mater.* **2023**, *13*, 2301505.
[92] W. Qu, Z. Lu, C. Geng, L. Wang, Y. Guo, Y. Zhang, W. Wang, W. Lv, Q. Yang, *Adv. Energy Mater.* **2022**, *12*, 2202232.
[93] J. Sun, Y. Liu, L. Liu, J. Bi, S. Wang, Z. Du, H. Du, K. Wang, W. Ai, W. Huang, *Adv. Mater.* **2023**, *35*, 2211168.
[94] J. Sun, Y. Liu, L. Liu, S. He, Z. Du, K. Wang, L. Xie, H. Du, W. Ai, *Nano Lett.* **2022**, *22*, 3728.
[95] D. Zhang, S. Wang, R. Hu, J. Gu, Y. Cui, B. Li, W. Chen, C. Liu, J. Shang, S. Yang, *Adv. Funct. Mater.* **2020**, *30*, 2002471.
[96] J. Offermann, E. Gayretli, C. Schmidt, J. Carstensen, H. G. Bremes, A. Würsig, S. Hansen, M. Abdollahifar, R. Adelung, *J. Colloid Interface Sci.* **2024**, *664*, 444.
[97] J. Wang, G. Li, D. Luo, Y. Zhang, Y. Zhao, G. Zhou, L. Shui, X. Wang, Z. Chen, *Adv. Energy Mater.* **2020**, *10*, 2002076.
[98] T. Wang, D. Luo, Y. Zhang, Z. Zhang, J. Wang, G. Cui, X. Wang, A. Yu, Z. Chen, *ACS Nano* **2021**, *15*, 19457.
[99] Y. Zhang, X. Liu, L. Wu, W. Dong, F. Xia, L. Chen, N. Zhou, L. Xia, Z. Y. Hu, J. Liu, H. S. H. Mohamed, Y. Li, Y. Zhao, L. Chen, B. L. Su, *J. Mater. Chem. A* **2020**, *8*, 2741.
[100] X. Long, Z.-H. Luo, W.-H. Zhou, S.-K. Zhu, Y. Song, H. Li, C.-N. Geng, B. Shi, Z.-Y. Han, G.-M. Zhou, W. Lv, J.-J. Shao, *Energy Storage Mater.* **2022**, *52*, 120.
[101] Z. Liang, C. Peng, J. Shen, J. Yuan, Y. Yang, D. Xue, M. Zhu, J. Liu, *Small* **2024**, *20*, 2309717.
[102] S. Tian, Q. Zeng, G. Liu, J. Huang, X. Sun, D. Wang, H. Yang, Z. Liu, X. Mo, Z. Wang, K. Tao, S. Peng, *Nano-Micro Lett.* **2022**, *14*, 196.
[103] X. Wu, R. Xie, D. Cai, B. Fei, C. Zhang, Q. Chen, B. Sa, H. Zhan, *Adv. Funct. Mater.* **2024**, *34*, 2315012.

[104] W. Li, H. Yao, K. Yan, G. Zheng, Z. Liang, Y.-M. Chiang, Y. Cui, *Nat. Commun.* **2015**, *6*, 7436.
[105] S. Dörfler, H. Althues, P. Härtel, T. Abendroth, B. Schumm, S. Kaskel, *Joule* **2020**, *4*, 539.
[106] Y. Chen, T. Wang, H. Tian, D. Su, Q. Zhang, G. Wang, *Adv. Mater.* **2021**, *33*, 2003666.
[107] W. Ren, W. Ma, S. Zhang, B. Tang, *Energy Storage Mater.* **2019**, *23*, 707.
[108] A. Tomaszewska, Z. Chu, X. Feng, S. O'Kane, X. Liu, J. Chen, C. Ji, E. Endler, R. Li, L. Liu, Y. Li, S. Zheng, S. Vetterlein, M. Gao, J. Du, M. Parkes, M. Ouyang, M. Marinescu, G. Offer, B. Wu, *eTransportation* **2019**, *1*, 100011.
[109] P. Wang, B. Xi, M. Huang, W. Chen, J. Feng, S. Xiong, *Adv. Energy Mater.* **2021**, *11*, 2002893.
[110] X. Fan, W. Sun, F. Meng, A. Xing, J. Liu, *Green Energy Environ.* **2018**, *3*, 2.
[111] R. Fang, G. Li, S. Zhao, L. Yin, K. Du, P. Hou, S. Wang, H. M. Cheng, C. Liu, F. Li, *Nano Energy* **2017**, *42*, 205.
[112] Z. Xiao, Z. Yang, H. Nie, Y. Lu, K. Yang, S. Huang, *J. Mater. Chem. A* **2014**, *2*, 8683.
[113] Y. C. Jeong, K. Lee, T. Kim, J. H. Kim, J. Park, Y. S. Cho, S. J. Yang, C. R. Park, *J. Mater. Chem. A* **2016**, *4*, 819.
[114] G. Zhou, L. Li, C. Ma, S. Wang, Y. Shi, N. Koratkar, W. Ren, F. Li, H. M. Cheng, *Nano Energy* **2015**, *11*, 356.
[115] G. Zhou, E. Paek, G. S. Hwang, A. Manthiram, *Nat. Commun.* **2015**, *6*, 7760.
[116] Z. Sun, J. Zhang, L. Yin, G. Hu, R. Fang, H.-M. Cheng, F. Li, *Nat. Commun.* **2017**, *8*, 14627.
[117] T. Wang, Q. Zhang, J. Zhong, M. Chen, H. Deng, J. Cao, L. Wang, L. Peng, J. Zhu, B. Lu, *Adv. Energy Mater.* **2021**, *11*, 2100448.
[118] J. Pu, W. Gong, Z. Shen, L. Wang, Y. Yao, G. Hong, *Adv. Sci.* **2022**, *9*, 2104375.
[119] R. Gao, M. Zhang, Z. Han, X. Xiao, X. Wu, Z. Piao, Z. Lao, L. Nie, S. Wang, G. Zhou, *Adv. Mater.* **2024**, *36*, 2303610.
[120] X. Zhang, C. Shang, E. M. Akinoglu, X. Wang, G. Zhou, *Adv. Sci.* **2020**, *7*, 2002037.
[121] J. S. Lee, W. Kim, J. Jang, A. Manthiram, *Adv. Energy Mater.* **2017**, *7*, 1601943.
[122] Z. Li, J. T. Zhang, Y. M. Chen, J. Li, X. W. Lou, *Nat. Commun.* **2015**, *6*, 8850.
[123] J. Xu, L. Yang, S. Cao, J. Wang, Y. Ma, J. Zhang, X. Lu, *Adv. Sci.* **2021**, *8*, 2101019.
[124] Z. H. Chen, X. L. Du, J. B. He, F. Li, Y. Wang, Y. L. Li, B. Li, S. Xin, *ACS Appl. Mater. Interfaces* **2017**, *9*, 33855.
[125] M. Zhong, J. Guan, J. Sun, X. Shu, H. Ding, L. Chen, N. Zhou, Z. Xiao, *Energy Storage Mater.* **2021**, *41*, 588.
[126] L. Huang, S. Shen, Y. Zhong, Y. Zhang, L. Zhang, X. Wang, X. Xia, X. Tong, J. Zhou, J. Tu, *Adv. Mater.* **2022**, *34*, 2107415.
[127] J. Wang, W. Han, *Adv. Funct. Mater.* **2022**, *32*, 2107166.
[128] K. Zou, W. Jing, X. Dai, X. Chen, M. Shi, Z. Yao, T. Zhu, J. Sun, Y. Chen, Y. Liu, Y. Liu, *Small* **2022**, *18*, 2107380.
[129] W. Deng, Z. Xu, Z. Deng, X. Wang, *J. Mater. Chem. A* **2021**, *9*, 21760.
[130] Q. Jin, L. R. Zhang, M. L. Zhao, L. Li, X. B. Yu, J. P. Xiao, L. Kong, X. T. Zhang, *Adv. Funct. Mater.* **2024**, *34*, 2309624.
[131] X. L. Fan, L. Q. Ping, F. L. Qi, Z. A. Ghazi, X. N. Tang, R. P. Fang, Z. H. Sun, H. M. Cheng, C. Liu, F. Li, *Carbon* **2019**, *154*, 90.
[132] L. Sun, D. Wang, Y. Luo, K. Wang, W. Kong, Y. Wu, L. Zhang, K. Jiang, Q. Li, Y. Zhang, J. Wang, S. Fan, *ACS Nano* **2016**, *10*, 1300.
[133] S. Xin, L. Gu, N. H. Zhao, Y. X. Yin, L. J. Zhou, Y. G. Guo, L. J. Wan, *J. Am. Chem. Soc.* **2012**, *134*, 18510.
[134] Z. Zhao, S. Wang, R. Liang, Z. Li, Z. Shi, G. Chen, *J. Mater. Chem. A* **2014**, *2*, 13509.
[135] R. Sahore, L. P. Estevez, A. Ramanujapuram, F. J. Disalvo, E. P. Giannelis, *J. Power Sources* **2015**, *297*, 188.
[136] G. W. Sun, C. Y. Zhang, Z. Dai, M. J. Jin, Q. Y. Liu, J. L. Pan, Y. C. Wang, X. P. Gao, W. Lan, G. Z. Sun, C. S. Gong, Z. X. Zhang, X. J. Pan, J. Li, J. Y. Zhou, *J. Colloid Interface Sci.* **2022**, *608*, 459.
[137] L. Li, Z. Ma, Y. Li, *Carbon* **2022**, *197*, 200.
[138] J. Li, H. Zhang, L. Luo, H. Li, J. He, H. Zu, L. Liu, H. Liu, F. Wang, J. Song, *J. Mater. Chem. A* **2021**, *9*, 2205.
[139] J. Cheng, Y. Liu, X. Zhang, X. Miao, Y. Chen, S. Chen, J. Lin, Y. Zhang, *Chem. Eng. J.* **2021**, *419*, 129649.
[140] Y. Song, X. Long, Z. Luo, C. Guo, C. N. Geng, Q. S. Ouyang, Z. Han, G. Zhou, J. J. Shao, *ACS Appl. Mater. Interfaces* **2022**, *14*, 32183.
[141] D. Cheng, Y. Zhao, X. Tang, T. An, X. Wang, H. Zhou, D. Zhang, T. Fan, *Carbon* **2019**, *149*, 750.
[142] J. Xie, J. Yang, X. Zhou, Y. Zou, J. Tang, S. Wang, F. Chen, *J. Power Sources* **2014**, *253*, 55.
[143] M. Li, X. Zhou, X. Ma, L. Chen, D. Zhang, S. Xu, D. Duan, C. Chen, Q. Yuan, S. Liu, *Chem. Eng. J.* **2021**, *409*, 128164.
[144] C. Zheng, S. Niu, W. Lv, G. Zhou, J. Li, S. Fan, Y. Deng, Z. Pan, B. Li, F. Kang, Q.-H. Yang, *Nano Energy* **2017**, *33*, 306.
[145] J. Lin, Y. Mo, S. Li, J. Yu, *J. Mater. Chem. A* **2022**, *10*, 690.
[146] Y. Peng, Y. Zhang, Z. Wen, Y. Wang, Z. Chen, B. J. Hwang, J. Zhao, *Chem. Eng. J.* **2018**, *346*, 57.
[147] H. Jiang, X. Liu, Y. Wu, Y. Shu, X. Gong, F. Ke, H. Deng, *Angew. Chemie* **2018**, *130*, 3980.
[148] S. Li, Z. Han, W. Hu, L. Peng, J. Yang, L. Wang, Y. Zhang, B. Shan, J. Xie, *Nano Energy* **2019**, *60*, 153.
[149] A. Abdul Razzaq, Y. Yao, R. Shah, P. Qi, L. Miao, M. Chen, X. Zhao, Y. Peng, Z. Deng, *Energy Storage Mater.* **2019**, *16*, 194.
[150] S. Ma, Z. Zhang, Y. Wang, Z. Yu, C. Cui, M. He, H. Huo, G. Yin, P. Zuo, *Chem. Eng. J.* **2021**, *418*, 129410.
[151] M. Yan, H. Chen, Y. Yu, H. Zhao, C. Li, Z. Hu, P. Wu, L. Chen, H. Wang, D. Peng, H. Gao, T. Hasan, Y. Li, B. Su, *Adv. Energy Mater.* **2018**, *8*, 1801066.
[152] G. C. Li, G. R. Li, S. H. Ye, X. P. Gao, *Adv. Energy Mater.* **2012**, *2*, 1238.
[153] J. Yan, B. Li, X. Liu, *Nano Energy* **2015**, *18*, 245.
[154] L. Li, J. Yang, G. Duan, C. Zhang, K. Liu, S. Jiang, H. Hou, *J. Energy Storage* **2024**, *90*, 111933.
[155] H. Xiang, N. Deng, H. Zhao, X. Wang, L. Wei, M. Wang, B. Cheng, W. Kang, *J. Energy Chem.* **2021**, *58*, 523.
[156] B. Wang, Y. Wang, Y. Lan, G. Lu, L. Liu, T. Tang, M. Li, Y. Cheng, J. Xiao, X. Li, *Angew. Chem., Int. Ed.* **2024**, *63*, 202406693.
[157] R. Gao, Q. Zhang, Y. Zhao, Z. Han, C. Sun, J. Sheng, X. Zhong, B. Chen, C. Li, S. Ni, Z. Piao, B. Li, G. Zhou, *Adv. Funct. Mater.* **2022**, *32*, 2110313.
[158] H. Kang, H. Kim, M. J. Park, *Adv. Energy Mater.* **2018**, *8*, 1802423.
[159] J. Liu, H. Li, J. Wang, Y. Zhang, D. Luo, Y. Zhao, Y. Li, A. Yu, X. Wang, Z. Chen, *Adv. Energy Mater.* **2021**, *11*, 2101926.
[160] Y. Tao, Y. Wei, Y. Liu, J. Wang, W. Qiao, L. Ling, D. Long, *Energy Environ. Sci.* **2016**, *9*, 3230.
[161] Z. W Seh, W. Li, J. J. Cha, G. Zheng, Y. Yang, M. T. McDowell, P.-C. Hsu, Y. Cui, *Nat. Commun.* **2013**, *4*, 1331.
[162] L. Ma, L. J. Yu, J. Liu, Y. Q. Su, S. Li, X. Zang, T. Meng, S. Zhang, J. Song, J. Wang, X. Zhao, Z. Cui, N. Wang, Y. Zhao, *Energy Storage Mater.* **2022**, *44*, 180.
[163] R. Xiao, D. Luo, J. Wang, H. Lu, H. Ma, E. M. Akinoglu, M. Jin, X. Wang, Y. Zhang, Z. Chen, *Adv. Sci.* **2022**, *9*, 2202352.
[164] R. Li, D. Rao, J. Zhou, G. Wu, G. G. Wang, Z. Zhu, X. Han, R. Sun, H. Li, C. Wang, W. Yan, X. Zheng, P. Cui, Y. Wu, G. G. Wang, X. Hong, *Nat. Commun.* **2021**, *12*, 3102.
[165] L. Niu, T. Wu, D. Zhou, J. Qi, Z. Xiao, *Energy Storage Mater.* **2022**, *45*, 840.
[166] J. Wang, G. Li, D. Luo, Y. Zhao, Y. Zhang, G. Zhou, L. Shui, X. Wang, *J. Mater. Chem. A* **2021**, *9*, 11160.
[167] Y. Zhou, C. Zhou, Q. Li, C. Yan, B. Han, K. Xia, Q. Gao, J. Wu, *Adv. Mater.* **2015**, *27*, 3774.

[168] J. Zhang, Z. Li, Y. Chen, S. Gao, X. W. Lou, *Angew. Chemie* **2018**, *130*, 11110.
[169] J. Y. Hwang, H. M. Kim, S. Shin, Y. K. Sun, *Adv. Funct. Mater.* **2018**, *28*, 1704294.
[170] W. Qiu, G. Li, D. Luo, Y. Zhang, Y. Zhao, G. Zhou, L. Shui, X. Wang, Z. Chen, *Adv. Sci.* **2021**, *8*, 2003400.
[171] Q. Liu, Z. Li, J. Li, L. Ma, W. Yue, *J. Energy Storage* **2024**, *81*, 110479.
[172] S. H. Chung, L. Luo, A. Manthiram, *ACS Energy Lett.* **2018**, *3*, 568.
[173] W. Sun, S. Liu, Y. Li, D. Wang, Q. Guo, X. Hong, K. Xie, Z. Ma, C. Zheng, S. Xiong, *Adv. Funct. Mater.* **2022**, *32*, 2205471.
[174] L. Luo, S. Chung, A. Manthiram, *Adv. Energy Mater.* **2018**, *8*, 1801014.
[175] R. Chu, T. T. Nguyen, Y. Bai, N. H. Kim, J. H. Lee, *Adv. Energy Mater.* **2022**, *12*, 2102805.
[176] D. Yang, Z. Liang, C. Zhang, J. J. Biendicho, M. Botifoll, M. C. Spadaro, Q. Chen, M. Li, A. Ramon, A. O. Moghaddam, J. Llorca, J. Wang, J. R. Morante, J. Arbiol, S. L. Chou, A. Cabot, *Adv. Energy Mater.* **2021**, *11*, 2101250.
[177] M. Li, D. Yang, J. J. Biendicho, X. Han, C. Zhang, K. Liu, J. Diao, J. Li, J. Wang, M. Heggen, R. E. Dunin-Borkowski, J. Wang, G. Henkelman, J. R. Morante, J. Arbiol, S. Chou, A. Cabot, *Adv. Funct. Mater.* **2022**, *32*, 2200529.
[178] Z. Zhou, Z. Chen, H. Lv, Y. Zhao, H. Wei, B. Chen, Y. Wang, *Energy Storage Mater.* **2022**, *51*, 486.
[179] M. Zheng, J. Zhao, W. Wu, R. Chen, S. Chen, N. Cheng, *Small* **2024**, *20*, 2303192.
[180] T. Zhou, W. Lv, J. Li, G. Zhou, Y. Zhao, S. Fan, B. Liu, B. Li, F. Kang, Q. H. Yang, *Energy Environ. Sci.* **2017**, *10*, 1694.
[181] R. Hou, S. Zhang, Y. Zhang, N. Li, S. Wang, B. Ding, G. Shao, P. Zhang, *Adv. Funct. Mater.* **2022**, *32*, 2200302.
[182] Y. Liu, X. Huang, H. Zhang, G. Qin, X. Wang, M. Song, H. Liang, J. Hong, Y. Huang, *J. Mater. Sci. Technol.* **2024**, *173*, 54.
[183] S. Huang, Y. Von Lim, X. Zhang, Y. Wang, Y. Zheng, D. Kong, M. Ding, S. A. Yang, H. Y. Yang, *Nano Energy* **2018**, *51*, 340.
[184] J. Cheng, D. Zhao, L. Fan, X. Wu, M. Wang, N. Zhang, K. Sun, *J. Mater. Chem. A* **2017**, *5*, 14519.
[185] X. Tian, Y. Zhou, B. Zhang, N. B. S. Selabi, G. Wang, *J. Energy Chem.* **2022**, *74*, 239.
[186] Y. H. Liu, W. Chang, J. Qu, Y. Q. Sui, Y. Abdelkrim, H. J. Liu, X. Z. Zhai, Y. G. Guo, Z. Z. Yu, *Energy Storage Mater.* **2022**, *46*, 313.
[187] R. Xiao, T. Yu, S. Yang, K. Chen, Z. Li, Z. Liu, T. Hu, G. Hu, J. Li, H. M. Cheng, Z. Sun, F. Li, *Energy Storage Mater.* **2022**, *51*, 890.
[188] C. Dong, C. Ma, C. Zhou, Y. Yu, J. Wang, K. Yu, C. Shen, J. Gu, K. Yan, A. Zheng, M. Gong, X. Xu, L. Mai, *Adv. Mater.* **2024**, *36*, 2407070.
[189] X. Wang, X. Zhang, Y. Zhang, J. Wang, J. Liu, S. Li, X. Liu, M. Jin, L. Zhao, G. Li, X. Wang, *Adv. Energy Mater.* **2024**, *14*, 2400926.
[190] Y. Wang, R. Zhang, J. Chen, H. Wu, S. Lu, K. Wang, H. Li, C. J. Harris, K. Xi, R. V. Kumar, S. Ding, *Adv. Energy Mater.* **2019**, *9*, 1900953.
[191] M. Li, Y. Zhang, X. Wang, W. Ahn, G. Jiang, K. Feng, G. Lui, Z. Chen, *Adv. Funct. Mater.* **2016**, *26*, 8408.
[192] C. Wen, X. Zheng, X. Li, M. Yuan, H. Li, G. Sun, *Chem. Eng. J.* **2021**, *409*, 128102.
[193] H. Wang, S. A. He, Z. Cui, C. Xu, J. Zhu, Q. Liu, G. He, W. Luo, R. Zou, *Chem. Eng. J.* **2021**, *420*, 129693.
[194] K. Guan, X. Li, Q. Xie, L. Huang, H. Zhang, G. Li, W. Lei, *Chem. Eng. J.* **2024**, *492*, 151978.
[195] Z. Zhu, Y. Zeng, Z. Pei, D. Luan, X. Wang, *Angew. Chem., Int. Ed.* **2023**, *62*, 202305828.
[196] X. Wang, C. Zhao, B. Liu, S. Zhao, Y. Zhang, L. Qian, Z. Chen, J. Wang, X. Wang, Z. Chen, *Adv. Energy Mater.* **2022**, *12*, 2201960.
[197] D. Yang, Z. Liang, P. Tang, C. Zhang, M. Tang, Q. Li, J. J. Biendicho, J. Li, M. Heggen, R. E. Dunin-Borkowski, M. Xu, J. Llorca, J. Arbiol, J. R. Morante, S. Chou, A. Cabot, *Adv. Mater.* **2022**, *34*, 2108835.
[198] M. Ma, X. Lu, Y. Guo, L. Wang, X. Liang, *TrAC Trends Anal. Chem.* **2022**, *157*, 116741.
[199] C. Altintas, I. Erucar, S. Keskin, *CrystEngComm* **2022**, *24*, 7360.
[200] W. Liu, L. Gong, Z. Liu, Y. Jin, H. Pan, X. Yang, B. Yu, N. Li, D. Qi, K. Wang, H. Wang, J. Jiang, *J. Am. Chem. Soc.* **2022**, *144*, 17209.
[201] H. Duan, K. Li, M. Xie, J. M. Chen, H. G. Zhou, X. Wu, G. H. Ning, A. I. Cooper, D. Li, *J. Am. Chem. Soc.* **2021**, *143*, 19446.
[202] B. Du, Y. Luo, Y. Yang, W. Xue, G. Liu, J. Li, *Chem. Eng. J.* **2022**, *442*, 135823.
[203] X. Song, D. Tian, Y. Qiu, X. Sun, B. Jiang, C. Zhao, Y. Zhang, L. Fan, N. Zhang, *Energy Storage Mater.* **2021**, *41*, 248.
[204] T. Chen, Z. Zhang, B. Cheng, R. Chen, Y. Hu, L. Ma, G. Zhu, J. Liu, Z. Jin, *J. Am. Chem. Soc.* **2017**, *139*, 12710.
[205] X. Zhao, Y. Guan, X. Du, G. Liu, J. Li, G. Li, *Chem. Eng. J.* **2022**, *431*, 134242.
[206] D. Yang, C. Zhang, J. J. Biendicho, X. Han, Z. Liang, R. Du, M. Li, J. Li, J. Arbiol, J. Llorca, Y. Zhou, J. R. Morante, A. Cabot, *ACS Nano* **2020**, *14*, 15492.
[207] Z. Ye, Y. Jiang, J. Qian, W. Li, T. Feng, L. Li, F. Wu, R. Chen, *Nano Energy* **2019**, *64*, 103965.
[208] Z. Li, L. Yin, *ACS Appl. Mater. Interfaces* **2015**, *7*, 4029.
[209] S. Lv, X. Ma, S. Ke, Y. Wang, T. Ma, S. Yuan, Z. Jin, J. L. Zuo, *J. Am. Chem. Soc.* **2024**, *146*, 9385.
[210] B. Li, S. Zhang, L. Kong, H. Peng, Q. Zhang, *Adv. Mater.* **2018**, *30*, 1707483.
[211] W. Yao, W. Zheng, K. Han, S. Xiao, *J. Mater. Chem. A* **2020**, *8*, 19028.
[212] J. Zhang, C. P. Yang, Y. X. Yin, L. J. Wan, Y. G. Guo, *Adv. Mater.* **2016**, *28*, 9539.
[213] J. He, L. Luo, Y. Chen, A. Manthiram, *Adv. Mater.* **2017**, *29*, 1702707.
[214] D. Luo, G. Li, Y. Deng, Z. Zhang, J. Li, R. Liang, M. Li, Y. Jiang, W. Zhang, Y. Liu, W. Lei, A. Yu, Z. Chen, *Adv. Energy Mater.* **2019**, *9*, 1900228.
[215] Q. Yang, S. Shen, Z. Han, G. Li, D. Liu, Q. Zhang, L. Song, D. Wang, G. Zhou, Y. Song, *Adv. Mater.* **2024**, *36*, 2405790.
[216] Z. Yu, X. Huang, M. Zheng, S. Zhang, Y. Yang, J. Lu, *Adv. Mater.* **2023**, *35*, 2300861.
[217] Q. Yang, C. Wang, L. Song, Y. Zhang, Z. Shen, W. Cai, Y. Song, *Angew. Chemie* **2025**, *137*, 202415078.
[218] H. Moon, M.-H. Ryou, A. Park, B.-Q. Li, H. N. Kim, N. Park, E. Lee, K. Y. Chung, J.-Q. Huang, T. Yim, W. B. Lee, S.-Y. Lee, *ACS Energy Lett.* **2025**, *10*, 1654.
[219] Z. Han, S. Li, R. Xiong, Z. Jiang, M. Sun, W. Hu, L. Peng, R. He, H. Zhou, C. Yu, S. Cheng, J. Xie, *Adv. Funct. Mater.* **2022**, *32*, 2108669.
[220] L. Yin, J. Wang, J. Yang, Y. Nuli, *J. Mater. Chem.* **2011**, *21*, 6807.
[221] H. Kim, J. Lee, H. Ahn, O. Kim, M. J. Park, *Nat. Commun.* **2015**, *6*, 7278.
[222] S. Zeng, L. Li, L. Xie, D. Zhao, N. Zhou, N. Wang, S. Chen, *Carbon* **2017**, *122*, 106.
[223] Y. Cao, Y. Jia, X. Meng, X. Fan, J. Zhang, J. Zhou, D. Matoga, C. W. Bielawski, J. Geng, *Chem. Eng. J.* **2022**, *446*, 137365.
[224] H. Pan, X. X. Huang, C. Wang, D. Liu, D. Wang, R. Zhang, S. Li, C. Lv, L. Zhao, J. Wang, X. X. Huang, *Chem. Eng. J.* **2021**, *410*, 128424.
[225] S. Cheng, J. Wang, S. Duan, J. Zhang, Q. Wang, Y. Zhang, L. Li, H. Liu, Q. Xiao, H. Lin, *Chem. Eng. J.* **2021**, *417*, 128172.
[226] J. Liu, G. Li, D. Luo, J. Li, X. Zhang, Q. Li, H. Li, Y. Zhang, Z. Chen, *Adv. Funct. Mater.* **2024**, *34*, 202303357.
[227] C. Chang, S. Di, G. Gao, B. Zhai, S. Chen, S. Wang, X. Liu, L. Li, *Chem. Eng. J.* **2022**, *435*, 135031.
[228] D. Deng, H. Xiong, Y. Luo, K. Yu, J. Weng, G. Li, J. Lei, Y. Li, M. Zheng, Q. Wu, *Adv. Mater.* **2024**, 2406135.
[229] W. Xiao, G. K. Kiran, K. Yoo, J. Kim, H. Xu, *Small* **2023**, *19*, 2206750.
[230] Z. Chen, Y. Hu, W. Liu, F. Yu, X. Yu, T. Mei, L. Yu, X. Wang, *ACS Appl. Mater. Interfaces* **2021**, *13*, 38394.

[231] X. Zhang, T. Yang, J. Liu, C. Hu, S. Gao, Z. Shi, Q. Wu, H. Li, Y. Zhang, Z. Chen, *Small* **2024**, *20*, 2311086.
[232] H. Zhu, S. Chen, X. Yao, K. Yang, W. Zhao, T. Chen, L. Yang, F. Pan, *Adv. Funct. Mater.* **2024**, *34*, 2401470.
[233] D. Li, H. Li, S. Zheng, N. Gao, S. Li, J. Liu, L. Hou, J. Liu, B. Miao, J. Bai, Z. Cui, N. Wang, B. Wang, Y. Zhao, *J. Colloid Interface Sci.* **2022**, *607*, 655.
[234] Y. Li, X. Wang, M. Sun, Z. Zhao, Z. Wang, J. Qiu, *J. Mater. Chem. A* **2022**, *10*, 5410.
[235] J. Li, Y. Xu, Y. Zhang, C. He, T. Li, *J. Mater. Chem. A* **2020**, *8*, 19544.
[236] J. Liu, S. Xiao, L. Chang, L. Lai, R. Wu, Y. Xiang, X. Liu, J. S Chen, *J. Energy Chem.* **2021**, *56*, 343.
[237] D. Tian, X. Song, Y. Qiu, X. Sun, B. Jiang, C. Zhao, Y. Zhang, X. Xu, L. Fan, N. Zhang, *ACS Nano* **2021**, *15*, 16515.
[238] C. Huang, J. Yu, C. Y. Zhang, Z. Cui, J. Chen, W. H. Lai, Y. J. Lei, B. Nan, X. Lu, R. He, L. Gong, J. Li, C. Li, X. Qi, Q. Xue, J. Y. Zhou, X. Qi, L. Balcells, J. Arbiol, A. Cabot, *Adv. Mater.* **2024**, *36*, 2400810.
[239] S. Li, P. Xu, M. K. Aslam, C. Chen, A. Rashid, G. Wang, L. Zhang, B. Mao, *Energy Storage Mater.* **2020**, *27*, 51.
[240] W. Xia, Y. Chen, M. Han, X. Wu, H. Yang, K. Fu, M. Chen, X. Wang, H. Shu, *Adv. Funct. Mater.* **2024**, *34*, 2400262.
[241] C. Zhang, J. J. Biendicho, T. Zhang, R. Du, J. Li, X. Yang, J. Arbiol, Y. Zhou, J. R. Morante, A. Cabot, *Adv. Funct. Mater.* **2019**, *29*, 1903842.
[242] L. Chen, Y. Xu, G. Cao, H. M. K. Sari, R. Duan, J. Wang, C. Xie, W. Li, X. Li, *Adv. Funct. Mater.* **2022**, *32*, 2107838.
[243] B. Wang, L. Wang, D. Ding, Y. Zhai, F. Wang, Z. Jing, X. Yang, Y. Kong, Y. Qian, L. Xu, *Adv. Mater.* **2022**, *34*, 2204403.
[244] W. Yao, C. Tian, C. Yang, J. Xu, Y. Meng, I. Manke, N. Chen, Z. Wu, L. Zhan, Y. Wang, R. Chen, *Adv. Mater.* **2022**, *34*, 2106370.
[245] C. Huang, J. Yu, C. Li, Z. Cui, C. Zhang, C. Zhang, B. Nan, J. Li, J. Arbiol, A. Cabot, *Adv. Funct. Mater.* **2023**, *33*, 2305624.
[246] W. Zhang, F. Ma, Q. Wu, Z. Zeng, W. Zhong, S. Cheng, X. Chen, J. Xie, *Energy Environ. Mater.* **2023**, *6*, 12369.
[247] X. Zhao, T. Gao, W. Ren, C. Zhao, Z. H. Liu, L. Li, *J. Energy Chem.* **2022**, *75*, 250.
[248] H. Wang, Z. Cui, S.-A. He, J. Zhu, W. Luo, Q. Liu, R. Zou, *Nano-Micro Lett.* **2022**, *14*, 189.
[249] R. Sun, Y. Bai, Z. Bai, L. Peng, M. Luo, M. Qu, Y. Gao, Z. Wang, W. Sun, K. Sun, *Adv. Energy Mater.* **2022**, *12*, 2102739.
[250] X. Sun, Y. Qiu, B. Jiang, Z. Chen, C. Zhao, H. Zhou, L. Yang, L. Fan, Y. Zhang, N. Zhang, *Nat. Commun.* **2023**, *14*, 291.
[251] D. Lu, X. Wang, Y. Hu, L. Yue, Z. Shao, W. Zhou, L. Chen, W. Wang, Y. Li, *Adv. Funct. Mater.* **2023**, *33*, 2212689.
[252] C. Ma, Y. Zhang, Y. Feng, N. Wang, L. Zhou, C. Liang, L. Chen, Y. Lai, X. Ji, C. Yan, W. Wei, *Adv. Mater.* **2021**, *33*, 2100171.
[253] J. Wang, W. Qiu, G. Li, J. Liu, D. Luo, Y. Zhang, Y. Zhao, G. Zhou, L. Shui, X. Wang, Z. Chen, *Energy Storage Mater.* **2022**, *46*, 269.
[254] R. Wang, R. Wu, X. Yan, D. Liu, P. Guo, W. Li, H. Pan, *Adv. Funct. Mater.* **2022**, *32*, 2200424.
[255] F. Cao, X. Zhang, Z. Jin, J. Zhang, Z. Tian, D. Kong, Y. Li, Y. Li, L. Zhi, *Adv. Energy Mater.* **2024**, *14*, 2303893.
[256] Y. Bai, T. T. Nguyen, H. Song, R. Chu, D. T. Tran, N. H. Kim, J. H. Lee, *Small* **2024**, *20*, 2402074.
[257] Z. Wang, C. Song, H. Shen, S. Ma, G. Li, Y. Li, *Adv. Mater.* **2024**, *36*, 2307786.
[258] L. Ni, G. Yang, Y. Liu, Z. Wu, Z. Ma, C. Shen, Z. Lv, Q. Wang, X. Gong, J. Xie, G. Diao, Y. Wei, *ACS Nano* **2021**, *15*, 12222.
[259] C. Tang, B. Q. Li, Q. Zhang, L. Zhu, H. F. Wang, J. Le Shi, F. Wei, *Adv. Funct. Mater.* **2016**, *26*, 577.
[260] X. Li, Y. Zuo, Y. Zhang, J. Wang, Y. Wang, H. Yu, L. Zhan, L. Ling, Z. Du, S. Yang, *Adv. Energy Mater.* **2024**, *14*, 2303389.
[261] Y. Zhang, G. Li, J. Wang, D. Luo, Z. Sun, Y. Zhao, A. Yu, X. Wang, Z. Chen, *Adv. Energy Mater.* **2021**, *11*, 2100497.
[262] K. Tian, C. Wei, Z. Wang, Y. Li, B. Xi, S. Xiong, J. Feng, *Small* **2024**, *20*, 2309422.
[263] J. Xia, W. Chen, Y. Yang, X. Guan, T. Yang, M. Xiao, S. Zhang, Y. Xing, X. Lu, G. Zhou, *EcoMat* **2022**, *4*, 12183.
[264] X. Wu, Q. Zhang, G. Tang, Y. Cao, H. Yang, H. Li, X. Ai, *Small* **2022**, *18*, 2106144.
[265] B. Sun, D. Wang, Y. Jiang, R. Wang, L. Lyu, G. Diao, W. Zhang, H. Pang, *Adv. Mater.* **2024**, *36*, 2415633.
[266] K. Xiao, J. Wang, Z. Chen, Y. Qian, Z. Liu, L. Zhang, X. Chen, J. Liu, X. Fan, Z. X. Shen, *Small* **2019**, *15*, 1901454.
[267] J. H. Yu, B. J. Lee, S. Zhou, J. H. Sung, C. Zhao, C. H. Shin, B. Yu, G. L. Xu, K. Amine, J. S. Yu, *ACS Nano* **2024**, *18*, 31974.
[268] G. Liu, K. Feng, H. Cui, J. Li, Y. Liu, M. Wang, *Chem. Eng. J.* **2020**, *381*, 122652.
[269] Y. Xiao, W. Gong, S. Guo, Y. Ouyang, D. Li, X. Li, Q. Zeng, W. He, H. Deng, C. Tan, Q. Zhang, S. Huang, *ACS Mater. Lett.* **2021**, *3*, 1684.
[270] J. Q. Huang, H. J. Peng, X. Y. Liu, J. Q. Nie, X. B. Cheng, Q. Zhang, F. Wei, *J. Mater. Chem. A* **2014**, *2*, 10869.
[271] W. Chang, J. Qu, W. Li, Y. Liu, X. Zhai, H. Liu, Y. Kang, Z. Yu, *Small* **2021**, *17*, 2101857.
[272] W. Chen, T. Lei, W. Lv, Y. Hu, Y. Yan, Y. Jiao, W. He, Z. Li, C. Yan, J. Xiong, *Adv. Mater.* **2018**, *30*, 1804084.
[273] J. Liu, Y. Ding, Z. Shen, H. Zhang, T. Han, Y. Guan, Y. Tian, P. V. Braun, *Adv. Sci.* **2022**, *9*, 2103517.
[274] Y. Wu, D. Li, J. Pan, Y. Sun, W. Huang, M. Wu, B. Zhang, F. Pan, K. Shi, Q. Liu, *J. Mater. Chem. A* **2022**, *10*, 16309.
[275] C. Ye, L. Zhang, C. Guo, D. Li, A. Vasileff, H. Wang, S. Qiao, *Adv. Funct. Mater.* **2017**, *27*, 1702524.
[276] G. Zeng, D. Chen, C. Zhen, C. Feng, Y. Pang, W. He, *Small* **2023**, *19*, 2302548.
[277] S. Wu, J. Shi, X. Nie, Y. Yao, F. Jiang, Q. Wei, F. Huang, *Energy Environ. Mater.* **2023**, *6*, 12319.
[278] Y. Zuo, X. Jiao, Z. Huang, J. Lei, M. Liu, L. Dong, W. Yan, J. Zhang, *Adv. Funct. Mater.* **2024**, *34*, 2405853.
[279] M. Liu, Z. Wu, S. Liu, T. Guo, P. Chen, X. Cao, S. Pan, T. Zhou, L. Pompizii, M. Najafov, A. Coskun, Y. Fu, *Angew. Chem., Int. Ed.* **2025**, *64*, 202417624.
[280] Z. A. Ghazi, X. He, A. M. Khattak, N. A. Khan, B. Liang, A. Iqbal, J. Wang, H. Sin, L. Li, Z. Tang, *Adv. Mater.* **2017**, *29*, 1606817.
[281] Y. Jiang, P. Liang, M. Tang, S. Sun, H. Min, J. Han, X. Shen, H. Yang, D. Chao, J. Wang, *J. Mater. Chem. A* **2022**, *10*, 22080.
[282] D. He, J. Meng, X. Chen, Y. Liao, Z. Cheng, L. Yuan, Z. Li, Y. Huang, *Adv. Funct. Mater.* **2021**, *31*, 2001201.
[283] B. Wei, C. Shang, X. Wang, G. Zhou, *Small* **2020**, *16*, 2002789.
[284] D.-Q. Cai, Y.-T. Gao, X.-Y. Wang, J.-L. Yang, S.-X. Zhao, *ACS Appl. Mater. Interfaces* **2022**, *14*, 38651.
[285] S. Deng, T. Guo, J. Heier, C. (John) Zhang, *Adv. Sci.* **2023**, *10*, 2204930.
[286] M. Luo, Y. Bai, R. Sun, M. Qu, M. Wang, Z. Yang, Z. Wang, W. Sun, K. Sun, *J. Energy Chem.* **2022**, *73*, 407.
[287] B. Hao, H. Li, W. Lv, Y. Zhang, S. Niu, Q. Qi, S. Xiao, J. Li, F. Kang, Q. H. Yang, *Nano Energy* **2019**, *60*, 305.
[288] Z. Q. Zhou, H. M. Wang, L. Bin Yang, C. Ma, J. T. Wang, W. M. Qiao, L. C. Ling, *New Carbon Mater* **2024**, *39*, 201.
[289] S. Huang, Z. Wang, Y. Von Lim, Y. Wang, Y. Li, D. Zhang, H. Y. Yang, *Adv. Energy Mater.* **2021**, *11*, 2003689.
[290] Z. Li, F. Zhang, T. Cao, L. Tang, Q. Xu, H. Liu, Y. Wang, *Adv. Funct. Mater.* **2020**, *30*, 2006297.
[291] P. Wang, Z. Shen, C. Xia, K. Lv, H. Zhang, P. He, H. Zhou, *ACS Appl. Mater. Interfaces* **2020**, *12*, 47590.
[292] J. Wang, J. Liang, J. Wu, C. Xuan, Z. Wu, X. Guo, C. Lai, Y. Zhu, D. Wang, *J. Mater. Chem. A* **2018**, *6*, 6503.
[293] Z. Gu, C. Cheng, T. Yan, G. Liu, J. Jiang, J. Mao, K. Dai, J. Li, J. Wu, L. Zhang, *Nano Energy* **2021**, *86*, 106111.

[294] S. H. Kim, J. S. Yeon, R. Kim, K. M. Choi, H. S. Park, *J. Mater. Chem. A* **2018**, *6*, 24971.
[295] Y. Chen, L. Zhang, H. Pan, J. Zhang, S. Xiang, Z. Cheng, Z. Zhang, *J. Mater. Chem. A* **2021**, *9*, 26929.
[296] X. Zhang, G. Li, Y. Zhang, D. Luo, A. Yu, X. Wang, Z. Chen, *Nano Energy* **2021**, *86*, 106094.
[297] L. Xie, Y. Xiao, Q. Zeng, Y. Wang, J. Weng, H. Lu, J. Rong, J. Yang, C. Zheng, Q. Zhang, S. Huang, *ACS Nano* **2024**, *18*, 12820.
[298] X. Zuo, M. Zhen, D. Liu, L. Fu, Y. Qiu, H. Liu, Y. Zhang, *Adv. Funct. Mater.* **2024**, *34*, 2405486.
[299] W. Sun, L. Xu, Z. Song, H. Lin, Z. Jin, W. Wang, A. Wang, Y. Huang, *Adv. Funct. Mater.* **2024**, *34*, 2313112.
[300] X. Wang, G. Li, M. Li, R. Liu, H. Li, T. Li, M. Sun, Y. Deng, M. Feng, Z. Chen, *J. Energy Chem.* **2020**, *53*, 234.
[301] T. Huang, Q. Cao, B. Jing, X. Wang, D. Wang, L. Liang, *Chem. Eng. J.* **2022**, *430*, 132677.
[302] W. Hua, Z. Yang, H. Nie, Z. Li, J. Yang, Z. Guo, C. Ruan, X. Chen, S. Huang, *ACS Nano* **2017**, *11*, 2209.
[303] W. Cai, G. Li, F. He, L. Jin, B. Liu, Z. Li, *J. Power Sources* **2015**, *283*, 524.
[304] G. Wang, Y. Lai, Z. Zhang, J. Li, Z. Zhang, *J. Mater. Chem. A* **2015**, *3*, 7139.
[305] C. Chang, C. Yang, Q. Wu, X. Wang, H. Nie, X. Zhou, X. Xie, B. Hwang, Y. Ye, *J. Power Sources* **2022**, *550*, 232115.
[306] X. Zhang, W. Yuan, H. Huang, M. Xu, Y. Chen, B. Zhao, X. Ding, S. Zhang, Y. Tang, L. Lu, *Int. J. Extrem. Manuf.* **2023**, *5*, 015501.
[307] W. Zhang, H. Li, R. Tao, C. Guo, K. Du, J. Wang, S. Yao, X. Liu, H. Li, P. Guo, J. Li, J. Liang, *Chem. Eng. J.* **2023**, *475*, 146133.
[308] J. Zhang, W. Xi, F. Yu, Y. Zhang, R. Wang, Y. Gong, B. He, H. Wang, J. Jin, *Chem. Eng. J.* **2023**, *475*, 146009.
[309] Z. Wang, J. Hu, J. Liu, Y. Von Lim, H. Song, Y. Wang, T. He, C. Huang, X. Yan, D. Zhang, S. Huang, *Small* **2022**, *18*, 2106716.
[310] X. Wang, L. Meng, X. Liu, Z. Yan, W. Liu, N. Deng, L. Wei, B. Cheng, W. Kang, *J. Colloid Interface Sci.* **2022**, *628*, 247.
[311] W. Yao, J. Xu, Y. Cao, Y. Meng, Z. Wu, L. Zhan, Y. Wang, Y. Zhang, I. Manke, N. Chen, C. Yang, R. Chen, *ACS Nano* **2022**, *16*, 10783.
[312] B. Qin, Y. Cai, X. Si, C. Li, J. Cao, W. Fei, J. Qi, *Chem. Eng. J.* **2022**, *430*, 132698.
[313] N. Shi, B. Xi, J. Liu, Z. Zhang, N. Song, W. Chen, J. Feng, S. Xiong, *Adv. Funct. Mater.* **2022**, *32*, 2111586.
[314] J. Liu, C. Lin, Q. Xie, D.-L. Peng, R.-J. Xie, *Chem. Eng. J.* **2022**, *430*, 133099.
[315] Z. Zhao, Y. Duan, F. Chen, Z. Tian, R. Pathak, J. W. Elam, Z. Yi, Y. Wang, X. Wang, *Chem. Eng. J.* **2022**, *450*, 138310.
[316] T. Wang, Y. Liu, X. Zhang, J. Wang, Y. Zhang, Y. Li, Y. Zhu, G. Li, X. Wang, *ACS Appl. Mater. Interfaces* **2021**, *13*, 56085.
[317] C. Wei, Y. Han, H. Liu, R. Gan, Q. Li, Y. Wang, P. Hu, C. Ma, J. Shi, *Carbon* **2021**, *184*, 1.
[318] Y. Li, T. Gao, D. Ni, Y. Zhou, M. Yousaf, Z. Guo, J. Zhou, P. Zhou, Q. Wang, S. Guo, *Adv. Mater.* **2022**, *34*, 2107638.
[319] Y. Ren, L. Hu, S. Chang, Y. Ma, B. Wang, H. Wu, F. Li, Y. Yang, S. Tang, X. Meng, *Small* **2024**, *20*, 2400068.
[320] L. Yang, Y. Li, Y. Wang, Q. Li, Y. Chen, B. Zhong, X. Guo, Z. Wu, Y. Liu, G. Wang, Y. Song, W. Xiang, Y. Zhong, *J. Power Sources* **2021**, *501*, 230040.
[321] Z. Cheng, J. Lian, Y. Chen, Y. Tang, Y. Huang, J. Zhang, S. Xiang, Z. Zhang, *CCS Chem.* **2024**, *6*, 988.
[322] A. Zhu, S. Li, Y. Yang, B. Peng, Y. Cheng, Q. Kang, Z. Zhuang, L. Ma, J. Xu, *Small* **2024**, *20*, 2305494.
[323] J. Feng, W. Liu, C. Shi, C. Zhang, X. Zhao, T. Wang, S. Chen, Q. Li, J. Song, *Energy Storage Mater.* **2024**, *67*, 103328.
[324] C. Li, K. Yang, Z. Ma, F. Zhao, J. Li, X. Xu, X. Hao, H. Qi, Y. He, *J. Mater. Chem. A* **2023**, *12*, 174.
[325] H. K. H. Liu, W. H. Lai, H. L. Yang, Y. F. Zhu, Y. J. Lei, L. Zhao, J. Peng, Y. X. Wang, S. L. Chou, H. K. H. Liu, *Chem. Eng. J.* **2021**, *408*, 127348.
[326] L. Fan, N. Deng, J. Yan, Z. Li, W. Kang, B. Cheng, *Chem. Eng. J.* **2019**, *369*, 874.
[327] Y. Liu, Y. Elias, J. Meng, D. Aurbach, R. Zou, D. Xia, Q. Pang, *Joule* **2021**, *5*, 2323.
[328] J. Brückner, S. Thieme, H. T. Grossmann, S. Dörfler, H. Althues, S. Kaskel, *J. Power Sources* **2014**, *268*, 82.
[329] T. Zhang, M. Marinescu, S. Walus, P. Kovacik, G. J. Offer, *J. Electrochem. Soc.* **2018**, *165*, A6001.
[330] T. Zhang, M. Marinescu, S. Walus, G. J. Offer, *Electrochim. Acta* **2016**, *219*, 502.
[331] A. Gupta, A. Bhargav, A. Manthiram, *Adv. Energy Mater.* **2019**, *9*, 1803096.
[332] L. Cheng, L. A. Curtiss, K. R. Zavadil, A. A. Gewirth, Y. Shao, K. G. Gallagher, Sparingly Solvating Electrolytes for High Energy Density Lithium-Sulfur Batteries, American Chemical Society, **2016**.
[333] H. Chu, J. Jung, H. Noh, S. Yuk, J. Lee, J. Lee, J. Baek, Y. Roh, H. Kwon, D. Choi, K. Sohn, Y. Kim, H. Kim, *Adv. Energy Mater.* **2020**, *10*, 2000493.
[334] H. Pan, K. S. Han, M. H. Engelhard, R. Cao, J. Chen, J. Zhang, K. T. Mueller, Y. Shao, J. Liu, *Adv. Funct. Mater.* **2018**, *28*, 1707234.
[335] H. Ye, Y. Li, *Nano Res. Energy* **2022**, *1*, 9120012.
[336] S. Zhang, K. Ueno, K. Dokko, M. Watanabe, S. Zhang, K. Ueno, K. Dokko, M. Watanabe, *Adv. Energy Mater.* **2015**, *5*, 1500117.
[337] L. Kong, L. Yin, F. Xu, J. Bian, H. Yuan, Z. Lu, Y. Zhao, *J. Energy Chem.* **2021**, *55*, 80.
[338] X. Kong, Y. Kong, L. He, W. Zhang, Y. Song, S. Liu, Y. Zhao, *J. Power Sources* **2022**, *551*, 232211.
[339] J. Zhou, Y. Guo, C. Liang, L. Cao, H. Pan, J. Yang, J. Wang, *Chem. Commun.* **2018**, *54*, 5478.
[340] Y. H. Xu, W. Z. Li, B. Fan, P. Fan, Z. K. Luo, F. Wang, X. H. Zhang, H. L. Ma, B. Xue, *Appl. Surf. Sci.* **2021**, *546*, 149034.
[341] C. Barchasz, J. C. Leprêtre, S. Patoux, F. Alloin, *Electrochim. Acta* **2013**, *89*, 737.
[342] J. Gao, M. A. Lowe, Y. Kiya, H. D. Abruña, *J. Phys. Chem. C* **2011**, *115*, 25132.
[343] M. Helen, T. Diemant, S. Schindler, R. J. Behm, M. Danzer, U. Kaiser, M. Fichtner, M. A Reddy, *ACS Omega* **2018**, *3*, 11290.
[344] H. M Joseph, M. Fichtner, A. R. Munnangi, *J. Energy Chem.* **2021**, *59*, 242.
[345] C. Kensy, D. Leistenschneider, S. Wang, H. Tanaka, S. Dörfler, K. Kaneko, S. Kaskel, *Batter. Supercaps* **2021**, *4*, 612.
[346] X. Li, M. Banis, A. Lushington, X. Yang, Q. Sun, Y. Zhao, C. Liu, Q. Li, B. Wang, W. Xiao, C. Wang, M. Li, J. Liang, R. Li, Y. Hu, L. Goncharova, H. Zhang, T.-K. Sham, X. Sun, *Nat. Commun.* **2018**, *9*, 4509.
[347] Z. Lin, Z. Liu, W. Fu, N. J. Dudney, C. Liang, *Adv. Funct. Mater.* **2013**, *23*, 1064.
[348] F. Ding, W. Xu, G. L. Graff, J. Zhang, M. L. Sushko, X. Chen, Y. Shao, M. H. Engelhard, Z. Nie, J. Xiao, X. Liu, P. V. Sushko, J. Liu, J. G. Zhang, *J. Am. Chem. Soc.* **2013**, *135*, 4450.
[349] J. Li, L. Zhang, F. Qin, B. Hong, Q. Xiang, K. Zhang, J. Fang, Y. Lai, *J. Power Sources* **2019**, *442*, 227232.
[350] F. Wu, J. T. Lee, N. Nitta, H. Kim, O. Borodin, G. Yushin, *Adv. Mater.* **2015**, *27*, 101.
[351] G. G. Eshetu, X. Judez, C. Li, O. Bondarchuk, L. M. Rodriguez-Martinez, H. Zhang, M. Armand, *Angew. Chem., Int. Ed.* **2017**, *56*, 15368.
[352] F. Wu, J. Qian, R. Chen, J. Lu, L. Li, H. Wu, J. Chen, T. Zhao, Y. Ye, K. Amine, *ACS Appl. Mater. Interfaces* **2014**, *6*, 15542.
[353] S. Xiong, X. Kai, X. Hong, Y. Diao, *Ionics (Kiel)*. **2012**, *18*, 249.

[354] J. W. Park, K. Ueno, N. Tachikawa, K. Dokko, M. Watanabe, *J. Phys. Chem. C* **2013**, *117*, 20531.
[355] Z. Guan, L. Bai, B. Du, *Materials* **2023**, *16*, 7504.
[356] X. Kong, Y. Kong, X. Liao, S. Liu, Y. Zhao, *SSRN Electron. J.* **2022**.
[357] H. Lu, Y. Zhu, B. Zheng, H. Du, X. Zheng, C. Liu, Y. Yuan, J. Fang, K. Zhang, *New J. Chem.* **2019**, *44*, 361.
[358] É. A. Santos, L. M. S. Barros, A. F. Anna, I. Galantini, J. M. Gonçalves, R. Maciel Filho, H. Zanin, *Chem. Eng. J.* **2024**, *493*, 152429.
[359] Y. Cao, P. Zuo, S. Lou, Z. Sun, Q. Li, H. Huo, Y. Ma, C. Du, Y. Gao, G. Yin, *J. Mater. Chem. A* **2019**, *7*, 6533.
[360] M. Agostini, Y. Aihara, T. Yamada, B. Scrosati, J. Hassoun, *Solid State Ionics* **2013**, *244*, 48.
[361] J. K. Song, M. Kim, S. Park, Y. J. Kim, *J. Energy Chem.* **2023**, *78*, 574.
[362] M. Jia, T. Li, D. Yang, L. Lu, L. Duan, J. Liu, T. Wu, *Batteries* **2023**, *9*, 488.
[363] S. Kim, Y. A. Chart, S. Narayanan, M. Pasta, *Nano Lett.* **2022**, *22*, 10176.
[364] M. Alkhedher, A. B. Al Tahhan, J. Yousaf, M. Ghazal, R. Shahbazian-Yassar, M. Ramadan, *J. Energy Storage* **2024**, *86*, 111172.
[365] P. GaneshKumar, V. Sivalingam, S. Divya, T. H. Oh, V. S. Vigneswaran, R. Velraj, *J. Energy Storage* **2024**, *87*, 111412.
[366] Y. Wu, Q. Wu, M. Sun, Z. Zeng, S. Cheng, J. Xie, *Adv. Funct. Mater.* **2025**, 2425698.
[367] P. Molaiyan, M. Abdollahifar, B. Boz, A. Beutl, M. Krammer, N. Zhang, A. Tron, M. Romio, M. Ricci, R. Adelung, A. Kwade, U. Lassi, A. Paolella, *Adv. Funct. Mater.* **2024**, *34*, 2311301.
[368] D. Petersen, M. Gronenberg, G. Lener, E. Leiva, G. L. Luque, S. Rostami, A. Paolella, B. J. Hwang, R. Adelung, M. Abdollahifar, *Mater. Horiz.* **2024**, *11*, 5914.
[369] S. Pal, X. Zhang, B. Babu, X. Lin, J. Wang, A. Vlad, *Oxford Open Mater. Sci.* **2022**, *2*, itac005.
[370] J. Offermann, A. Paolella, R. Adelung, M. Abdollahifar, *Chem. Eng. J.* **2024**, *502*, 157920.
[371] M. Abdollahifar, *Carbon* **2025**, *233*, 119914.
[372] M. Horst, J. K. Burmeister, M. Abdollahifar, S. Pillitteri, A. Kwade, *J. Power Sources* **2023**, *587*, 233675.

Jakob Offermann is currently a doctoral students at the Chair of Functional Nanomaterials (Prof. Dr. Rainer Adelung) in the Department of Engineering at the Christian-Albrechts-University of Kiel, Germany. He received his M.Sc. degree in materials science and engineering from Kiel University in 2020 and was awarded for the best master thesis of the year. His current research focuses on the combination of high performance and eco-friendly silicon–sulfur batteries, as well as surface structuring of metals for improved mechanical bonding of various materials.

Sheikh Najeeb Ul Haq is a doctoral candidate in the Nanoscience and Energy Research lab (NERL) at the Department of Physics, School of Natural Sciences, Shiv Nadar Institution of Eminence, Delhi-NCR, India. He earned his 5-year integrated B.Sc.–M.Sc. in physics from the Central University of Kashmir, Jammu & Kashmir, India. His research is centered on the development of advanced electrode and electrolyte materials for rechargeable metal–sulfur batteries, with a particular emphasis on the fabrication of cathodes and electrocatalysts for lithium–sulfur batteries.

Kai-Xing Wang is a master's student at Chung Yuan Christian University (CYCU), specializing in advanced battery technology, with a focus on lithium–sulfur and anode-free lithium metal batteries. His research covers areas such as energy density, dendrite formation, and electrode modification. Additionally, he is working on creating self-assembled porous structures (breath figures) using inorganic materials like cobalt sulfide, applied to the cathode surface of batteries.

Rainer Adelung is a professor and holder of the Chair of Functional Nanomaterials in the Department of Materials Science at the Faculty of Engineering at Kiel University (Germany). He specializes in various nanostructures, mainly in the synthesis and design of porous materials. Applications range from energy technology such as batteries and supercapacitors to sensor devices, antiviral agents and advanced adhesion technology in engineering.

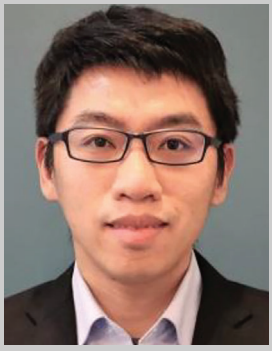

Shu-Hao Chang is currently an assistant professor in the Department of Chemical Engineering at Chung Yuan Christian University (CYCU). He received his Ph.D. in chemical engineering from National Tsing Hua University (NTHU), Taiwan, in 2014. His research expertise includes the synthesis and characterization of nanomaterials, as well as the development of electrode materials for batteries such as lithium-ion, lithium-sulfur, and zinc-ion batteries, along with pressure sensor devices.

Binson Babu is an assistant professor and leader of the Nanoscience and Energy Research Lab (NERL) at the Department of Physics, School of Natural Science at the Shiv Nadar Institution of Eminence, Delhi-NCR, India. He earned his Ph.D. from IISER Thiruvananthapuram in 2019 and completed postdocs at Friedrich-Schiller-University, Jena, and Université catholique de Louvain, Belgium. In 2023, he received the HORIZON-MSCA-PF fellowship and an SRG from ANRF (SERB), India. His research focuses on developing novel electrode and electrolyte materials for rechargeable batteries, supercapacitors, and hybrid-ion capacitors.

Mozaffar Abdollahifar received his doctorate in chemical engineering, focused on energy storage materials, from National Taiwan University (NTU) in 2018. Before becoming a battery group leader at Kiel University (Germany), he worked as a scientist for several years at NTU and then at the Battery LabFactory Braunschweig (BLB, TU Braunschweig, Germany). He is interested in developing supercapacitors and battery materials for Li, Na and sulfur chemistries, anode-free batteries, and electrode engineering, as well as recycling end-of-life batteries.